Resonant Switched Reluctance Motor Drive and Its Power Conditioning with Switched-Capacitor Techniques

Yeung Yiu Pun Benny

Ph.D.

THE HONG KONG
POLYTECHNIC UNIVERSITY

2004

The Hong Kong Polytechnic University

Department of Electrical Engineering

Resonant Switched Reluctance Motor Drive and Its Power Conditioning with Switched-Capacitor Techniques

Yeung Yiu Pun Benny

A thesis submitted in partial fulfilment

of the requirements for the Degree

of

Doctor of Philosophy

January 2004

CERTIFICATE OF ORIGINALITY

I hereby declare that this thesis is my own work and that, to the best of my knowledge and belief, it reproduces no material previously published or written nor material which has been accepted for the award of any other degree or diploma, except where due acknowledgement has been made in the text

_____(Signed)

Yeung Yiu Pun Benny_____(Name of student)

Abstract

In the past, switched-capacitor DC-DC converters were mainly used on low power applications for doubling voltage or invert voltage. They are not suitable for high power applications because of their current stress problem and low efficiency. In this project, families of switched-capacitor DC-DC resonant converters are developed. Current stress problems have been solved in the circuits so that they can work under high power operation. All transistors in the circuits are switched under zero-current switching condition to improve the efficiency. Since the improvements are done, the switched-capacitor techniques can be used for power conditioning for applications such as motor drives. Implementation of high power switched-capacitor resonant converter is done.

Switched reluctance motor (SRM) has the advantages of high power density, fast response and robust. To drive a SRM, electronic circuit is need. A newly designed switched reluctance motor drive is introduced in the thesis. Active-clamp resonant technique is applied in the motor drive to provide soft-switching for all high switching frequency transistors. Performances of both electromagnetic interference (EMI) and efficiency of the motor drive are improved.

Performance of Switched reluctance motor is usually poor when its speed is high because of its long regenerating stage. A method by using switched-capacitor based power conditioning is proposed in the thesis.

Waveforms of the commutating current of the SRM are modified by a switched-capacitor front-end converter. In the whole system, all high frequency transistors are switched under zero-voltage switching condition.

Mathematical Analysis, Computer simulation, and experiments have been done for all proposed circuits. Description and explanation of the results are provided in the thesis.

List of Publications

Accepted Journal Papers

1. Y.P.B.Yeung and K.W.E.Cheng, "Zero-current Switching Fixed Frequency Resonant-Transition Square Wave Converters", *IEE Proc. Electr. Power Appl.*, vol.148, No. 6, pp. 475-480, Nov. 2001.

2. Y.P.B.Yeung, K.W.E.Cheng and D.Sutanto, "Investigation of Multiple Output Operation for Switched-capacitor Resonant Converters", *Int. J. Cct. Theory & Appl.*, vol. 30, No. 4, pp. 411-423, March 2002.

3. Y.P.B.Yeung, K.W.E.Cheng, D.Sutanto and S.L.Ho, "Zero-current Switching Switched-capacitor Quasi-resonant Step-down Converter", *IEE Proc. Electr. Power Appl.*, vol. 149, No. 2, pp. 111-121, March 2002.

4. Y.P.B.Yeung, K.W.E.Cheng, S.L.Ho and D.Sutanto, "Generalised Analysis of Switched-capacitor Step-down Quasi-resonant Converter", *IEE Electron. Letters*, vol. 38, No. 6, pp. 263-264, March 2002.

5. Y.P.B.Yeung, K.W.E.Cheng, S.L.Ho, K.K.Law and D.Sutanto, "Unified Analysis of Switched-capacitor Resonant Converters", *IEEE Trans. on Ind. Electron.*, vol. 51, No. 4, pp. 864-873, Aug. 2004.

Accepted Conference Papers

1. K.W.E.Cheng and Y.P.Yeung, "Investigation of Zero-current Switching Fixed Frequency Resonant-transition Square Wave Converters", *IEEE PEDS 1999*, vol. 2, pp. 755-760, 1999.

2. K.W.E.Cheng, Y.P.B.Yeung, C.Y.Tang, X.D.Xue and D.Sutanto, "Topology Analysis of Switched Reluctance Drives for Electric Vehicles", *IEE PEVD 2000*, pp. 512-517, 2000.

3. Y.P.B.Yeung, K.W.E.Cheng and X.D.Xue, "High Order Output Design for Switched-capacitor Resonant Converters", *EPE 2001*, Graz, Austria, 2001.

4. Y.P.B.Yeung, K.W.E.Cheng and D.Sutanto, "Multiple and Fractional Voltage Conversion Ratios for Switched-capacitor Resonant Converters", *IEEE PESC 2001*, vol. 3, pp. 1289-1294, 2001.

5. Y.P..Yeung, K.W.E.Cheng and K.K.Law, "Switched-capacitor Based Step-Down Resonant Converters", *14th Conf. of China Power Supply Society,* Sep. 2001, pp. 125-128, 2001.

6. K.W.E.Cheng, K.K.Law, Y.P.B.Yeung, D.Sutanto and D.K.W.Cheng, "Development of Multiple Output Operation Based on Single Stage

Switched-Capacitor Resonant Converters", *IEEE PESC 2002*, Vol. 3, pp. 1325 –1330, 2002.

7. Y.P.B.Yeung, K.W.E.Cheng, D.Sutanto and S.L.Ho, "Exploring Zero-voltage Switching in SRM drive Design", *EPE-PEMC 2002*, Cavtat & Dubrovnik, Croatia, 2002.

8. Y.P.B.Yeung, K.W.E.Cheng, D.Sutanto, and S.L.Ho, "Analysis of Partial Soft-switching Converter for Switched Reluctance Motor Drive Achieved by Active-clamp Topology", *Proc. of ASPCOM 2003,*vol. 1, pp. 174-178, 2003.

9. Y.P.B.Yeung, C.Y.Tang, and K.W.E.Cheng, "Application of Conductive Adhesive Planar Inductor on a Power Conversion", *Proc. of ASPCOM 2003,* vol. 1, pp. 179-184, 2003.

Acknowledgements

I would like to express thanks to my supervisor, Professor Ka Wai Eric Cheng, for his continuing guidance and encouragement throughout the course of my studies since 1997. I would also like to give thanks to everyone in my department, department of research committee, and research office, especially to the head of department, Professor Kit Po Wong, associate head of department, Professor Siu Lau Ho, my co-supervisor, Professor Danny Sutanto, and Ms. Shirley Tsang of research office. I would also gratefully acknowledge the financial support of the Research Grant Council, Hong Kong, for the project. I would like to also thank to everyone in my department, especially the head of department.

A special thank goes to Mr. Tze Kong Cheung. He has given me great technical supports and suggestions. I would give thanks to my colleagues, Mr. Yiu Lun Ho, Mr. Xiang Dong Xu and Mr. Ka Yin Tse, and my friends in my life for their great supports. I am also thankful to the members in my band, Mr. Paul Hung, Mr. Karl Cheng and Mr. Maurice Fong.

Most of all, I wish to express my sincerest gratitude to Ms. Bonnie Fan, my father, Yeung Koon To, my grandfather, Kan Kee, my grandmother, Ko Fung Po, and my aunts, Kan Yuk Ha and Kan Yuk Bing, for their warm loves and encouragement.

Table of Contents

List of Figures

List of Tables

Chapter 1. Introduction

1.1. Background

This thesis concerns switched reluctance motor drives and switched-capacitor techniques. Backgrounds of these technologies will be briefly introduced in this session.

1.1.1. Switched Reluctance Motors

According to records, the first switched reluctance motor (SRM), commonly known as variable reluctance motor in U.S., was built by Davidson in Scotland in 1838 [B2]. Controlling the motor, switched reluctance motor was not popular in industry. Electronics has been well developed since the early 70's. In 1971 and 1972, Bedford and Hoft introduced a modern switched reluctance motor with its circuit topology of power electronic controller. Since this "reinvention" of SRM, the use of such machines has been widespread and became popular in the industry. Many companies have started developing their own SRMs and motor drives for industrial applications. The first commercial application of SRM in the United States was the Hewlett-Packard servo drive used in the Draftmaster computer-plotter. As new technologies of power electronics such as soft-switching techniques developed, switched reluctance motor has become a great interest in research today. The advantages and disadvantages of SRMs are summarized below:

Advantages of SRMs:

(i) Its structure is simple and robust.

(ii) It has neither winding nor permanent magnet on the rotor and hence reducing manufacturing cost of rotor.

(iii) It has no permanent magnet in the machine so that its material cost is low.

(iv) It has low rotor inertia. Because there is no winding on the rotor, size, weight and moment of inertia of the rotor are low. The machine can produce high starting torque and good dynamic response.

(v) It has slightly higher power density compared with induction motor but lower power density than DC brushless machine.

(vi) It has fault tolerance characteristic. Each phase winding in the stator is electrically separated from each other, with negligible mutual coupling. Generally, electrical fault in one phase does not affect the operation of other phases and hence, increase reliability of the machine.

(vii) It is a kind of brushless machine. There is no problem of commutation brush damage as in traditional DC motors. It can provide high reliability.

(viii) It can operate in a wide range of speed.

(ix) It is fully controllable for four-quadrant operation.

Disadvantages of SRMs:

(i) It does not have line-start capability. It requires a power electronic converter for motor drives. Nowadays, power electronic components are less expensive. It can overcome the problem of the expense of motor drives.

(ii) Torque ripple is high, but some controlling phase current techniques have been proposed to reduce the torque ripple.

(iii) High acoustic noise, but it has been reduced by some techniques in as described in a number of literatures [B4] and [B6].

(iv) Position sensors are required to control the machine, increasing manufacturing cost. Some sensorless control techniques have thus been proposed to solve this problem, such as inductance-sensing method and observer-based rotor position estimation method.

Features of switched reluctance motors are attractive in industrial or commercial applications. However, there is still resistance of using or manufacturing this kind of motors in industry or commercial products as, unlike

induction motors, SRMs are comparatively new machines. The AC drives are entrenched in the marketplace, and customers are knowledgeable in the old driving system. The expense of retraining of their personnel is high if replacing a SRM system instead of another traditional driving system in existing applications. Also, manufacturers of motor drives may not be willing to install additional, new manufacturing lines that may cannibalize their existing product line, require capital investment, and thus decrease profit in the short term.

Although switched reluctance motors are not popular in old applications, but because of its advantages, companies do accept using SRMs on newer applications or newer products, especially in variable speed drive applications.

1.1.2. Switched-capacitor Power Supplies

Switched-mode power supplies (SMPSs) are devices for transforming voltage from one level to another by controlling durations of turning on and off of switching devices to store energy in energy storage components and release energy to the output. Typical power supplies use both capacitors and inductors or transformers as the energy storage components. Since SMPSs can operate at significantly high switching frequencies, power densities of the devices are high. This kind of devices has become very popular in industrial and domestic applications.

Size and weight of energy storage components can be reduced by high switching frequencies of SMPSs. However, those of magnetic components,

such as inductors and transformers, occupy a very high ratio of the whole size and total weight in typical SMPSs. For some common SMPS topologies, like buck, boost, buck-boost, and flyback converters, their output voltage is highly dependent on their output power when they operate in discontinuous mode. In this case, closed-loop control is necessary to regulate the output voltage, especially at light load, although very accurate output voltage is not required.

Switched-capacitor power supplies are also a kind of SMPS. One feature of this SMPS is that capacitors in the circuit are the only components for energy storage. In other word, this kind of power supplies does not have any magnetic component. Since the capacitor does not have magnetic saturation problem, the weight of the capacitor is lighter and the size of the capacitor is smaller than the magnetic component in the same power level. Size and weight of the switched-capacitor power supplies are about 50% of those in typical SMPS.

Applications of integrated circuit (IC) chips have rapidly increased in the last twenty years. Nowadays, demand for power conversion devices internally built in IC chips is high for providing good responsibility to the integrated circuits. Switched-capacitor power supplies are developed for this application. The main difference of this kind of SMPS is that it has no magnetic component inside the circuit. Only capacitors are used for energy storage, so that they can be fabricated in IC chips. This technology has been used in many IC chips for low power applications recently. As high switching frequency techniques are more and more mature, the integrated switched capacitor power supplies can be

used in higher power applications.

Switching devices in switched-capacitor power supplies are responsible for routing different charging and discharging paths of switched-capacitors to produce different conversion ratio. Their structures are usually simple if the power supplies are used for producing output voltage with double, half or negative level of input voltage. If for producing other voltage conversion ratios, most of them need a number of switching devices for routing the complicated charging and discharging paths. Switching loss and costs of switching devices drivers are high. Another drawback of switched-capacitor power supplies is that the switched-capacitors in the power supplies are charged by transient current from the power sources. This leads to high current stress problem, such that this kind of power supplies is suitable for low power applications only.

1.2. Previous Researches

1.2.1. Principles of Switched Reluctance Motor Drives

Switched reluctance motor is a kind of brushless motor and reluctance motor. Definition of reluctance motor is that it is an electric motor in which torque is produced by the tendency of its moveable part to move to a position where the inductance of the excited winding is maximized [B1]. Fig. 1.1 shows a SRM with 8 stator poles and 6 rotor poles (8/6 SRM).

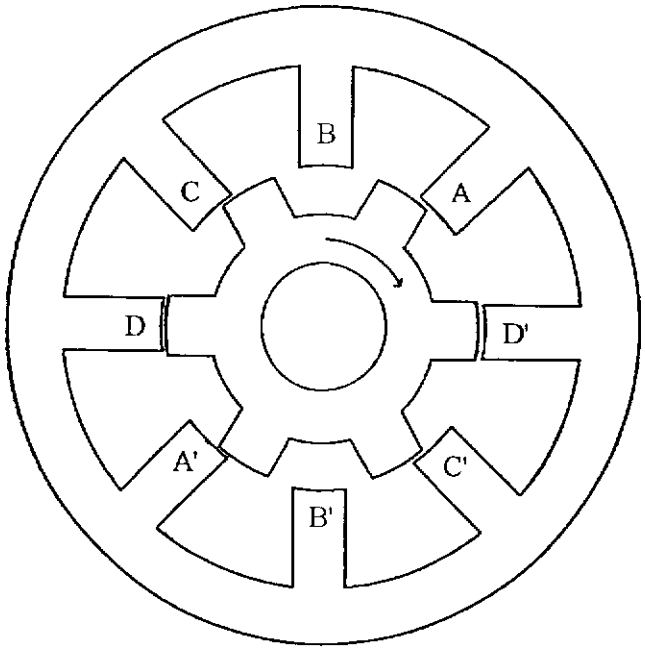

Fig. 1.1. 8/6 switched reluctance motor

In Fig 1.1, the rotor is in intermediate position relative to phase A. When phase A is energized, there is a torque to rotate the rotor towards the position that aligns the rotor pole to phase A, i.e. clockwise direction in this case. Inductance of phase A is in maximum when in aligned position. In aligned position, there is no torque to the rotor. In the SRM, only one phase can be energized at each moment. To keep the rotation continuous, the phases of motor are energized in the sequence phase B, C, D, A,... and so on.

Fig. 1.2 shows a characteristic of inductance of one phase of SRM. Inductance of the phase in SRM is changed when the rotor rotates to a different position. Because of the saturation of the phase windings, inductance of the phase is dependent on input current. In short, phase inductance is a function of phase current and angular position.

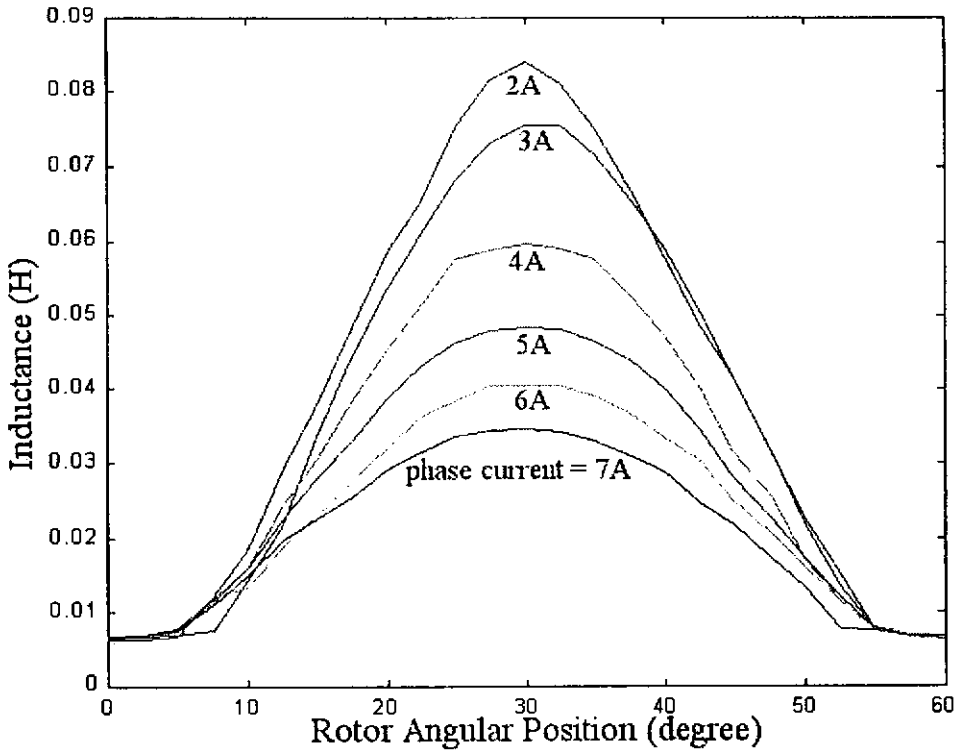

Fig. 1.2. Phase inductance characteristic of switched reluctance motor

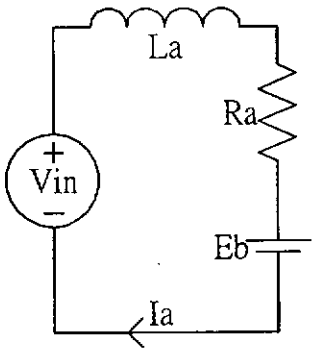

Fig. 1.3. Per-phase equivalent circuit of switched reluctance motor in motoring stage

Equivalent circuit of per-phase of SRM in motoring stage is shown in Fig. 1.3. L_a is inductance of the phase windings, R_a is DC resistance of the phase windings, V_{in} is input voltage, i_a is phase current and E_b is back EMF of the machine to this phase. From the equivalent circuit, it gives the equations:

$$V_{in} = R_a i_a + L_a(i_a, \theta)\frac{di_a}{dt} + E_b \tag{1.1}$$

therefore,

$$V_{in} = R_a i_a + L_a \frac{di_a}{dt} + \frac{d\varphi_a}{dt} \tag{1.2}$$

where φ_a is phase flux linkage and θ is angular position.

Equation (1.2) can be rewritten as:

$$V_{in} = R_a i_a + L_a \frac{di_a}{dt} + i_a \frac{\partial L_a}{\partial \theta} \times \frac{d\theta}{dt} \tag{1.3}$$

Torque produced by one phase is:

$$T_a = \frac{1}{2} i_a^2 \frac{\partial L_a}{\partial \theta} \tag{1.4}$$

Let T_b, T_c and T_d be torque produced by another phases of the motor, J be total moment of inertia of the rotor, and B be total damping factor of the load and the motor, net torque of a 4-phase SRM is:

$$T_{net} = J \frac{d\omega_m}{dt} + B\omega_m T = T_a + T_b + T_c + T_d - T_L \tag{1.5}$$

1.2.2. Traditional Switched Reluctance Motor Drives

A number of different switched reluctance motor drive circuits have been proposed and described in [B1], [B2], [B14] and [B15]. They include basic asymmetric bridge SRM converter circuit, (n+1)-switch circuit, 2(n+1)-switch circuit, Oulton™ circuit and C-dump circuit. A basic SRM converter circuit and a 2(n+1)-switch circuit are shown in Fig. 1.4 and Fig. 1.5, respectively.

Both (n+1)-switch circuit and 2(n+1)-switch circuit are modified from the basic converter circuit shown in Fig. 1.4. Comparing the circuits in Fig. 1.4 and Fig. 1.5, the 2(n+1)-switch circuit uses 2 transistors and 2 diodes fewer than the basic converter circuit. This lowers manufacturing cost.

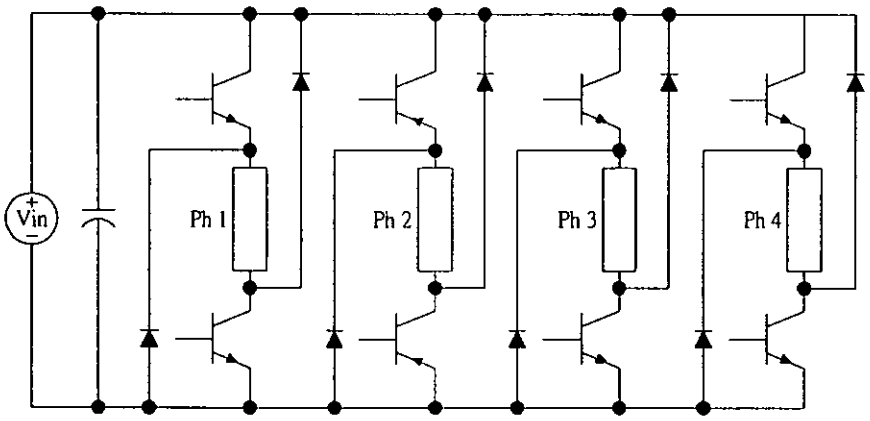

Fig. 1.4. Basic asymmetric bridge circuit for switched reluctance motor drives

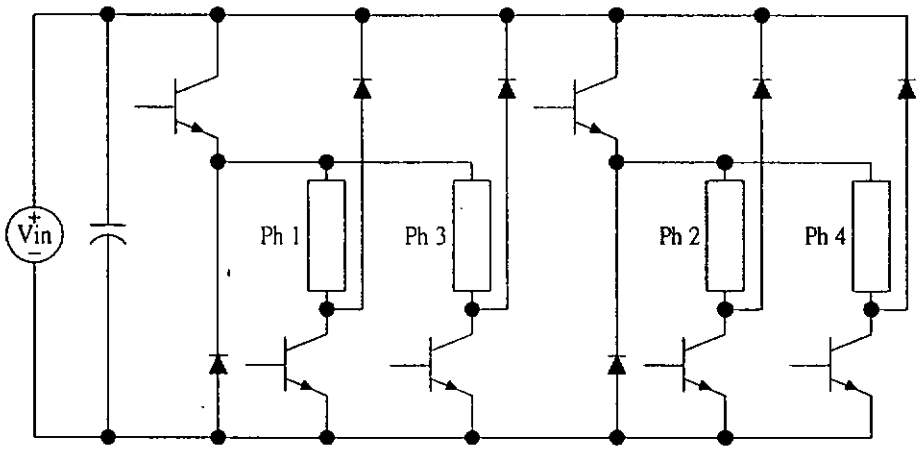

Fig. 1.5. 2(n+1)-switch circuit for switched reluctance motor drives

Fig. 1.6 shows per-phase equivalent circuits of switched reluctance motor drive in different states of operation. These equivalent circuits are for both basic converter and 2(n+1)-switch circuits. There are three states of operation. The motor is in motoring stage in both State I and State II, and in regenerating

stage in State III.

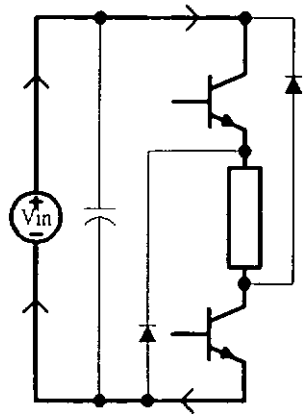

(a) State I

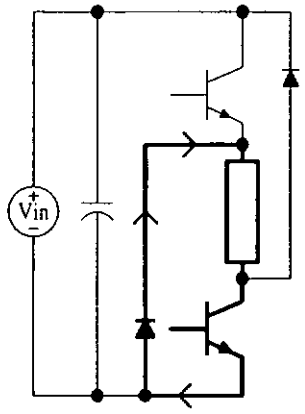

(b) State II

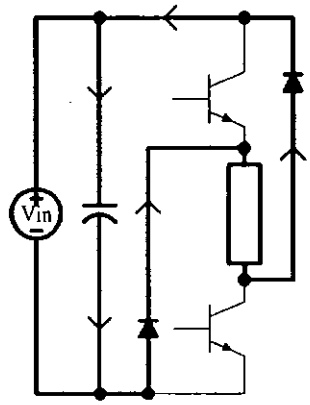

(c) State III

Fig. 1.6. States of operation of per-phase switched reluctance motor drive

In State I as shown in Fig. 1.6(a), both chopping transistor (upper transistor) and commutation transistor (lower transistor) are turned on. V_{in} is connected to the phase winding and phase current increases. In State II as shown in Fig. 1.6(b), the chopping transistor is turned off and the commutating transistor is still on. Because the inductance of the phase windings is high, phase current freewheels through a freewheeling diode and decreases gradually by the resistance of the winding. The circuit operates in State I and State II alternately. When the rotor reaches aligned position, or when the other phase needs to be energized to maintain smooth rotation of the motor, the circuit operates in State III as shown in Fig. 1.6(c). In this state, all transistors are turned off and all diodes are in forward bias. Input voltage is in reverse polarity to the phase winding. The phase current decreases to zero.

1.2.3. Conventional Soft-switching Converters for Switched Reluctance Motor Drives

Soft-switching technique by using resonance method is a trend in power electronics. This technique has advantages of low switching loss, low switching transient, and low electromagnetic interference (EMI). Higher frequency can be used in soft-switching circuits than that in hard-switching circuits to improve performance of the circuits such as reducing the current ripple and the torque ripple in the motoring stage in current control. Soft-switching techniques have been widely used on SMPSs for many years. Many different soft-switching topologies of SMPS have been proposed [A1-A14], however, , only few research articles about soft-switching SRM drives for switched

reluctance motors have been published [B5], [B7-B11], [B13-B15].

Operation of SRM requires a complicated control system. Generally, computers or microprocessors are used for the control systems for reducing hardware cost and to avoid the need for designing complicated hardware circuits. In the past, speed of computers and microprocessors were low, and could not provide a high frequency operation environment for the machine. In the past few years, performance of digital signal processors (DSPs) has been much improved and the cost much lowered. DSPs have been commonly used in the market. Because of their high speed, they can operate in high frequency. Nowadays, switched reluctance motor controllers are often based on DSPs for providing better performance. Soft-switching techniques are suitable for high frequency operation. Applying these techniques in SRM drives to improve efficiency is a great concern.

1.2.3.1. Quasi-resonant Circuits

Quasi-resonant soft-switching topologies have been widely used in DC-DC converters and AC-DC converters [A1-A8]. Generally, these techniques involve adding one or more resonant tanks in the circuit to provide resonance environment in each switching period. The transistors are switched under zero-voltage switching or zero-current switching conditions. Thus, switching loss of the transistors can be reduced. References [B5], [B7-B11], [B14] and [B16] introduced some soft-switching switched reluctance motor drives based on quasi-resonant topologies.

The topologies introduced in references [B9–B11] are similar to the traditional resonant transition DC-DC converters proposed in reference [A5]. In these two papers, when the motor is in motoring stage, the drive circuits are considered as buck converters. On the other hand, in regenerating stage, the circuits are considered as boost converters. By applying resonant transition methods in the circuits, zero-current switching and zero-voltage switching condition can be obtained, respectively.

1.2.3.2. Resonant DC Link Circuits

References [B5], [B8] and [B13] proposed a topology of actively clamped resonant DC link circuit (ACRDCL) applied on SRMs. The concept of ACRDCL for AC drives has been well-developed. The idea proposed in these papers applies the resonant AC drive concept in SRM drive. In fact, the ACRDCL SRM drives are very similar to ACRDCL inverter for AC drives. In this SRM drive, resonant DC link is provided by an ACRDCL circuit after DC input. The DC link voltage is clamped by a large clamping capacitor to limit its maximum voltage. The SRM operates with hard-chopping. By controlling the resonant DC link voltage, soft-switching for all transistors is obtained.

1.2.4. Commutation Current Modification Methods

Performance of switched reluctance motors is dependent on the shapes of commutation current of its phase windings. The ideal commutation current of

each phase winding of SRM is a square wave. However, the ideal waveform of commutation current cannot be achieved practically due to the inductance of the phase windings. Fig. 1.7 shows the ideal and practical shapes of commutation current of a 3-phase SRM.

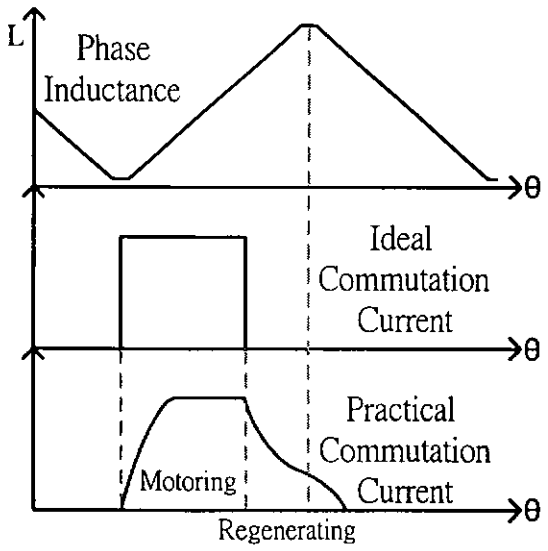

Fig. 1.7. Commutation current of 3-phase switched reluctance motor

The disadvantage of the practical shape of commutation current is that current cannot rise from zero to the maximum current nor fall to zero rapidly. The slow rising of current in the beginning of motoring stage limits maximum input and output power of the SRM. In regenerating state, energy is recovered and stored in voltage source or capacitors. If the duration of regenerating state is long, in practice, conduction loss due to the regenerating commutation current is high. In some cases, commutation current may not fall to zero when the angular rotor position is beyond aligned position. If the current is positive in the region that the change of inductance is negative, negative torque is produced. This leads to higher torque ripples and lower efficiency. The influence of the practical current shape is particularly significant at high speed.

References [B3], [B12], [B17] and [B19] proposed methods for squaring up commutation current of SRMs. Most of them use voltage boost method for increasing the rate of change of current in the beginning and the end of motoring state. In their proposed circuits, a boost-capacitor is used. The capacitor is responsible for storing energy from the phase winding in regenerating state and releasing energy to the phase winding in motoring state. In regenerating state, phase winding regenerates current to the voltage source through the boost-capacitor so that the capacitor is charged. Voltage of the capacitor increases. By connecting the capacitor in series with the voltage source, in regenerating state, the negative voltage applied on the phase winding is higher than the normal DC link voltage. Commutation current hence falls to zero more quickly. In the beginning of motoring state, the DC link voltage is higher than the normal one. Current thus increases to the peak value more quickly, until the energy of the capacitor is totally released.

1.2.5. Vibration and Acoustic Noise Cancellation Techniques in Switched Reluctance Motor Drive

As the features of SRM such as brushless, low rotor inertia, and low manufacturing costs, SRM is an attractive machine. The main disadvantage of this machine is that it induces high acoustic noise and vibration due to its operation principles. In fact, acoustic noise is closely related to vibration. Some researchers have analysed the causes of vibration induced in SRM. [B4] This literature introduced the experiments for analysing the machine in both static tests and rotary tests. By the time domain analysis with the experiments,

the causes of vibration and acoustic noise in SRM were found.

[B4] proposed a technique for reducing the vibration and acoustic noise. [B6] is a further research of [B4]. This literature proposed three techniques to reduce the vibration as well. All the techniques proposed in these literatures are using reducing the step change of voltage applied on the phase windings and vibration cancellation methods by producing an opposite vibration on the SRM. Vibration sensor is not needed by using these methods. However, as the level of vibration is related to the material and construction of the SRM, an initial test is required to find the natural frequency of the stator.

1.2.6. Switched-capacitor DC-DC converter

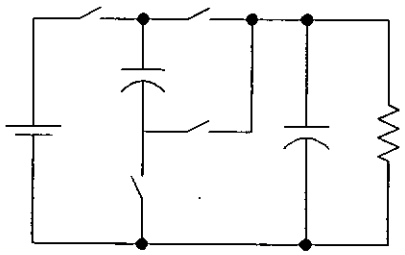

(a) half-mode

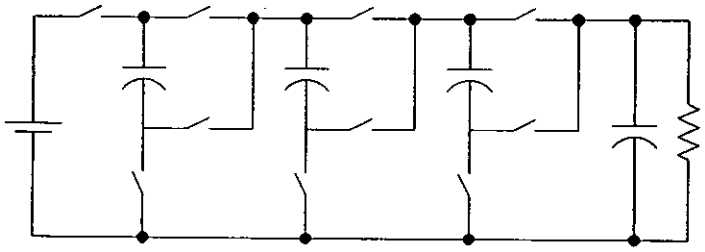

(b) 1/5-mode

Fig. 1.8. Conventional switched-capacitor DC-DC step-down converters

For most switched mode power supplies, energy storage relies on large capacitors or magnetic components like transformers or inductors. These magnetic components are usually wire-wounded on a magnetic core or air-core, limiting the reduction of size and weight of the circuits. Some switched-capacitor converters have been proposed in References [C1-C10] to solve this problem. Conventional switched capacitor DC-DC step-down converters are shown in Fig. 1.8. In this kind of converters, instead of magnetic components, only capacitors are used for energy storage. Electrical energy conversion is achieved by controlling the routines of charging and discharge of the capacitors, known as switched-capacitors. These routines are controlled by transistors. Because of the advantage of eliminating magnetic components in the circuit, converters can be fabricated in integrated chips.

Switched capacitor converters generally have some common disadvantages as listed below:

(i) Most switched capacitor converters operate in hard-switching. This causes high switching loss and high electromagnetic interference.

(ii) There is current spike problem when charging the switched capacitors. This limits the power level and current level of the circuits.

(iii) A number of transistors are needed for routing the charging and discharging paths of switched-capacitors.

(iv) It is difficult to control output voltages of the circuits. Some switched-capacitor converter control techniques are proposed in references [C1-C4], [C6] and [C7]. They use equivalent series resistance (ESR) of the switched capacitors to control the charging level of the capacitors. Because the charging time of capacitor is very short, it is very difficult to control its charging time by controlling duty ratio of turn on time of transistors. It is easier to control the charging level of the switched-capacitors if the ESR is high; however, this causes high power losses in charging and discharging the capacitors.

1.3. Outline of Thesis

The main results and contribution of this thesis are outlined as follows:

(i) Two families of newly designed single-stage switched-capacitor DC-DC step-down converters are introduced in Chapter 2. Circuits in one family are for producing positive stepped down voltage, while circuits in the other are for producing negative stepped down voltage. All circuits have only two transistors for switching. All transistors in the circuits are under zero-current switching condition, obtaining high efficiency. The new circuits do not have the common current stress problem of switched-capacitor converters. Operation principles of the circuits are described in this chapter, and explained by mathematical analysis and computer simulation. Design method of the circuits describes suggested methods to obtain zero-current switching in the circuits. A

prototype was tested in experiment to verify the operation of the circuits.

(ii) A family of multi-stage switched-capacitor step-up converter is introduced in Chapter 3. They produce positive step-up voltage. These circuits not only provide low current stress and zero-current switching, but also provide more than one output voltages other than the single-stage circuit. Operation principles of the circuit are discussed by mathematical analysis, computer simulation results and experiment results.

(iii) Chapter 4 introduces a new resonant converter for SRMs. All high frequency transistors in the circuit are under zero-voltage switching. This chapter explains the reason that chopping transistors need soft-switching in switched reluctance motor under soft-chopping condition. Active-clamp features and principles of operation of the converter are explained by computer simulation, mathematical analysis and experiments.

(iv) Chapter 5 suggests a method for improving performance of SRM by using power electronics for power conditioning. A switched-capacitor converter is used for stepping down the voltage from the voltage source when the voltage of the source is too high for the SRM. An experiment of implementation of switched-capacitor converter in high power operation is provided and discussed. In the whole driving system, the SRM regenerates the high voltage source. Duration of

regenerating stage is shorter. This can improve the performance of the machine. Mathematical analysis and computer simulation are used to discuss the performance.

(v) Chapter 6 concludes contributions of this thesis. Further study of the switched-capacitor resonant converters and the switched-reluctance motor drive is recommended.

Chapter 2. Single-stage Zero-current switching Quasi-resonant Switched-capacitor Step-down Converters

2.1. Introduction

Most switched-capacitor converters face a current spike problem when charging switched-capacitors in the circuits. This problem limits power of applications of the converters. It also causes high electromagnetic interference because of the rapid change of current. Most conventional circuits use hard-switching techniques to operate the converters, causing high switching loss. Hard-switching circuits are not suitable for operating in high frequency and hence, sizes of capacitors in the circuits are large and their power density is comparatively low. Another drawback of switched-capacitor converters is that a variation of the voltage conversion ratio can only be achieved by adding more switches. This means that more transistor drive circuits will be required for additional switches and hence, manufacturing cost and transistor drive loss are increased.

To solve the above problems, two families of single-stage zero-current switching quasi-resonant switched-capacitor step-down converters have been designed [C5], [C8] and [C10]. It includes non-inverting mode circuits and inverting mode circuits. By using zero-current switching quasi-resonant technique in these circuits, their charging and discharging currents of the switched-capacitor are half sinusoidal waves. This solves the current spike problem. All switching devices in the circuits are switched on and off under

zero-current switching condition. Switching loss and electromagnetic interference are both low, and hence, high efficiency is obtained. Further, a simple switched-capacitor cell is proposed. This switched-capacitor cell consists of only one capacitor and three diodes. By adding the switched-capacitor cell to the converters, voltage conversion ratios of the converters decrease fractionally. No additional transistor is required for changing the voltage conversion ratio.

2.2. Family of Circuits

Circuit diagrams of non-inverting mode circuits of zero-current switching quasi-resonant switched-capacitor step-down converters are shown in Fig. 2.1 and circuit diagrams of the inverting mode circuits are shown in Fig. 2.2. The circuits in Fig. 2.1(a), 2.1(b), 2.1(c), 2.1(d), 2.2(a), 2.2(b) 2.2(c), and 2.2(d) give output voltages equal to 1/2, 1/3, 1/4, 1/n, -1, -1/2, -1/3 and –1/n input voltage, respectively.

Output voltages of both non-inverting mode and inverting mode converters are based on the number of switched-capacitor cells, shown in Fig. 2.3, applied on the converter circuit. Referring to Fig. 2.1, in each cell for the proposed converters, Terminal a and Terminal b are connected across the capacitor of the former cell. Terminal c is connected to the node between D_1 and D_2. Terminal d is connected to the anode of the D_b of the next cell. Terminal e is connected to the cathode of D_b of the former cell. Terminal f is connected to L_r.

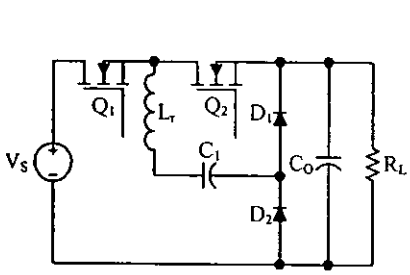

(a) 1/2-mode

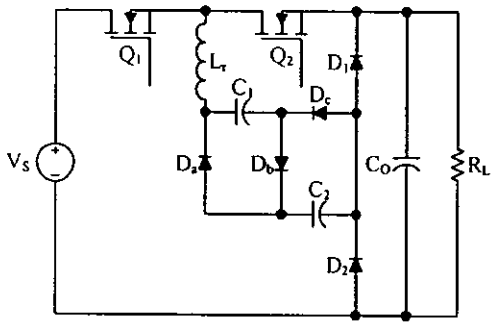

(b) 1/3-mode

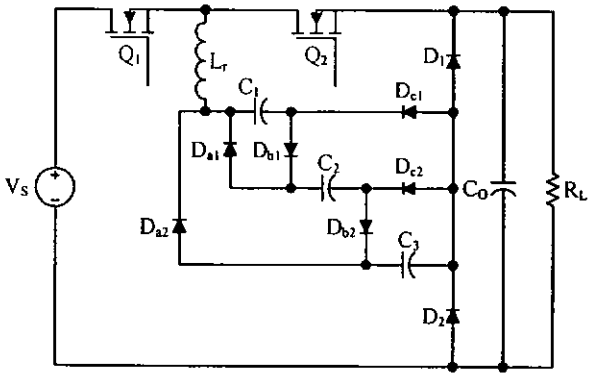

(c) 1/4-mode

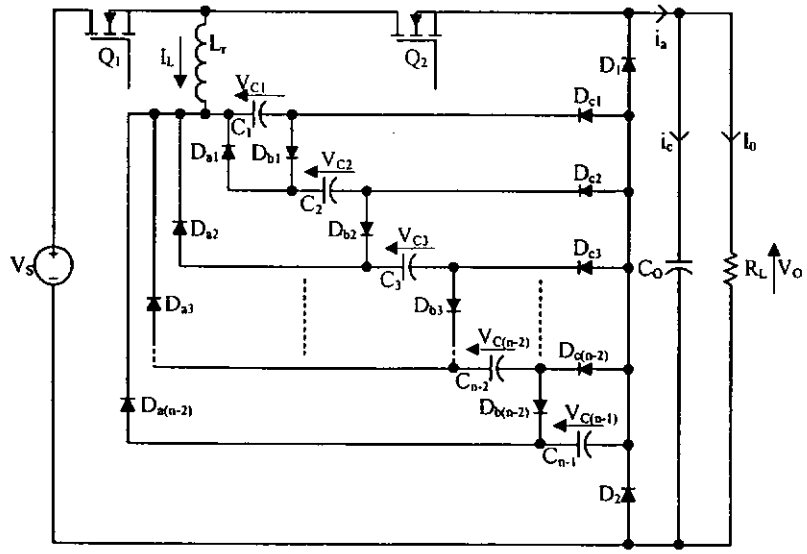

(d) 1/n-mode

Fig. 2.1 Circuit diagrams of non-inverting single-stage zero-current switching quasi-resonant step-down converters

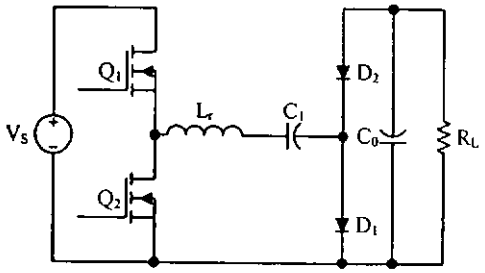

(a) –1-mode

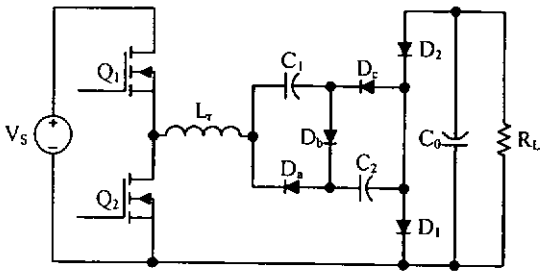

(b) –1/2-mode

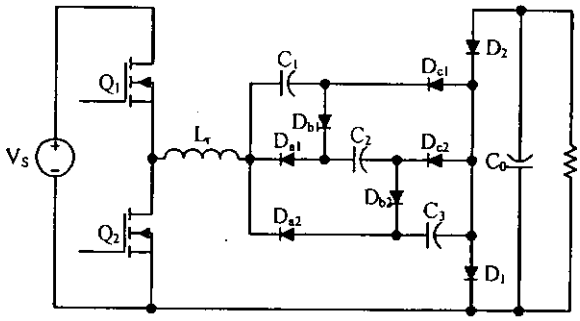

(c) –1/3-mode

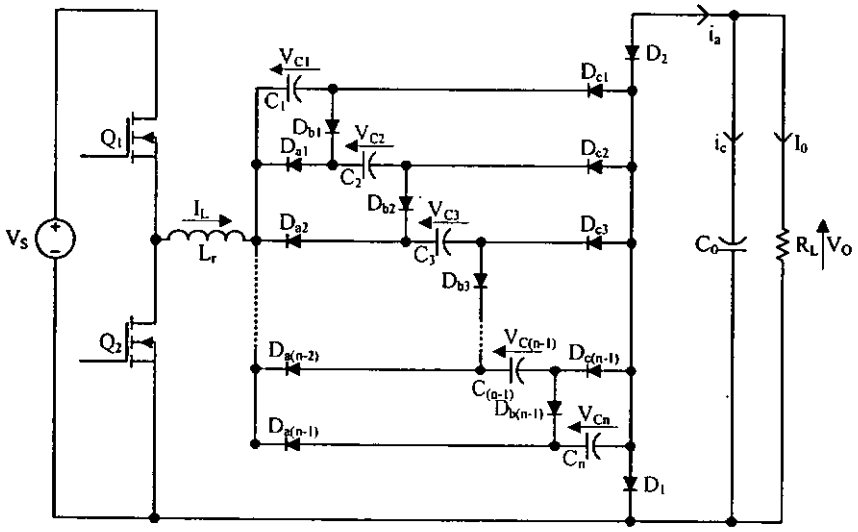

(d) –1/n-mode

Fig. 2.2 Circuit diagrams of inverting single-stage zero-current switching quasi-resonant step-down converters

Each capacitor in the switched-capacitor cells is for sharing the input voltage in series and releasing the energy in parallel with C_f to the load where the diodes are used for determining the direction of the current flow to charge the capacitors. Using this method, the converter can step down the input voltage fractionally. For a converter with 1/n voltage conversion ratio (1/n-mode converter), there are n-2 switched-capacitor cells.

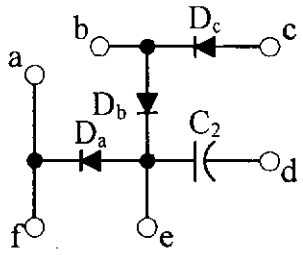

Fig. 2.3 Switched-capacitor cell

2.3. Principles of Operation

2.3.1. Non-inverting Mode Step-down Resonant Converters

The non-inverting 1/3-mode switched-capacitor resonant step-down converter is analysed. There are a total of 4 states of operation in each switching period. Fig. 2.4 shows the equivalent circuits of each state of operations of the non-inverting 1/3-mode step-down converter.

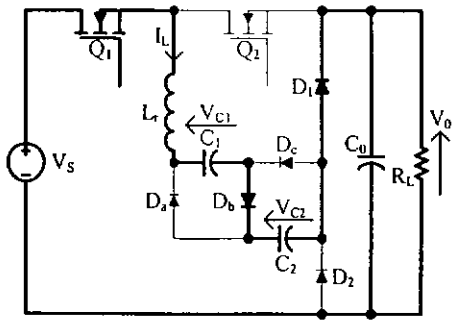

(a) State I

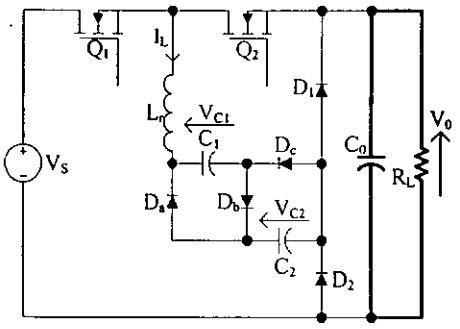

(b) State II

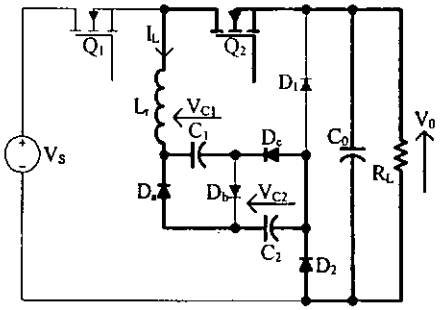

(c) State III

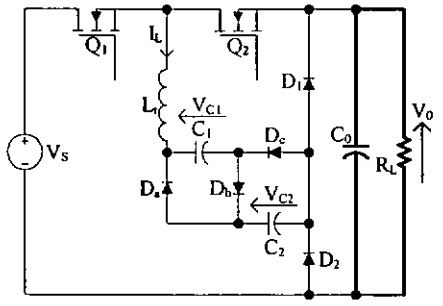

(d) State IV

Fig. 2.4 States of operation of non-inverting 1/3-mode switched-capacitor resonant step-down converter

Fig. 2.5 shows the simulation waveforms of the converter. The input voltage is 90V. The output power is 80W. The switching frequency is 200kHz. C_1 and C_2 are 0.22μF. L_r is 1μH. C_0 is 50μF. Assuming the output capacitor, C_0, is very large to maintain constant output voltage, the capacitance of C_1 is equal to that of C_2 (called C), and there is no power loss in the circuit, analysis of each state follows:

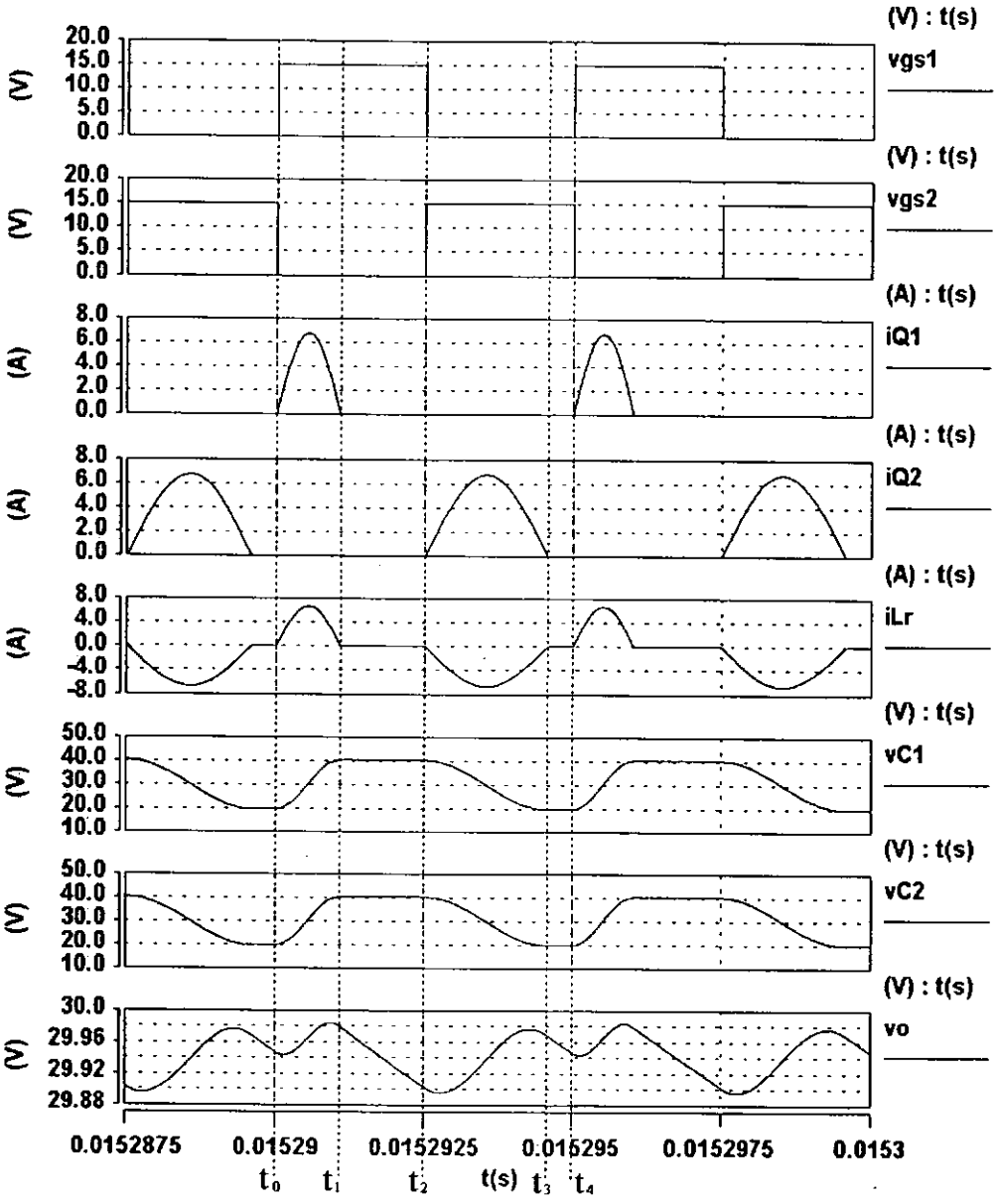

Fig. 2.5. Idealised simulation waveforms of the non-inverting 1/3-mode switched-capacitor resonant step-down converter

2.3.1.1. States of Operation of 1/3-mode Converter

(i) State I $[t_0 - t_1]$

At t_0, Q_1 is switched on while Q_2 is switched off. C_1 and C_2 are charged in series with D_b, D_1, L_r and the load. At this moment, C_1 and C_2 resonate with L_r in series. The charging current of the capacitors resonates from zero at t_0, to the peak, and then back to the zero at t_1, in a sinusoidal waveform. Q_1 is switched on under zero-current switching condition. The equations of this state are:

$$V_S = L_r \frac{di_L}{dt} + 2v_C + V_0 \tag{2.1}$$

$$i_L = C \frac{dv_C}{dt} \tag{2.2}$$

where V_S is the input voltage, V_0 is the output voltage, V_C is the resonant capacitor (C_1 or C_2) voltage, and i_L is the resonant inductor (L_r) current.

Let V_{C0} be the value of V_C at t_0, the solutions of the differential equations (2.1) and (2.2) are:

$$v_C = \frac{V_S - V_0}{2} - \left(\frac{V_S - V_0 - 2V_{C0}}{2} \right) \cos \omega_0 (t - t_0) \tag{2.3}$$

$$i_L = \left(\frac{V_S - V_0 - 2V_{C0}}{Z_0} \right) \sin \omega_0 (t - t_0) \tag{2.4}$$

The angular resonant frequency of this state is:

$$\omega_0 = \sqrt{\frac{2}{L_r C}} \tag{2.5}$$

The resonant impedance of this state is:

$$Z_0 = \sqrt{\frac{2L_r}{C}} \tag{2.6}$$

(ii) State II $[t_1 - t_2]$

Q_1 remains on and Q_2 is still off. At t_1, the inductor current reaches zero, and the diodes D_b and D_1 stop the resonance. Both the inductor current and the input current are equal to zero. C_0 is discharged to the load. Let V_{C1} be the voltage of C at t_1. The equations of this state are:

$$v_C = V_{C1} \tag{2.7}$$

$$i_L = 0 \tag{2.8}$$

(iii) State III $[t_2 - t_3]$

Q_1 is switched off and Q_2 is switched on at t_2. C_1 and C_2 are discharged in parallel to L_r and the load. D_a and D_c and D_2 are conducting. The two capacitors resonate with L_r in a sinusoidal manner, similar to State I. Q_1 is zero-current switched off while Q_2 is zero-current switched on at t_2. At t_3, the inductor current is resonated to zero. The equations of this state are:

$$v_C + L_r \frac{di_L}{dt} = V_0 \tag{2.9}$$

$$i_L = 2C \frac{dv_C}{dt} \tag{2.10}$$

The solutions of these two differential equations (2.9) and (2.10) are:

$$v_C = V_0 - (V_0 - V_{C2}) \cos \omega_1 (t - t_2) \tag{2.11}$$

$$i_L = \frac{V_0 - V_{C2}}{Z_1} \sin \omega_1 (t - t_2) \tag{2.12}$$

where V_{C2} is the voltage of C at t_2.

The angular resonant frequency of this state is:

$$\omega_1 = \sqrt{\frac{1}{2L_r C}} \tag{2.13}$$

The resonant impedance of this state is:

$$Z_1 = \sqrt{\frac{L_r}{2C}} \tag{2.14}$$

(iv) State IV [$t_3 - t_4$]

Similar to State II, the diodes stop the resonance at t_3. Inductor current is equal to zero and only C_0 is discharged to the load. Q_2 is switched off under zero-current switching condition at t_4. The equations of this state are:

$$v_C = V_{C3} \tag{2.15}$$

$$i_L = 0 \tag{2.16}$$

where V_{C3} is the voltage of C at t_3.

2.3.1.2. Generalised Equations of 1/3-mode converter

By using input and output power balancing,

$$V_S I_{in} = V_0 I_0 \tag{2.17}$$

the generalised equations of each state of 1/3-mode converter are:

(i) State I

$$V_S \int_0^{t_1} i_L dt = V_0 I_0 T_S \tag{2.18}$$

By solving equation (2.18), and assuming the voltage conversion ratio is 1/3, then,

$$v_C = V_0 - \frac{\pi I_0 T_S Z_0}{6T_0} \cos \omega_0 (t - t_0) \tag{2.19}$$

$$i_L = \frac{\pi I_0 T_S}{3T_0} \sin \omega_0 (t - t_0) \tag{2.20}$$

where T_S is the switching period, T_0 is the resonant period in State I, and I_0 is the output current.

(ii) State II

$$v_C = V_0 + \frac{\pi I_0 T_S Z_0}{6T_0} \tag{2.21}$$

$$i_L = 0 \tag{2.22}$$

(ii) State III

$$V_S \int_{t_2}^{t_3} i_L dt = V_0 (I_0 - I_{in}) T_S \tag{2.23}$$

By solving equation (2.23), it gives

$$v_C = V_0 + \frac{2\pi I_0 T_S Z_1}{3T_1} \cos \omega_1 (t - t_2) \tag{2.24}$$

$$i_L = -\frac{2\pi I_0 T_S}{3T_1}\sin\omega_1(t-t_2) \tag{2.25}$$

where T_1 is the resonant period of State III.

(iv) State IV

$$v_C = V_0 - \frac{2\pi I_0 T_S Z_1}{3T_1} \tag{2.26}$$

$$i_L = 0 \tag{2.27}$$

2.3.1.3. Generalised Equations of 1/n-mode Converter

Generalised equations of each state of 1/n-mode converter are:

(i) State I

$$v_C = V_0 - \frac{\pi I_0 T_S Z_0}{n(n-1)T_0}\cos\omega_0(t-t_0) \tag{2.28}$$

$$i_L = \frac{\pi I_0 T_S}{nT_0}\sin\omega_0(t-t_0) \tag{2.29}$$

where

$$\omega_0 = \sqrt{\frac{n-1}{L_r C}} \tag{2.30}$$

$$Z_0 = \sqrt{\frac{(n-1)L_r}{C}} \tag{2.31}$$

(ii) State II

$$v_C = V_0 + \frac{\pi I_0 T_S Z_0}{n(n-1)T_0} \tag{2.32}$$

$$i_L = 0 \tag{2.33}$$

(iii) State III

$$v_C = V_0 + \frac{(n-1)\pi I_0 T_S Z_1}{nT_1} \cos \omega_1 (t - t_2) \tag{2.34}$$

$$i_L = -\frac{(n-1)\pi I_0 T_S}{nT_1} \sin \omega_1 (t - t_2) \tag{2.35}$$

where

$$\omega_1 = \sqrt{\frac{1}{(n-1)L_r C}} \tag{2.36}$$

$$Z_1 = \sqrt{\frac{L_r}{(n-1)C}} \tag{2.37}$$

(iv) State IV

$$v_C = V_0 - \frac{(n-1)\pi I_0 T_S Z_1}{nT_1} \tag{2.38}$$

$$i_L = 0 \tag{2.39}$$

2.3.2. Inverting Mode Step-down Resonant Converters

Each state of the operation of the inverting -1/2-mode step-down converter is analysed. Fig. 2.6 shows the equivalent circuits of each state of operation of the converter.

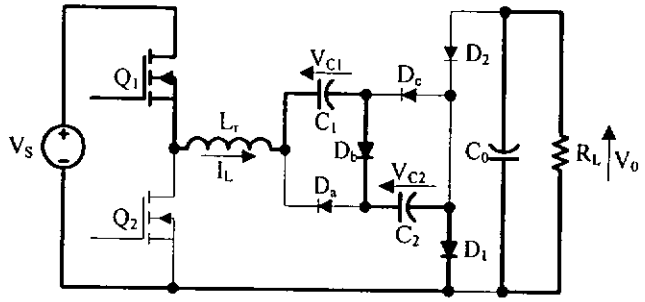

(a) State I

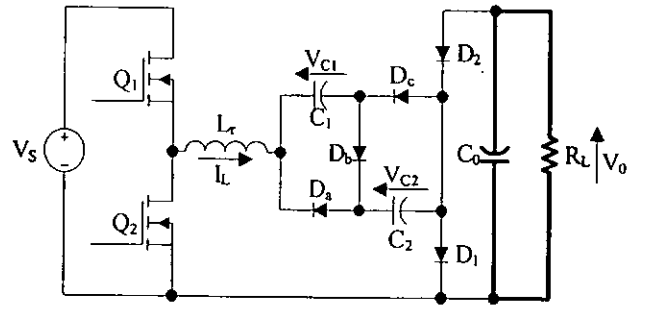

(b) State II

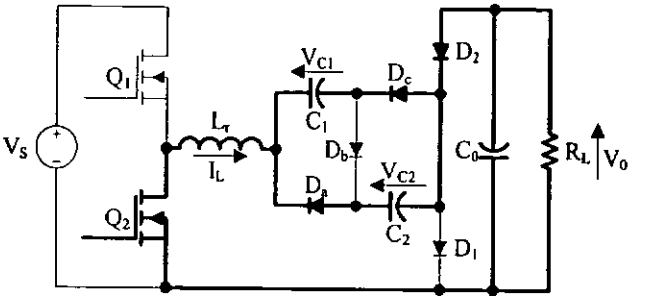

(c) State III

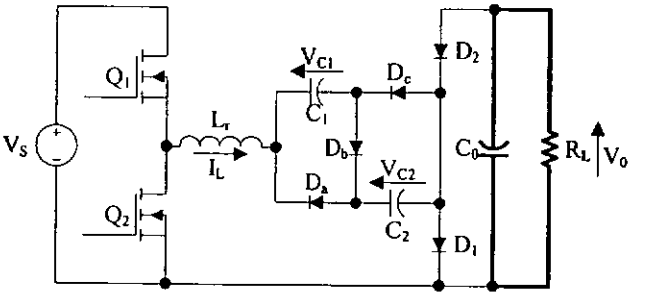

(d) State IV

Fig. 2.6 States of operation of inverting -1/2-mode switched-capacitor resonant step-down converter

Fig. 2.7 shows the simulation waveforms of the converter. The input voltage is 90V. The output power is 80W. The switching frequency is 200kHz. C_1 and C_2 are 0.22μF. C_0 is 50μF. L_r is 1μH. Assuming the converter has no power loss and its output filtering capacitor, C_0, is very large to maintain a constant output voltage, equations of the converter are given below:

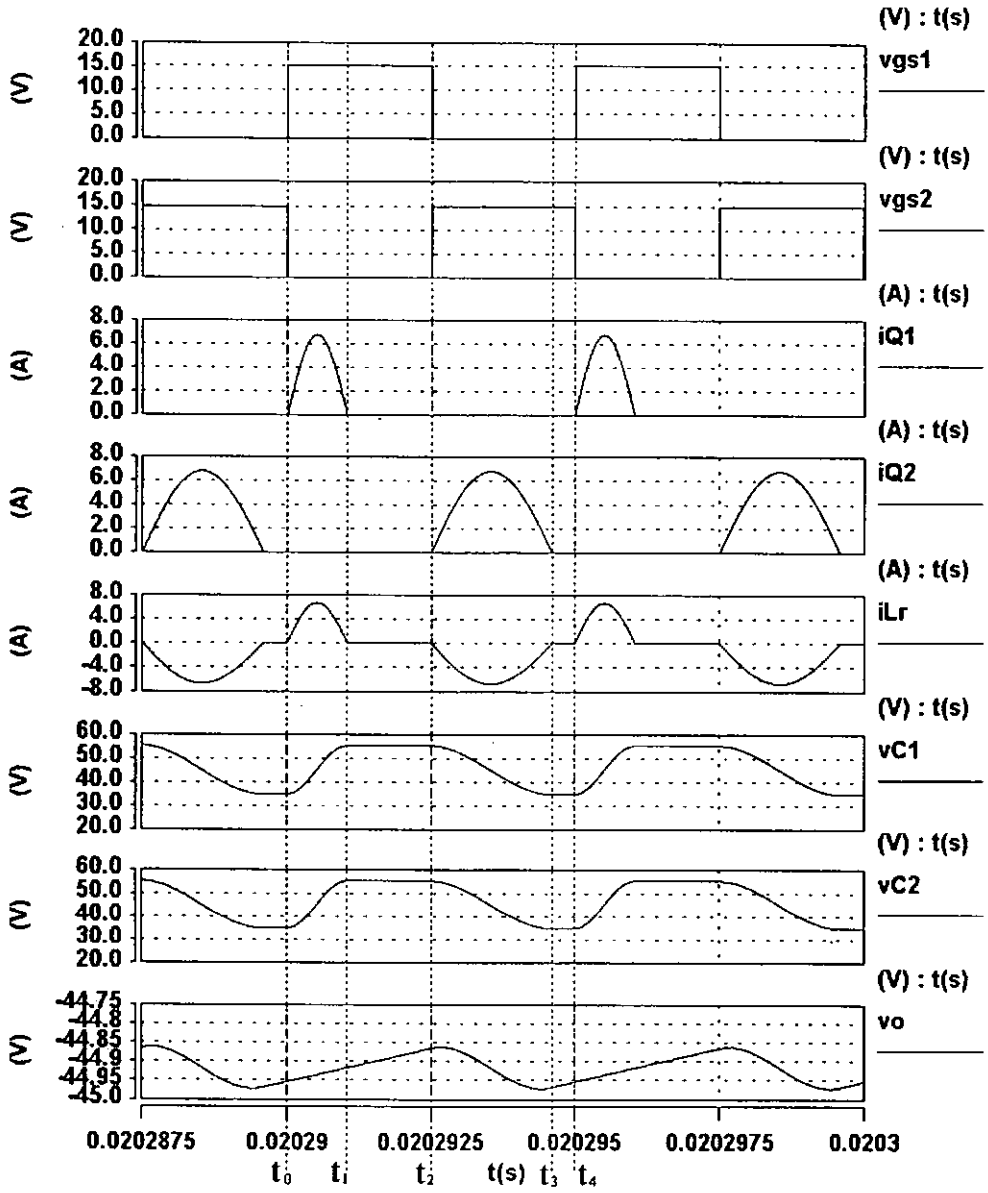

Fig. 2.7 Idealised simulation waveforms of the inverting -1/2-mode switched-capacitor resonant step-down converter

2.3.2.1. States of Operation of -1/2-mode Converter

(i) State 1 $[t_0 - t_1]$

Q_1 is switched on and Q_2 is switched off. Current passing through L_r, D_b and D_1 from the source is charging the capacitors C_1 and C_2 in series. The output capacitor C_0 is discharged to the load. Inductor current i_L starts resonating with C_1 and C_2 in a sinusoidal manner. Zero-current switching-on of Q_1 is achieved. The resonant inductor current decreases from zero at t_0, to the negative peak, and then increases from the peak to zero. It reaches zero again at t_1. The equations of this state are:

$$V_S = L_r \frac{di_L}{dt} + 2v_C \tag{2.40}$$

$$i_L = C \frac{dv_C}{dt} \tag{2.41}$$

By solving the differential equations (2.40) and (2.41),

$$v_C = \frac{V_S}{2} - \frac{V_S - 2V_{C0}}{2} \cos \omega_0 (t - t_0) \tag{2.42}$$

$$i_L = \frac{V_S - 2V_{C0}}{Z_0} \sin \omega_0 (t - t_0) \tag{2.43}$$

where V_{C2} is the voltage of C at t_2.

The angular resonant frequency of this state is:

$$\omega_0 = \sqrt{\frac{2}{L_r C}} \tag{2.44}$$

The resonant impedance of this state is:

$$Z_0 = \sqrt{\frac{2L_r}{C}} \tag{2.45}$$

(ii) State II [$t_1 - t_2$]

Q_1 is on and Q_2 is off. At t_1, the inductor current reaches zero. The resonance is stopped by the reverse bias of the diodes. The current is maintained at zero. C_0 is still discharging to the load in this state. The equations of this state are:

$$v_C = V_{C1} \tag{2.46}$$

$$i_L = 0 \tag{2.47}$$

(iii) State III [$t_2 - t_3$]

Q_1 is switched off and Q_2 is switched on. The inductor current is zero at t_2 when Q_1 is switched off. Q_1 is switched off under zero-current condition. At t_2, C_1 and C_2 are discharged to the load through L_r, D_a, D_b and D_2. The current starts resonating at t_2 in a sinusoidal manner which is similar to state I and hence, Q_2 is switched on under zero-current switching condition. The inductor current i_L starts decreasing from zero at t_2 to the peak and then increases to zero at t_3. The equations of this state are:

$$v_C + L_r \frac{di_L}{dt} + V_0 = 0 \tag{2.48}$$

$$i_L = 2C \frac{dv_C}{dt} \tag{2.49}$$

The solution of these two differential equations (2.48) and (2.49) are:

$$v_C = -V_0 + (V_0 + V_{C2})\cos\omega_1(t - t_2) \tag{2.50}$$

$$i_L = -\frac{V_0 + V_{C2}}{Z_1}\sin\omega_1(t - t_2) \tag{2.51}$$

where V_{C2} is the voltage of C at t_2.

The angular resonant frequency and the resonant impedance of this state are:

$$\omega_1 = \sqrt{\frac{1}{2L_rC}} \tag{2.52}$$

$$Z_1 = \sqrt{\frac{L_r}{2C}} \tag{2.53}$$

(iv) State IV $[t_3 - t_4]$

Q_1 is off and Q_2 is on. Similar to state II, the resonance of the inductor current is stopped by the reverse bias of the diodes. The inductor current is zero in this state. The output capacitor C_0 is discharged to the load. Q_2 is zero-current switched off at t_4. The equations of this state are:

$$v_C = V_{C3} \tag{2.54}$$

$$i_L = 0 \tag{2.55}$$

2.3.2.2. Generalised Equations of –1/2-mode converter

By using input and output power balancing as equation (2.56),

$$V_S \int_0^t i_L dt = V_0 I_0 T_S \tag{2.56}$$

the generalised equations of –1/2-mode converter are:

(i) State I

Assuming the voltage conversion ratio is –1/2, then,

$$v_C = -V_0 + \frac{\pi I_0 T_S Z_0}{4T_0} \cos \omega_0 (t - t_0) \tag{2.57}$$

$$i_L = -\frac{\pi I_0 T_S}{2T_0} \sin \omega_0 (t - t_0) \tag{2.58}$$

where T_S is the switching period, T_0 is the resonant period in State I, and I_0 is the output current.

(ii) State II

$$v_C = -V_0 - \frac{\pi I_0 T_S Z_0}{4T_0} \tag{2.59}$$

$$i_L = 0 \tag{2.60}$$

(iii) State III

$$\int_{t_2}^{t_3} i_L dt = I_0 T_S \tag{2.61}$$

By solving equation (2.61),

$$v_C = -V_0 - \frac{\pi I_0 T_S Z_1}{T_1} \cos \omega_1 (t - t_2) \tag{2.62}$$

$$i_L = \frac{\pi I_0 T_S}{T_1} \sin \omega_1 (t - t_2) \tag{2.63}$$

where T_1 is the resonant period of State III.

(iv) State IV

$$v_C = -V_0 + \frac{\pi I_0 T_S Z_1}{T_1} \tag{2.64}$$

$$i_L = 0 \tag{2.65}$$

2.3.2.3. Generalised Equations of -1/n-mode converter

For a -1/n-mode converter, the generalised equations are:

(i) State I

$$v_C = -V_0 + \frac{\pi I_0 T_S Z_0}{n^2 T_0} cos\, \omega_0 (t - t_0) \tag{2.66}$$

$$i_L = -\frac{\pi I_0 T_S}{n T_0} \sin \omega_0 (t - t_0) \tag{2.67}$$

where

$$\omega_0 = \sqrt{\frac{n}{L_r C}} \tag{2.68}$$

$$Z_0 = \sqrt{\frac{n L_r}{C}} \tag{2.69}$$

(ii) State II

$$v_C = -V_0 - \frac{\pi I_0 T_S Z_0}{n^2 T_0} \tag{2.70}$$

$$i_L = 0 \tag{2.71}$$

(iii) State III

$$v_C = -V_0 - \frac{\pi I_0 T_S Z_1}{T_1} \cos \omega_1 (t - t_2) \tag{2.72}$$

$$i_L = \frac{\pi I_0 T_S}{T_1} \sin \omega_1 (t - t_2) \tag{2.73}$$

where

$$\omega_1 = \sqrt{\frac{1}{nL_r C}} \tag{2.74}$$

$$Z_1 = \sqrt{\frac{L_r}{nC}} \tag{2.75}$$

(iv) State IV

$$v_C = -V_0 + \frac{\pi I_0 T_S Z_1}{T_1} \tag{2.76}$$

$$i_L = 0 \tag{2.77}$$

2.4. Design Method

2.4.1. Conditions of Zero-current Switching.

For obtaining zero-current switching, inductor current, i_L, needs to be able to resonate to zero in all resonant operation states, i.e., state I and state III, for both inverting and non-inverting circuits. Because of the different combinations of switched-capacitor in the resonant states, different resonant operation states have different angular resonant frequency.

Let d_1 and d_2 be duty ratios of gate signals of the transistors, Q_1 and Q_2,

respectively, and assuming the circuits are lossless, conditions of zero-current switching for both non-inverting and inverting circuits are:

$$d_1 T_S > \frac{\pi}{\omega_0} \tag{2.78}$$

$$d_2 T_S > \frac{\pi}{\omega_1} \tag{2.79}$$

2.4.2. Voltage Ratings of Components

2.4.2.1. Non-inverting Circuits

Table 2.1. Voltage Ratings of Components of 1/n-mode Non-inverting Converter

Components	Minimum Voltage Rating
Q_1 and Q_2	$\frac{V_S(n-1)}{n}$
$C_1 - C_{n-1}$	V_{cmax}
C_0	V_S/n
D_1 and D_2	V_S/n
D_{am}	mV_{cmax}
D_{bm}	V_{cmax}
D_{cm}	$(n-1-m)V_{cmax}$

Assuming all switched capacitors are ideal with the same value, from equation (2.28), maximum voltage of each switched-capacitor, V_{cmax}, is:

$$V_{c\max} = \frac{V_S}{n} + \frac{\pi I_0 T_S Z_0}{n(n-1)} \tag{2.80}$$

Considering 1/n-mode circuit, and m and n are integers such that $1 \leq m \leq n-2$, minimum voltage ratings of each component in the circuit are shown in Table 2.1.

2.4.2.2. Inverting Circuits

Assuming all switched-capacitors are ideal and their values are the same, maximum voltage of each switched-capacitor, V_{cmax}, is:

$$V_{c\max} = \frac{V_S}{n} - \frac{\pi I_0 T_S Z_0}{n^2 T_0} \tag{2.81}$$

It should be noted that the average output current of the converter, I_0, is negative.

Table 2.2. Voltage Ratings of Components of -1/n-mode Inverting Converter

Components	Minimum Voltage Rating
Q_1 and Q_2	V_S
$C_1 - C_{n-1}$	V_{cmax}
C_0	V_S/n
D_1 and D_2	V_S/n
D_{am}	mV_{cmax}
D_{bm}	V_{cmax}
D_{cm}	$(n-m)V_{cmax}$

Considering -1/n-mode circuit, and m and n are integers such that $1 \leq m \leq n-1$, minimum voltage ratings of each component in the circuit are shown in Table 2.2.

2.4.3. Current Ratings of Components

2.4.3.1. Non-inverting Circuits

Considering the routines of input current and output current, current rating of the circuit can be found. Current ratings of each components of 1/n-mode non-inverting circuit are shown in Table 2.3. I_0 is the average output current in each switching period.

Table 2.3 Current Ratings of Components of 1/n-mode Non-inverting Converter

Components	Minimum Current Rating
Q_1	I_0/n
Q_2	$I_0(n-1)/n$
L_r	$I_0(n+1)/n$
D_1	I_0/n
D_2	$I_0(n-1)/n$
D_a and D_c	$I_0/(n-1)$
D_b	I_0/n

2.4.3.2. Inverting Circuits

Current ratings of each components of -1/n-mode inverting circuit are shown in Table 2.4.

Table 2.4 Current Ratings of Components of -1/n-mode Inverting Converter

Components	Minimum Current Rating
Q_1	I_0/n
Q_2	I_0
L_r	$I_0(n+1)/n$
D_1	I_0/n
D_2	I_0
D_a, D_b and D_c	I_0/n

2.4.4. Selection of Resonant Components

2.4.4.1. Non-inverting Circuits

Considering equations (2.28) and (2.38), relationship between voltage ripples of switched capacitors and resonant impedances of Z_0 and Z_1 of 1/n-mode non-inverting converter can be derived, respectively. Let ΔV_c be voltage ripple of each switched-capacitor, referring to equation (2.28), gives:

$$Z_0 = \frac{n(n-1)f_S \Delta V_C}{2\pi I_0 f_0} \tag{2.82}$$

where f_S is switching frequency and f_0 is resonant frequency in State I.

To ensure the circuit operates in zero-current switching condition, f_0 should be higher than f_S. Substituting the value of required voltage ripple of switched capacitors and the ratio of f_S and f_0 to equation (2.82), Z_0 can be found.

Referring to the equations (2.30) and (2.31), values of resonant inductance and switched-capacitors can be found by the equations:

$$L_r = \frac{Z_0}{2\pi f_0} \tag{2.83}$$

$$C = \frac{n-1}{2\pi f_0 Z_0} \tag{2.84}$$

2.4.4.2. Inverting Circuits

Considering equation (2.66), and let ΔV_c be the voltage ripple of each switched-capacitor, the relationship between ΔV_c and resonant impedance is:

$$Z_0 = \frac{n^2 f_S \Delta V_C}{2\pi I_0 f_0} \tag{2.85}$$

Referring to the equations (2.68) and (2.69), values of the resonant inductance and the switched-capacitors can be found by the equations:

$$L_r = \frac{Z_0}{2\pi f_0} \tag{2.86}$$

$$C = \frac{n}{2\pi f_0 Z_0} \tag{2.87}$$

2.4.5. Calculation of Output Voltage Ripple

2.4.5.1. Non-inverting Circuits

According to Fig. 2.1(d), i_a is equal to the sum of the absolute values of i_L. For 1/n-mode non-inverting circuit, from equations (2.29), (2.33), (2.35) and (2.39), it gives:

$$i_a = \begin{cases} \dfrac{\pi I_0 T_S}{nT_0} \sin \omega_0 (t - t_0) & t_0 \le t \le t_1 \\ 0 & t_1 \le t \le t_2 \\ \dfrac{(n-1)\pi I_0 T_S}{nT_1} \sin \omega_1 (t - t_2) & t_2 \le t \le t_3 \\ 0 & t_2 \le t \le t_4 \end{cases} \tag{2.88}$$

and:

$$i_c = i_a - I_0 \tag{2.89}$$

Assuming output filtering capacitor, C_0, is very large and output current, I_0, is constant, by using the equation,

$$i_c = C_0 \frac{dV_0}{dt} \tag{2.90}$$

output voltage ripple of 1/n non-inverting circuit, ΔV_0, is approximately equal to:

$$\Delta V_0 \approx \frac{I_0}{2C_0} \left[\frac{(n+2)(1+\cos\theta)}{nf_S} + \frac{2}{f_0} \left(\frac{\theta}{\pi} - 1 \right) - \frac{f_1 - f_S}{f_1 f_S} \right] \tag{2.91}$$

where

$$\theta = \sin^{-1} \frac{nT_0}{\pi T_S} \tag{2.92}$$

2.4.5.2. Inverting Circuits

Referring to Fig. 2.2(d), equations (2.67), (2.71), (2.73), and (2.77), gives:

$$i_a = \begin{cases} -\dfrac{\pi I_0 T_S}{n T_0} \sin\omega_0(t-t_0) & t_0 \le t \le t_1 \\ 0 & t_1 \le t \le t_2 \\ \dfrac{\pi I_0 T_S}{T_1} \sin\omega_1(t-t_3) & t_2 \le t \le t_3 \\ 0 & t_2 \le t \le t_4 \end{cases} \tag{2.93}$$

Considering equations (2.89), (2.90) and (2.93), and assuming output current of the circuit, I_0, is constant, output voltage ripple of –1/n inverting circuit, ΔV_0, is approximately equal to:

$$\Delta V_0 \approx \frac{-I_0}{C_0}\left[\frac{\cos\theta}{f_S} + \frac{1}{f_1}\left(\frac{\theta}{\pi} - \frac{1}{2}\right)\right] \tag{2.94}$$

where

$$\theta = \sin^{-1}\frac{T_1}{\pi T_S} \tag{2.95}$$

2.5. Experimental Results

Non-inverting 1/3-mode Step-down resonant converter as shown in Fig. 2.8 has been tested. The circuit is very similar to that shown in Fig. 2.1(b) except that a filtering capacitor C_{in} was added to eliminate effects from the inductance of the conduction line between the power source and the input of the converter. For output voltage ripple less than 2%, specification of prototype of the circuit is shown in Table 2.5.

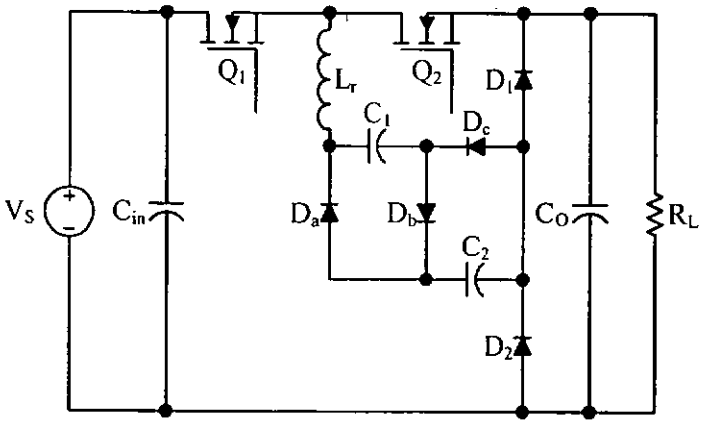

Fig. 2.8. Prototype of 1/3-mode non-inverting step-down resonant converter

Table 2.5 Specification of Prototype of 1/3-mode Non-inverting Converter

Descriptions	Model Numbers	Values	Units
Input Voltage		90	V
Expected Output Voltage		30	V
Switching Frequency		200	kHz
Output Power		10-80	W
Q_1 and Q_2	IRF630		
D_1, D_2, D_a, D_b and D_c	MBR10100		
D_1 and D_2	MBR10100		
C_1, C_2		0.22	μF
C_0		50	μF
L_r		1	μH

Since the main power flows through both C_{r1} and C_{r2} in the resonant state, the equivalent series resistance of these capacitors should be very low. High ESR may lead to high power loss and high temperature of the capacitors which may exceed the rated temperature of the capacitors. For this reason, polyester capacitors were chosen for these switched-capacitors.

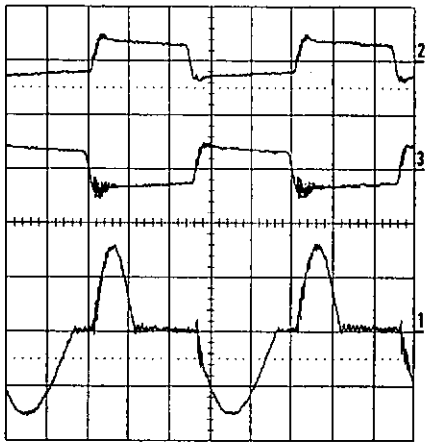

2: gate signal of Q_1, 40V/div; 3: gate signal of Q_2, 40V/div; 1: I_L, 5A/div

(a)

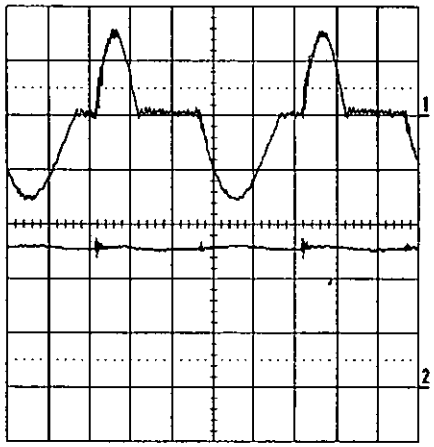

1: I_L, 5A/div; 3: output voltage, 10V/div

(b)

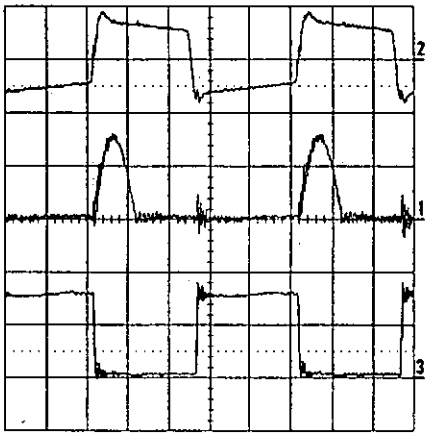

2: Gate signal of Q_1, 20V/div; 1: Q_1 current, 5A/div; 3: Vds of Q_1, 40V/div

(c)

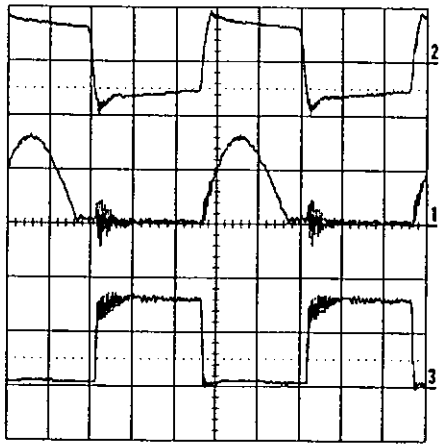

1: gate signal of Q_2, 20V/div; 2: Q_2 current, 5A/div; 3: Vds of Q_2, 40V/div

(d)

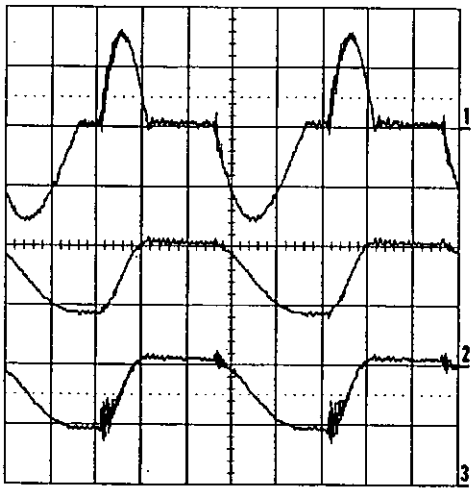

1: I_L, 5A/div; 2: V_{C1}, 20V/div; 3: V_{C2}, 20V/div

(e)

Time base = 1μs/div for (a) to (e)

Fig. 2.9 Measured waveforms of the non-inverting 1/3-mode switched-capacitor resonant step-down converter

Measured waveforms of the converter operating with 80W output power are shown in Fig. 2.9. Fig. 2.9(a) shows the resonant inductor current. Fig. 2.9(c) and Fig. 2.9(d) shows the currents and drain to source voltages of the transistors. By comparing Fig. 2.9(c) and Fig. 2.9 (d), it can be observed that

the resonant inductor current consists of the transistors Q_1 and Q_2 currents.

Output voltage of the converter is shown in Fig. 2.9(b). The measured output voltage of the converter was 25.84V when the output power is 80W. The measured output voltage is lower than the expected output voltage (30V) and the practical simulated output voltage because of the drain to source resistance of the transistors and the voltage drop of the diodes in forward bias. The resistance of wires and inductors, and the equivalent series resistance (ESR) of all capacitors cause an output voltage drop and power loss in the circuit. To minimise the influence of the ESR of the capacitors, polypropylene capacitors, which have low ESR, are used as the switched capacitors.

Fig. 2.9(c) and Fig. 2.9(d) show that the transistor currents resonate in a sinusoidal manner. The resonance stops when the current reaches zero while the drain to source voltage of the corresponding transistors is zero. The transistors are switched off when the currents are equal to zero so that zero-current switching condition is obtained. This is very similar to the simulated waveforms. Fig. 2.9(e) shows that the resonant inductor current and the voltages of switched capacitors resonate together. The voltage waveform of C_1 is almost the same as that of C_2. The amplitude of voltage of switched-capacitor is lower than those in simulation waveforms because of the voltage drop of the transistors, diodes and the wires.

Diagrams of v-i trajectory of each transistor of the circuit are shown in Fig. 2.10. Both Fig. 2.10(a) and Fig. 2.10(b) again confirm that both transistors are

in zero-current switching condition.

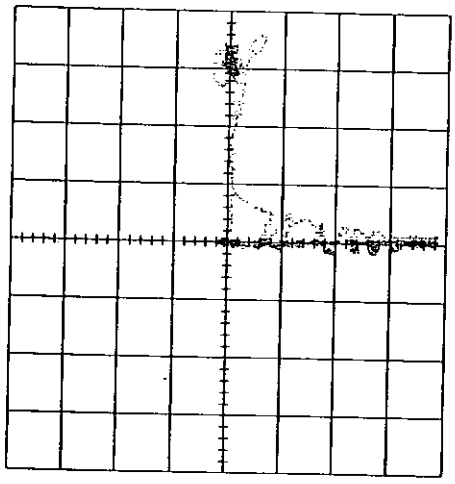

X-axis: Q_1 current, 2A/div; Y-axis: V_{ds} of Q_1, 20V/div

(a) v-i trajectory of Q_1

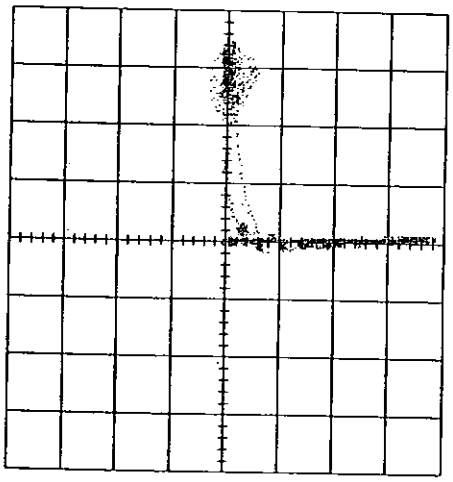

X-axis: Q_2 current, 2A/div; Y-axis: V_{ds} of Q_2, 20V/div

(b) v-i trajectory of Q_2

Fig. 2.10 v-i trajectory of the non-inverting 1/3-mode switched-capacitor resonant step-down converter

Fig. 2.11 shows the graph of the relationship between efficiency and output power of the converter. By testing the circuit with the output power between

10W to 80W, the efficiency varied between 85.5% at both 10W and 80W output power to 93.2% at 22W output power. Fig. 2.12 shows the graph of voltage conversion ratio against output power of the converter. The voltage conversion ratio varies between 0.325 at 10W output power to 0.287 at 80W output power. Fig. 2.11 shows that the efficiency was highest when the output power was 22W. At light load, power loss of the circuit is mainly due to the diodes, which have voltage drop in forward bias. At heavy load, the power loss is mainly due to drain-to-source resistance (R_{ds}) of the transistors. Besides, power loss occurs in the manner of switching loss of the transistors, and conduction losses of the conductor, inductor and the equivalent series resistance (ESR) of the capacitors. On the other hand, Fig. 2.12 shows that the voltage conversion ratio decreases when the output power increases. Other than the voltage drop on the diodes, when the current increases, the voltage drop on both transistors increases, and, voltage conversion ratio decreases.

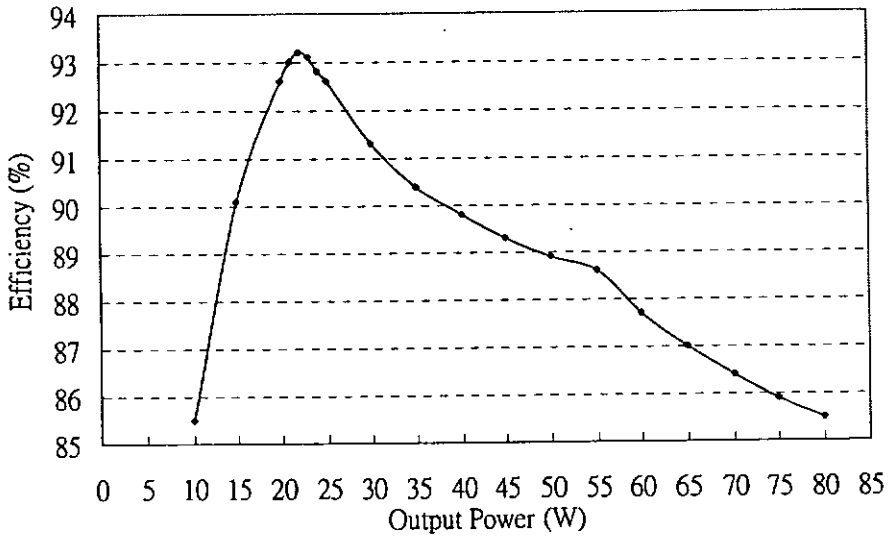

Fig. 2.11. Measured efficiency and output power of the non-inverting 1/3-mode switched-capacitor resonant step-down converter

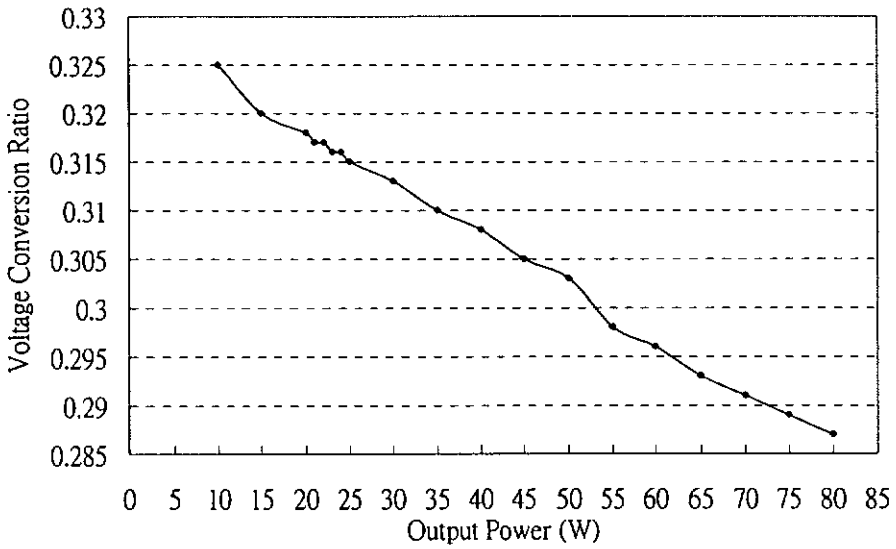

Fig. 2.12. Measured voltage conversion Ratio and output power of the non- inverting 1/3-mode switched-capacitor resonant step-down converter

2.6. Discussion

The structure of the resonant switched-capacitor converters is simple. The efficiency of the converters is high which is evident in the experiment. The high efficiency is obtained by the technique of quasi-resonant zero-current switching technique. The switched-capacitors in the circuit have to be charged and discharged in fixed periods, half resonant period for zero-current switching. Unlike the traditional switched-capacitor converters, the charging and discharging periods of the switched-capacitors are fixed. The output voltage cannot be regulated or controlled by controlling the charging and discharging periods.

The zero-current switching technique can much reduce the switching loss of the transistors. Switching loss still occurs in the drain-to-source junction

capacitors of the transistors. The switching loss is directly proportional to the switching frequency. For higher fraction conversion ratio of the resonant switched-capacitor converters, more diodes are needed for routing the charging and discharging current. Efficiency of the converters will be lower because of forward voltage of the diodes.

2.7. Summary

Two families of switched-capacitor circuits are introduced in this chapter. One is non-inverting converter and the other is inverting converter. All circuits in both families operate under zero-current switching. The inherent disadvantage of high current stress has been eliminated. The number of transistors needed is low. Complete analysis of the converters has also been presented. Each circuit in the families has a number of fractional output voltage conversion converters. Generalised equations of each family of circuits have been provided. Obtaining zero-current switching condition for all transistors has been confirmed by the computer simulation and the experiments.

Chapter 3. Multi-stage Zero-current Switching Quasi-resonant Switched-capacitor Step-up Converters

3.1. Introduction

Chapter 2 has introduced two families of switched-capacitor dc-dc converters based on zero-current switching quasi-resonant topology. It is noticed that the circuits are single-stage circuits. They are not designed to provide more than one voltage output or step up voltage.

A family of multi-stage zero-current switching quasi-resonant switched-capacitor step-up converters is introduced in this chapter [C9]. Similar to the circuits introduced in the previous chapter, there are only two transistors in each circuit. All transistors in the circuits are switched both on and off in zero-current switching condition. There is no large magnetic component. Each circuit has only one very small resonant inductor for resonating with switched-capacitors. Current stress of the components is low. The circuits are suitable for both low power and high power applications. Other than the basic circuit [C5] and [C8], all circuits in this family provide more than one voltage outputs with common ground without the need for additional transistors.

3.2. Family of Circuits

Fig. 3.1 shows the circuit diagrams of the converters in this family. The circuits were designed based on the basic circuit of the single-stage zero-current switching quasi-resonant switched-capacitor step-up converters. Circuit diagrams of the basic circuit are shown in Fig. 3.1(a).

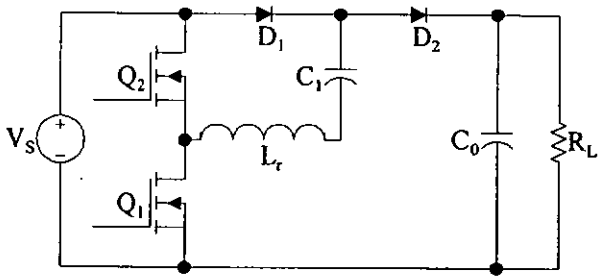

(a) Basic circuit of non-inverting resonant step-up converter

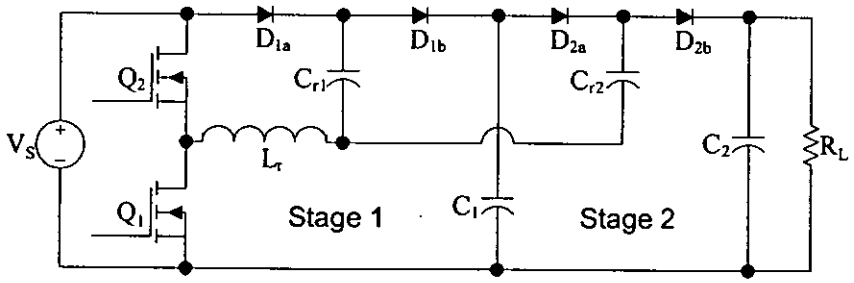

(b) 3-mode step-up converter

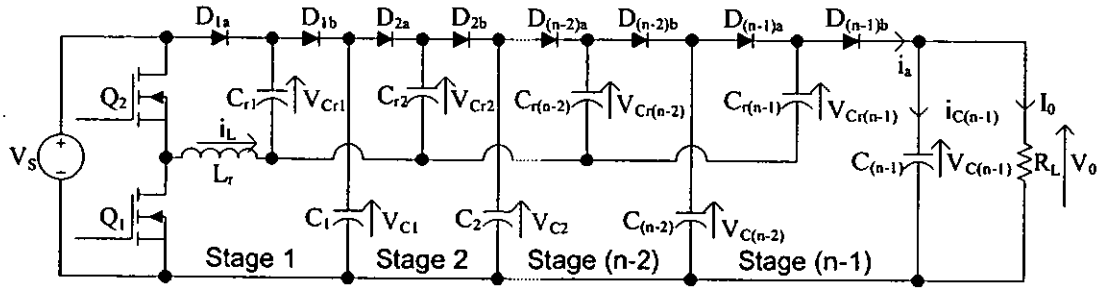

(c) n-mode step-up converter

Fig. 3.1 Circuit diagrams of family of zero-current switching quasi-resonant switched-capacitor step-up converters

A switched-capacitor cell shown in Fig 3.2 has been designed for this family of circuits. By adding the switched-capacitor cells into the basic circuit, output voltage can be multiplied and stepped up. Fig. 3.1 (b) and (c) show the circuit with 3 times step-up voltage and n times step-up voltage, respectively. As seen in Fig. 3.1 (c), n-time output voltage, V_0, is stepped up stage by stage. Output of each stage, V_{C1}, V_{C2}, to $V_{C(n-2)}$, can be considered as individual voltage outputs. These outputs provide voltage from $2V_S$ to nV_S. Other than the basic circuit, all circuits in this family provide more than one voltage outputs.

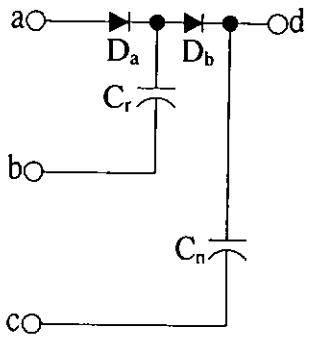

Fig. 3.2 Switched-capacitor cell for multi-stage zero-current switching quasi-resonant switched-capacitor step-up converters

Referring to Fig. 3.2, one switched-capacitor cell consists of two diodes, D_a and D_b, one switched-capacitor, C_r, and one filtering capacitor, C_n. The switched-capacitor is for storing energy from the voltage source or the previous stage of the circuit and release energy to the next stage of the circuit or the voltage output. It can also be considered as a resonant capacitor as it can resonate with the resonant inductor to provide zero-current switching condition for all transistors. As a result, each stage of the circuit has one resonant condition with the same resonant inductor. The filtering capacitor is for

storing energy from its own stage of circuit and filtering high frequency components of the voltage to provide smooth DC voltage for the next stage. It can also be considered as a filtering capacitor of voltage output. In the circuits of the family, each individual voltage output is across each filtering capacitor. Referring to Fig. 3.1 and Fig. 3.2, Terminal a of the cell is connected to the positive side of the filtering capacitor of the previous stage. Terminal b is connected in series with the resonant inductor, L_r. Terminal c is connected the common rail of the circuit. Terminal d is connected to the positive side of the load or to another cell of the next stage.

3.3. Analysis of the Circuits

3.3.1. Principles of Operation of 3-mode Converter

Fig. 3.3 shows equivalent circuits of each state of operation of the 3-mode converter. There are a total of 4 states of operation in one switching period. Computer simulation of the 3-mode circuit has been done. The simulation results, shown in Fig. 3.4, are used for analyzing the circuit. Theoretically, Q_1 and Q_2 can be switched on and off alternatively up to 50% duty ratio. In practice, a dead time between turn on and off Q_1 and Q_2 is applied to avoid short circuit due to finite fall time and off time of the transistors. Operation of the circuit of each state is described in the followings:

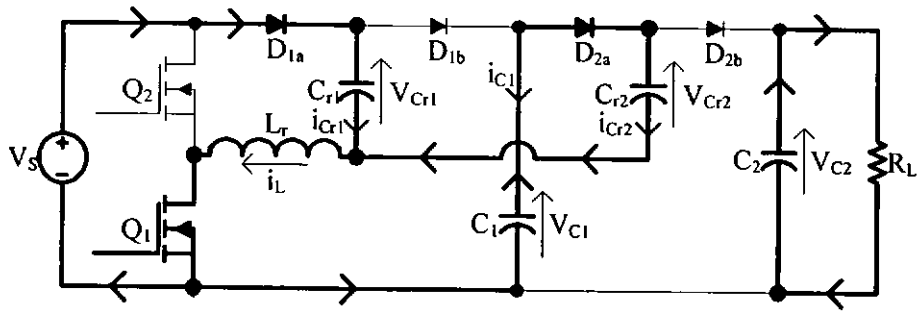

(a) State I

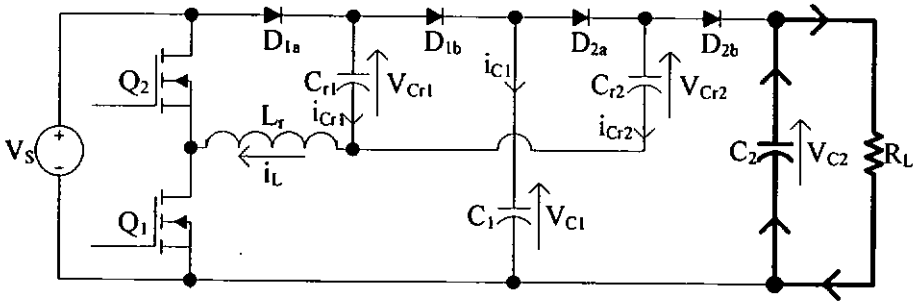

(b) State II

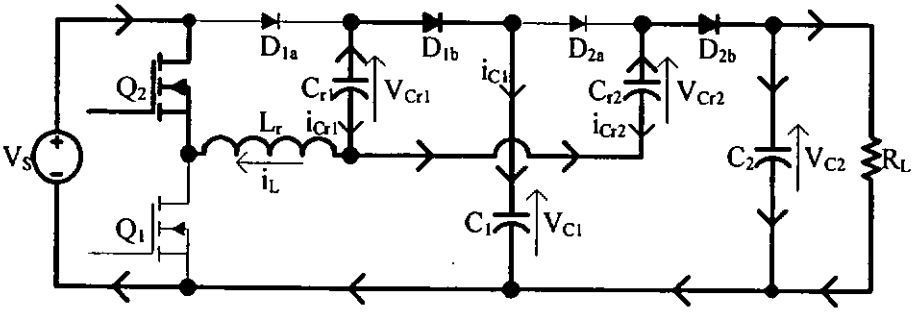

(c) State III

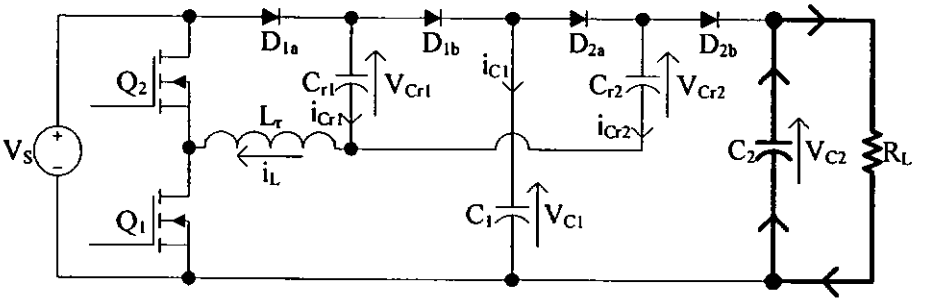

(d) State IV

Fig. 3.3 States of operation of non-inverting 3-mode switched-capacitor resonant step-up converter

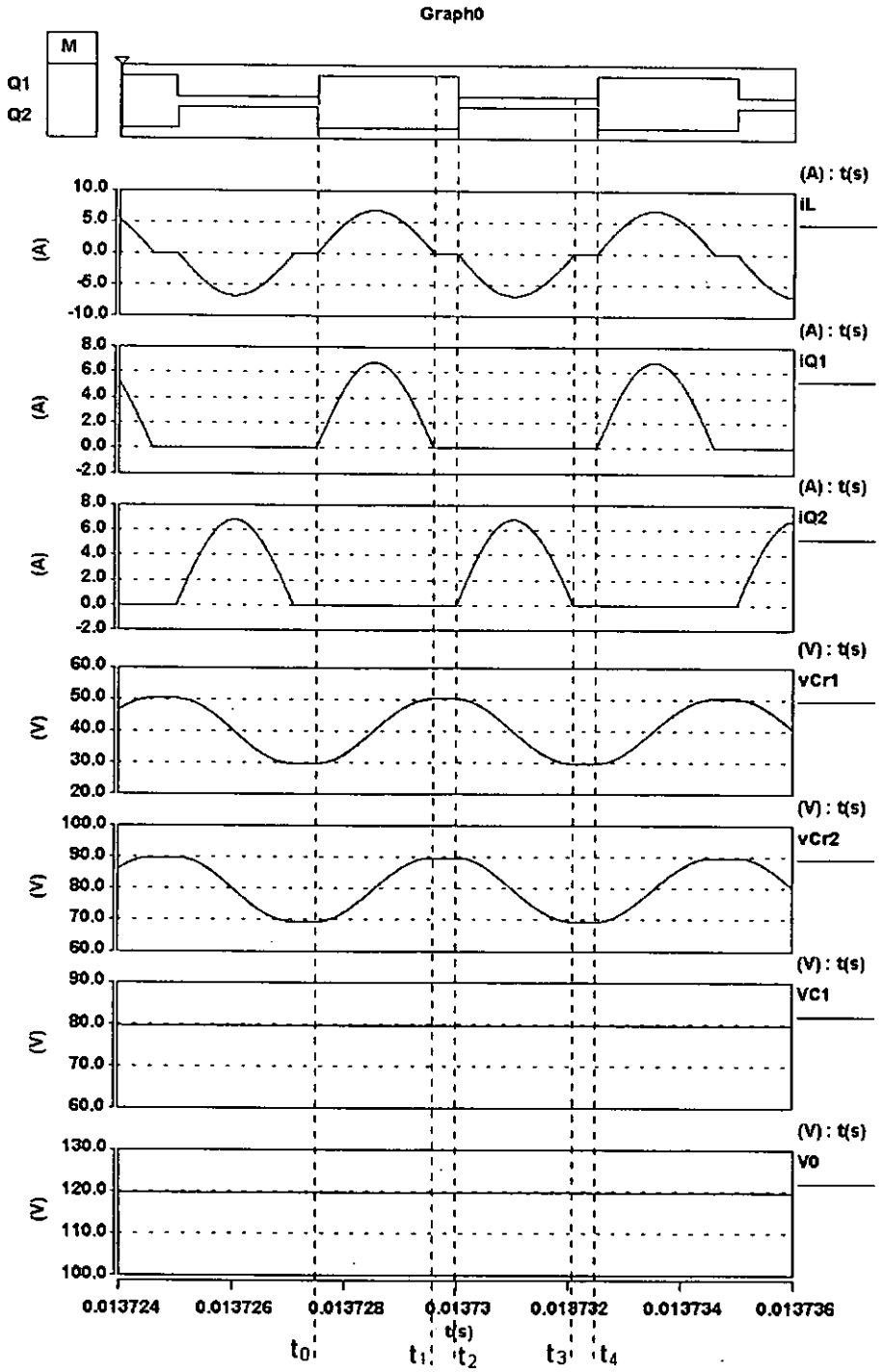

Fig. 3.4. Simulation results of 3-mode switched-capacitor resonant converter

3.3.1.1. State I

Q_1 is switched on at t_0 while Q_2 is off. In Stage 1 of the circuit, C_{r1} is charged from the voltage source, V_S, through D_{1a}, L_r, and Q_1 in a resonant manner. Meanwhile, in Stage 2 of the circuit, C_1 discharges to C_{r2} through D_{2a},

L_r and Q_1 in a resonant manner as well. In other words, Q_1 is zero-current switched on at t_0. There are 2 individual resonance produced by C_{r1} and L_r, and C_{r2} and L_r, respectively. When resonant current of C_{r1} resonates to zero at t_1, D_{1a} becomes reverse bias. The resonance stops at this moment. Similarly, in Stage 2, resonance stops when the resonant current of C_{r2} reaches zero. If C_{r1} is equal to C_{r2}, their resonance stops at the same moment because of their same resonant frequency. Average voltage across C_{r1} is equal to V_S and that of C_{r2} equal to the voltage across C_1, i.e., $2V_S$. C_2 discharges for the whole duration of this state to provide constant current to the load, R_L. Assuming capacitance of C_1 and C_2 is very large such that they can maintain their voltage as constants, the equations of this state are:

$$V_S = L_r \frac{di_{Cr1}}{dt} + v_{Cr1} \tag{3.1}$$

$$i_{Cr1} = C_{r1} \frac{dv_{Cr1}}{dt} \tag{3.2}$$

$$V_{C1} = L_r \frac{di_{Cr2}}{dt} + v_{Cr2} \tag{3.3}$$

$$i_{Cr2} = C_{r2} \frac{dv_{Cr2}}{dt} \tag{3.4}$$

where v_{Cr1} is the voltage of C_{r1}, v_{Cr2} is the voltage of C_{r2}, i_{Cr1} is the current of C_{r1}, i_{Cr2} is the current of C_{r2}, V_{C1} is the voltage of C_1.

Let V_{Cr10} and V_{Cr20} be the voltage of C_{r1} and C_{r2}, respectively, at t_0, and assume the capacitance of C_{r1} and C_{r2} is the identical and equal to C, the systems of differential equations (3.1) to (3.4) are solved as:

$$v_{Cr1} = V_S - (V_S - V_{Cr10})\cos\omega_0(t - t_0) \tag{3.5}$$

$$i_{Cr1} = \frac{V_S - V_{Cr10}}{Z_0} \sin \omega_0 (t - t_0) \tag{3.6}$$

$$v_{Cr2} = V_{C1} - (V_{C1} - V_{Cr20}) \cos \omega_0 (t - t_0) \tag{3.7}$$

$$i_{Cr2} = \frac{V_{C1} - V_{Cr20}}{Z_0} \sin \omega_0 (t - t_0) \tag{3.8}$$

where ω_0 is the angular resonant frequencies of both resonances of C_{r1} with L_r and C_{r2} with L_r. Z_0 is the resonant impedance of the resonances. The equations of ω_0 and Z_0 are:

$$\omega_0 = \frac{1}{\sqrt{L_r C}} \tag{3.9}$$

$$Z_0 = \sqrt{\frac{L_r}{C}} \tag{3.10}$$

3.3.1.2. State II

At t_1, although Q_1 is still on, because of the reverse bias of all diodes, no current flows in the circuit except the discharging of C_2 to the load. Let V_{Cr11} and V_{Cr21} be the voltage of C_{r1} and C_{r2}, respectively, at t_1, the equations of this state are:

$$v_{Cr1} = V_{Cr11} \tag{3.11}$$

$$v_{Cr1} = V_{Cr21} \tag{3.12}$$

$$i_{Cr1} = i_{Cr2} = 0 \tag{3.13}$$

3.3.1.3. State III

Q_1 is switched off under zero-current switching condition at t_2. Q_2 is switched on at this moment. In Stage 1, C_{r1} discharges to charge C_1 in a resonant manner through D_{1b}, L_r, and V_S. Since C_1 has very large capacitance, in steady state, voltage of C_1 is equal to $2V_S$. In Stage 2, C_{r2} discharges to the load and charges C_2 in resonant manner through D_{2b}, L_r and V_S. Because D_{2b} is in forward bias and polarities of V_S and C_{r2} are the same, and because capacitance of C_2 is very large, V_0 is equal to $3V_S$ in steady state. Because both C_{r1} and C_{r2} discharge in resonant manner, Q_2 is zero-current switched on at t_2. Assuming capacitance of C_{r1} and C_{r2} the same, resonance stops at t_3 because both D_{2a} and D_{2b} are in reverse bias. The equations of this state are:

$$V_{C1} - V_S = L_r \frac{di_{Cr1}}{dt} + v_{Cr1} \tag{3.14}$$

$$i_{Cr1} = C_{r1} \frac{dv_{Cr1}}{dt} \tag{3.15}$$

$$V_{C2} - V_S = L_r \frac{di_{Cr2}}{dt} + v_{Cr2} \tag{3.16}$$

$$i_{Cr2} = C_{r2} \frac{dv_{Cr2}}{dt} \tag{3.17}$$

where V_{C2} is the voltage of C_2. For the 3-mode circuit, V_{C2} is also the output voltage.

Let V_{Cr12} and V_{Cr22} are the voltage of C_{r1} and C_{r2}, respectively, at t_2, the differential equations (3.14) to (3.17) are solved as:

$$v_{Cr1} = V_{C1} - V_S - (V_{C1} - V_S - V_{Cr12}) \cos \omega_0 (t - t_2) \tag{3.18}$$

$$i_{Cr1} = \frac{V_{C1} - V_S - V_{Cr12}}{Z_0} \sin \omega_0 (t - t_2) \tag{3.19}$$

$$v_{Cr2} = V_{C2} - V_S - (V_{C2} - V_S - V_{Cr22}) \cos \omega_0 (t - t_2) \tag{3.20}$$

$$i_{Cr1} = \frac{V_{C2} - V_S - V_{Cr22}}{Z_0} \sin \omega_0 (t - t_2) \tag{3.21}$$

3.3.1.4. State IV

Similar to State II, no current flows in the circuit except the discharging of C_2 to the load. At t_4, Q_1 is switched on and Q_2 is switched off. Since current of Q_2 is zero before Q_2 is switched off, zero-current switched off of Q_2 is obtained. Let V_{Cr13} and V_{Cr14} be the voltage of C_{r1} and C_{r2}, respectively, at t_3, the equations of this state are:

$$v_{Cr1} = V_{Cr11} \tag{3.22}$$

$$v_{Cr1} = V_{Cr21} \tag{3.23}$$

$$i_{Cr1} = i_{Cr2} = 0 \tag{3.24}$$

3.3.2. Generalised Equations of 3-mode Converter

Ideally, the output voltage of the converter is equal to 3 times input voltage and the voltage of C_1 is 2 times input voltage. Considering these assumption, equations (3.5) and (3.7) can be derived as:

$$V_{Cr12} = V_S - V_{Cr10} \tag{3.25}$$

$$V_{Cr22} = 4V_S - V_{Cr20} \tag{3.26}$$

Using input and output balancing of C_1,

$$\int_0^1 i_{Cr2}\,dt = \int_2^3 i_{Cr1}\,dt \tag{3.27}$$

equation of (3.27) is solved as:

$$V_{Cr12} = 3V_S - V_{Cr20} \tag{3.28}$$

Considering input and output balancing of the whole converter gives:

$$\int_0^1 i_{Cr1}\,dt + \int_2^3 i_{Cr1}\,dt + \int_2^3 i_{Cr2}\,dt = I_0 T_S \tag{3.29}$$

where I_0 is the average output current of the converter and T_S is the switching period.

Current of the resonant inductor is:

$$i_L = i_{Cr1} + i_{Cr2} \tag{3.30}$$

Solving the equation (3.30) and considering the information from the equations (3.25), (3.26) and (3.29), V_{Cr10}, V_{Cr20}, V_{Cr12} and V_{Cr22} can be solved. Substituting the solutions of these initial values of C_{r1} and C_{r2} in different states to the equations (3.5) to (3.8), (3.11), (3.12), (3.18) to (3.23), and (3.30), generalised equations of the 3-mode circuit are developed below:

(i) State I

$$v_{Cr1} = V_S - \frac{\pi I_0 T_S Z_0}{T_0}\cos\omega_0(t - t_0) \tag{3.31}$$

$$v_{Cr2} = 2V_S - \frac{\pi I_0 T_S Z_0}{T_0}\cos\omega_0(t - t_0) \tag{3.32}$$

$$i_L = \frac{2\pi I_0 T_S}{T_0} \sin \omega_0 (t - t_0) \tag{3.33}$$

where T_0 is the resonant period such that:

$$T_0 = \frac{2\pi}{\omega_0} \tag{3.34}$$

(ii) State II

$$v_{Cr1} = V_S + \frac{\pi I_0 T_S Z_0}{T_0} \tag{3.35}$$

$$v_{Cr2} = 2V_S + \frac{\pi I_0 T_S Z_0}{T_0} \tag{3.36}$$

$$i_L = 0 \tag{3.37}$$

(iii) State III

$$v_{Cr1} = V_S + \frac{\pi I_0 T_S Z_0}{T_0} \cos \omega_0 (t - t_3) \tag{3.38}$$

$$v_{Cr2} = 2V_S + \frac{\pi I_0 T_S Z_0}{T_0} \cos \omega_0 (t - t_3) \tag{3.39}$$

$$i_L = -\frac{2\pi I_0 T_S}{T_0} \sin \omega_0 (t - t_3) \tag{3.40}$$

(iv) State IV

$$v_{Cr1} = V_S - \frac{\pi I_0 T_S Z_0}{T_0} \tag{3.41}$$

$$v_{Cr2} = 2V_S - \frac{\pi I_0 T_S Z_0}{T_0} \tag{3.42}$$

$$i_L = 0 \tag{3.43}$$

3.3.3. Generalised Equations of n-mode Converter

Similar to the previous sections, during States I, C_{r1} in Stage 1 is connected in series with V_S and L_r while C_{r2} in Stage 2 is connected in series with L_r and its source C_1. This implies that all switched-capacitors in all stages are connected to their own sources and L_r. The previous section also implies that all switched-capacitors are connected in series with V_S and L_r and the sources of their next stage or the load in the final stage. Analysing an n-mode circuit, assumption are made, including that all filtering capacitors (C_1, C_2,..., $C_{(n-1)}$) are very large to maintain constant voltage, capacitance of all switched-capacitors (C_{r1}, C_{r2},..., $C_{r(n-1)}$) are equal and called C, and that the circuit is lossless. Considering m and n are integers such that $1 \leq m \leq n-1$, generalised equations for all stages of the step-up circuit are derived as below:

(i) State I

$$v_{Crm} = mV_s - \frac{\pi I_0 T_S Z_o}{T_0} \cos \omega_0 (t - t_0) \tag{3.44}$$

$$i_L = \frac{(n-1)\pi I_0 T_S}{T_0} \sin \omega_0 (t - t_0) \tag{3.45}$$

(ii) State II

$$v_{Crm} = mV_s + \frac{\pi I_0 T_S Z_0}{T_0} \tag{3.46}$$

$$i_L = 0 \tag{3.47}$$

(iii) State III

$$v_{Crm} = mV_s + \frac{\pi I_0 T_S Z_o}{T_0}\cos\omega_o(t-t_2) \tag{3.48}$$

$$i_L = -\frac{(n-1)\pi I_0 T_S}{T_0}\sin\omega_o(t-t_2) \tag{3.49}$$

(iv) State IV

$$v_{Crm} = mV_s - \frac{\pi I_0 T_S Z_o}{T_0} \tag{3.50}$$

$$i_L = 0 \tag{3.51}$$

3.4. Design Method

3.4.1. Conditions of Zero-current Switching

For obtaining zero-current switching, similar to the circuits in Chapter 2, i_L needs to resonate to zero in both state I and state III for all stages. Let d_1 and d_2 be duty ratios of gate signals of the transistors, Q_1 and Q_2, respectively, and assuming the circuits are lossless, conditions of obtaining zero-current switching of all circuits in the family are:

$$d_1 T_S > \frac{\pi}{\omega_0} \tag{3.52}$$

and

$$d_2 T_S > \frac{\pi}{\omega_0} \tag{3.53}$$

3.4.2. Voltage Ratings of the Components

Assuming all switched-capacitors are ideal and identical, from the equation (3.44), maximum voltage of v_{Crm}, $V_{Crm(max)}$, is:

$$v_{Crm(\max)} = mV_s + \frac{\pi I_0 T_S Z_0}{2T_0} \tag{3.54}$$

The minimum voltage ratings of the components in the n-mode converter are shown in Table 3.1.

Table 3.1 Voltage Ratings of Components of n-Mode Switched-capacitor Resonant Step-up Converter

Components	Minimum Voltage Ratings
Q_1 and Q_2	V_S
C_m	$(m+1)V_S$
C_{rm}	$V_{Crm(max)}$
$D_{1a} - D_{(n-1)a}$ and $D_{1b} - D_{(n-1)b}$	V_S

3.4.3. Current Rating of Components

For n-mode circuit, there are a total of (n-1) stages in the circuit. Resonant current of all stages pass through the same resonant inductor, L_r. Total current of the inductors is equal the total resonant current in all stages. Absolute values of the positive average resonant current of m Stage, $|\overline{i_{LPm}}|$, and the negative average resonant current of m Stage, $|\overline{i_{LNm}}|$, are:

$$\left|\overline{i_{LPm}}\right| = \left|\overline{i_{LNm}}\right| = I_0 \tag{3.55}$$

By using equation (3.55), minimum current ratings of each component are estimated. This is shown in Table 3.2.

Table 3.2 Current Ratings of Components of n-Mode Switched-capacitor Resonant Step-up Converter

Components	Minimum Current Ratings
Q_1 and Q_2	$(n-1)I_0$
L_r	$2(n-1)I_0$
$D_{1a} - D_{(n-1)a}$ and $D_{2b} - D_{(n-1)b}$	I_0

3.4.4. Selection of Resonant Components

From the equations (3.44) and (3.48), it can be found that amplitudes of voltage ripple of the switched-capacitors in all stages in an n-mode circuit are equal. Relationship between Z_0 and the voltage ripple of the switched-capacitors, ΔV_{Cr}, is:

$$Z_0 = \frac{4 f_S \Delta V_{Cr}}{\pi I_0 f_0} \tag{3.56}$$

such that

$$f_0 = \frac{\omega_0}{2\pi}, \quad f_S = \frac{1}{T_S} \tag{3.57}$$

where f_S is the switching frequency and f_0 is the resonant frequency.

To obtain zero-current switching, f_0 should be higher than f_S when the duty

ratios of gate signals of the transistors in the circuit are 50%. Substituting values of ΔV_{Cr}, f_S and f_0, Z_0 can be found.

By the equations (3.9) and (3.10), equations of L_r and C_r can be re-arranged as:

$$L_r = \frac{Z_0}{2\pi f_0} \tag{3.58}$$

$$C = \frac{1}{2\pi f_0 Z_0} \tag{3.59}$$

Substituting the equations (3.56) and (3.57) to the equations (3.58) and (3.59), values of the switched-capacitors, C, and the resonant inductor, L_r, can be found.

3.4.5. Calculation of Voltage Ripple

3.4.5.1. Output Voltage Ripple

As described in the state of operation in Section 3.3.1, filtering capacitor in the last stage of the multi-stage converter, i.e., output filtering capacitor, is charged in State III only. For the n-mode circuit, referring to Fig. 3.1(c) and equations (3.45) (3.47), (3.49) and (3.51), i_a is:

$$i_a = \begin{cases} 0 & t_0 \le t \le t_1 \\ 0 & t_1 \le t \le t_2 \\ \dfrac{\pi I_0 T_S}{T_0} \sin \omega_o (t - t_2) & t_2 \le t \le t_3 \\ 0 & t_2 \le t \le t_4 \end{cases} \tag{3.60}$$

and

$$i_{C(n-1)} = i_a - I_0 \tag{3.61}$$

Assuming output filtering capacitor, $C_{(n-1)}$, is very large to maintain output current, I_0, to be constant, according to the following equation:

$$i_{C(n-1)} = C_{(n-1)} \frac{dV_0}{dt} \tag{3.62}$$

output voltage ripple of the n-mode converter, ΔV_0, is approximately equal to:

$$\Delta V_0 \approx \frac{I_0}{2C_0}(2T_S - T_0) \tag{3.63}$$

3.4.5.2. Voltage Ripple of Filtering Capacitors

For providing constant DC voltage for each stage in the n-mode converter, the capacitance of all filtering capacitors is large. Calculating the voltage ripple of all filtering capacitors is necessary to choose suitable capacitance values of the capacitors. The capacitance of C_m is assumed to be very large that it does not affect the resonance in the circuits. If the voltage across the filtering capacitors is not for voltage output, for $1 \le m \le n-2$, current flowing to C_m is:

$$i_{Cm} = \begin{cases} \dfrac{\pi I_0 T_S}{T_0} \sin \omega_o (t - t_2) & t_0 \le t \le t_1 \\ 0 & t_1 \le t \le t_2 \\ -\dfrac{\pi I_0 T_S}{T_0} \sin \omega_o (t - t_2) & t_2 \le t \le t_3 \\ 0 & t_2 \le t \le t_4 \end{cases} \tag{3.64}$$

Since

$$i_{Cm} = C_m \frac{dV_{Cm}}{dt} \tag{3.65}$$

the voltage of V_{Cm} is:

$$\Delta V_{Cm} = \frac{I_0 T_S}{C_m T_0} \tag{3.66}$$

3.5. Experimental Results

Table 3.3. Specification of Prototype of 3-mode Switched-capacitor Resonant Converter

Descriptions	Values	Units
Input Voltage	40	V
Expected Output Voltage	120	V
Switching Frequency	200	kHz
Maximum Tested Output Power	105	W

Table 3.4. List of Components of Prototype of 3-mode Switched-capacitor Resonant Converter

Descriptions	Model Numbers	Values	Units
Q_1 and Q_2	IRF530		
D_1 and D_2	MBR10100		
C_{r1} and C_{rb}		0.22	μF
C_1 and C_2		100	μF
L_r		1	μH

A prototype circuit of 3-mode switched-capacitor resonant step-up converter has been constructed to verify its proposed operation. The specification and list of components of the prototype circuit are listed in Table 3.3 and Table 3.4, respectively. Since the main power flows through both C_{r1} and C_{r2} in the resonant state, the equivalent series resistance of these capacitors should be very low. High ESR may lead to high power loss and high temperature of the capacitors which may exceed the rated temperature of the capacitors. For this reason, polyester capacitors were chosen for these switched-capacitors.

Experimental waveforms of the 3-mode converters are shown in Fig 3.5. The current of Q_1 and Q_2 are equal to the current of resonant inductor, I_L, when the transistors are conducting. Examination of the amplitude and the frequency of the measured waveforms show that they all agree with the theoretical findings as derived in Session 3.3.2. They also show that zero-current switching was achieved when both switching on and off the transistors.

Fig. 3.6 shows characteristics of the efficiency and the voltage conversion ratio of the converter measured in the experiment. Because of the conduction loss and the forward bias of the diodes, there was a small reduction in the amplitude of the DC output voltage of the circuit. The output voltage of the circuit was not exactly constant. Amplitude of the output voltage was slightly dependent on the output power. Experimental results show that the output voltage varies by about 10% only as the load varies by 400%. Efficiency of the circuit is relatively high. In the experiment, efficiency was over 90% over the range of output power from 20W to 85W.

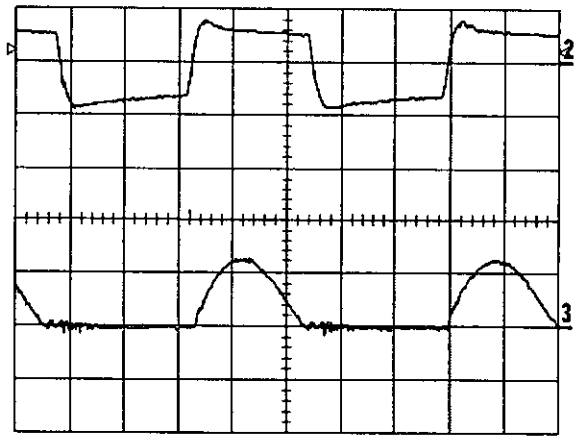

2: Gate signal of Q_1, 20V/div; 3: Drain current of Q_1, 5A/div

(a)

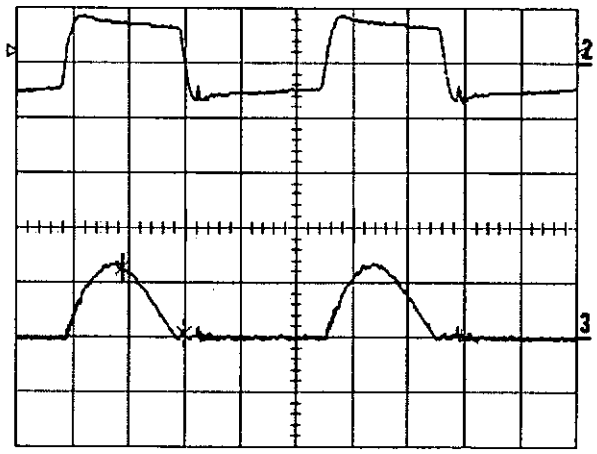

2: Gate signal of Q_2, 20V/div; 3: Drain current of Q_2, 5A/div

(b)

Time base: 1μs/div for both (a) and (b)

Fig. 3.5. Measured waveforms of the 3-mode switched-capacitor resonant step-up converter at 67W

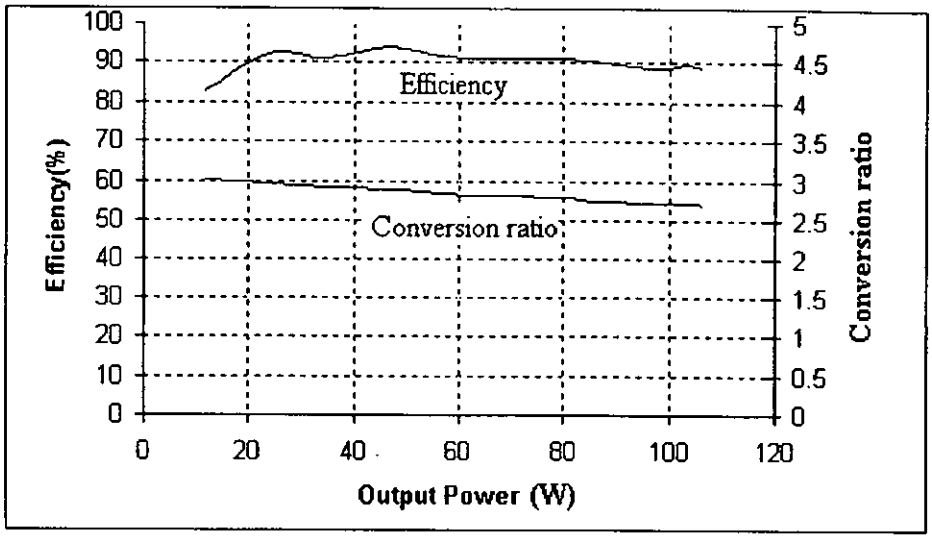

Fig. 3.6. Measured efficiency and conversion ratio of the 3-mode switched-capacitor resonant step-up converter against output power

3.6. Discussion

Similar to the families of the Single-stage step-down resonant switched-capacitor converters discussed in Chapter 2, the multi-stage step-up resonant switched-capacitor converters need more diodes for routing the charging and discharging current for obtaining higher multiplication of output voltage. In practical, schottky diodes may be used for this application. Their forward voltage is from 0.5V to 0.8V, depending on their ratings. The higher number of diodes leads to higher conduction loss due to their forward voltage. It also leads to the higher voltage drop of the output voltage.

When higher multiplication of the voltage conversion ratio is obtained, number of stages is higher. Number of filtering capacitors is also higher. The size of the converter will be higher because not only the total size of the

diodes is higher but also that of the capacitors is higher. However, in practical, the filtering capacitors are electrolytic capacitors. They have high capacitance values with small size and light weight. The total size of the capacitors will not much increases.

Because of the discontinuous discharging current of the switched-capacitors to the load, comparing with a continuous mode traditional SMPS, the capacitance value of the output capacitor is higher. In practical, the output capacitor is an electrolytic capacitor. The size of the capacitor is slightly bigger than that in a traditional SMPS.

3.7. Summary

This chapter introduced a family of the Multi-stage step-up DC-DC converters based on switched-capacitor method. In each circuit, only 2 transistors and a very small resonant inductor are needed. By adding a special switched-capacitor cell, different voltage conversions can be obtained without adding additional transistors. Mathematical analysis, computer simulation and experiments of these circuits verified that all transistors in the circuits are switched both on and off under zero-current switching condition, reducing switching loss. Experiments also showed that efficiency of this family of the converter is high. The main contributions of this research are:

(i) Propose a simple method to convert traditional switched-capacitor converter to have zero-current switching features.

(ii) Quantify the need of the inductor so that switching current can be expected whereas the classical switched-capacitor has an uncontrolled spike current due to the parasitic inductance.

(iii) Limit spike of current for charging switched-capacitors whereas current stress in traditional switched-capacitor converters is very high.

(iv) Produce families of converters with a wide range of numerical conversion ratios.

(v) Produce theoretical analysis of the operation and their associated general circuit equations.

(vi) Experimental results for validating the operations.

Chapter 4. Active-clamp Resonant Converter for Switched Reluctance Motor

4.1. Introduction

Although switched reluctance motor was first introduced over 150 years ago, it has come into attention for only about 30 years. Because of the rapid development of power electronics and the advantages of SRM, such as low rotor inertia, high dynamic response, high starting torque, and fault tolerance, this motor has high potential for common use in the future. Some industrial applications and commercial products like washing machines and hard disk drives have been using SRM [B2], [B9-11] and [B17]. It can also be applied on electric vehicles, trains and many automation machines [B16].

Nowadays, soft-switching techniques have been well developed [A1-A14], [B5-B7], [B8-B10], [B13-B16], [C5], and [C8-C10]. Many literatures have proposed topologies of soft-switching techniques. It contributes to improved efficiency, reduction of induced electromagnetic interference, and increase of switching frequency in power electronic circuits. It has been widely used in switched mode power supplies and AC motor drives.

In this chapter, an active-clamp soft-switching converter for SRM is introduced. Zero-voltage switching resonant and active-clamp techniques are applied on this proposed circuit. Fig. 4.1 shows a 2(n+1)-switch 4-phase SRM converter. Q_a and Q_b are the chopping transistors. Q_1, Q_2, Q_3 and Q_4 are the

commutation transistors. When the motor operates by soft-chopping, switching frequencies of the commutation transistors are low, especially when the speed of motor is low. Obtaining soft-switching condition for these transistors over the whole range of speed of the motor is also very difficult, as their switching frequencies depend on the speed of the motor. Soft-switching is also very costly if the switching frequency is low as large resonant capacitors and resonant inductors are needed. In fact, the main power loss of the commutation transistors is not switching loss but conduction loss. As a result, soft-switching condition of the commutation transistors cannot quite improve the performance of the SRM, while the resonant circuits actually increase the cost of the converter.

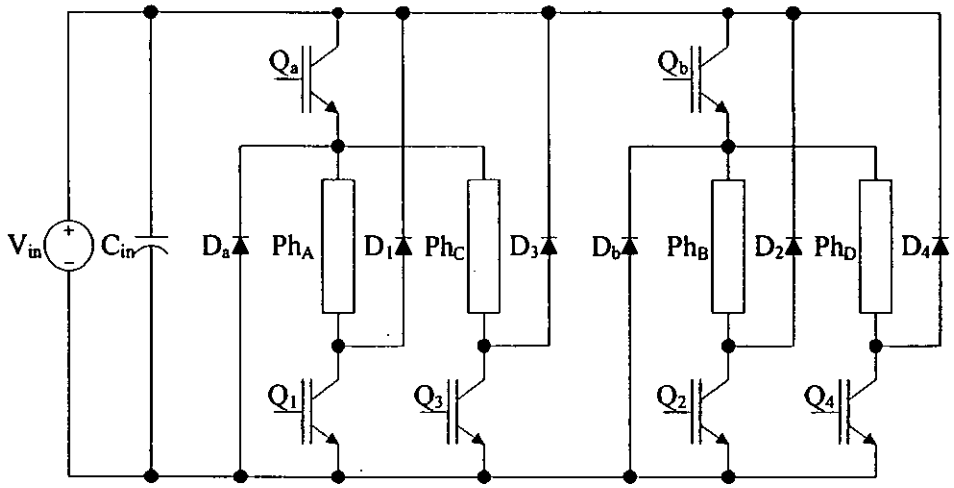

Fig. 4.1. Typical 2(n+1) switch converter for 4-phase switched reluctance motor

An active-clamp resonant converter for 4-phase SRM is proposed in this chapter. Unlike the commutation transistors, switching frequency of the chopping transistors is high if the SRM operates with pulse-width-modulation or constant current mode chopping method [B2] and [B18]. Therefore, in this newly designed circuit, soft-switching condition is provided for the chopping

transistors. Zero-voltage switching condition is provided by two resonant tanks and two active-clamp circuits. Switching loss can be reduced. Structure and switching sequence of the circuit are simple. The circuit can be controlled by both constant current mode and pulse-width modulation (PWM). The resonant voltage of the chopping transistors is clamped by the active-clamp circuits. Voltage stress of the chopping transistors is reduced.

4.2. Modelling of Switched Reluctance Motor

To analyse the proposed resonant converter for SRM by mathematical analysis and computer simulation, a mathematical model of SRM is built. Fig. 4.2 shows a diagram of the structure of a 4-phase 8/6 SRM. Referring to Ph_A, the unaligned position are at -30° and 30° while the aligned position is at 0°. Fig. 4.3 shows an ideal variation of inductance of Ph_A when the rotor position changes from -30° to 30°. It shows that the highest phase inductance position is at the aligned position because the air gap between the rotor and stator yokes are the smallest and the reluctance is the lowest. On the other hand, the phase inductance is the lowest when the rotor is at the unaligned position because the air gap is the largest and the reluctance is the highest. As a result, the phase inductance is a function of the angular position of the rotor.

The voltage applied on the phase winding is equal to the sum of the resistive voltage drop and the rate of the flux linkages. This gives an equation:

$$V_a = R_a i_a + \frac{dL_a i_a}{dt} \tag{4.1}$$

Equation (4.1) can be re-written as:

$$V_a = R_a i_a + L_a \frac{di_a}{dt} + E_{ba} \tag{4.2}$$

where V_a is the voltage applied on the phase winding. R_a is the phase resistance. L_a is the phase inductance. E_{ba} is the back electromotive force (emf) induced in the phase winding, L_a is a function of i_a and angular rotor position, θ.

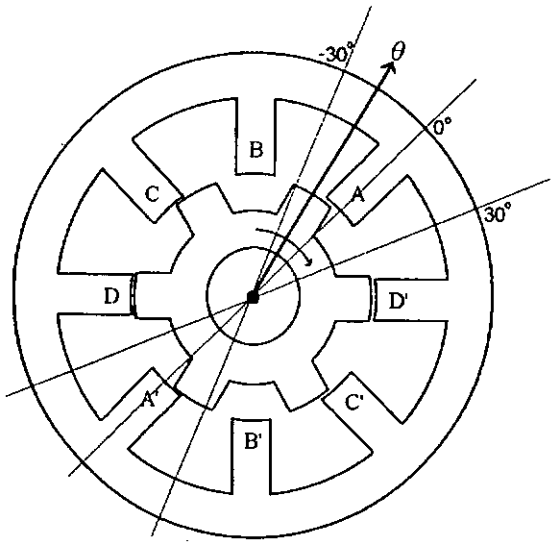

Fig. 4.2. Structure of 8/6 switched reluctance motor

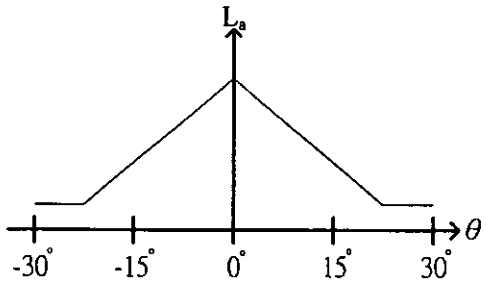

Fig. 4.3 Inductance of Ph_A of switched reluctance motor

According to Equation (4.2), a per-phase equivalent circuit of a SRM can be built as shown in Fig. 4.4.

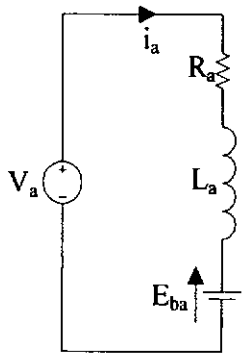

Fig.4.4. Per-phase equivalent Circuit of switched reluctance motor

Since

$$E_{ba} = i_a \frac{\partial L_a}{\partial \theta} \times \frac{d\theta}{dt} \tag{4.2}$$

equation (1) can be derived as:

$$V_a = R_a i_a + L_a \frac{di_a}{dt} + i_a \frac{\partial L_a}{\partial \theta} \times \frac{d\theta}{dt} \tag{4.3}$$

Also, instantaneous torque produced by a phase winding is:

$$T_a = \frac{1}{2} i_a^2 \frac{\partial L_a}{\partial \theta} \tag{4.4}$$

Total instantaneous new torque produced by the SRM is:

$$T_{net} = T_a + T_b + T_c + T_d - T_L \tag{4.5}$$

and

$$T_{net} = J \frac{d\omega_m}{dt} + B\omega_m \tag{4.6}$$

where T_b, T_c and T_d are the instantaneous torque produced by each phase of the SRM. T_L is the torque of the load. J is the moment of inertia and B is the

damping factor internally built in the motor. ω_m is the angular velocity of the rotor such that:

$$\omega_m = \frac{d\theta}{dt} \tag{4.7}$$

Table 4.1 shows the measured phase inductance of one phase winding with respect to phase current of an 8/6 SRM. The item "Phase Current" represents the current of the phase winding for measuring its inductance at different angular rotor positions. The item "Angle" represents the angular rotor position of the motor. The graph of the measured phase inductance is shown in Fig. 4.5. The period of the change of phase inductance in the 8/6 SRM is 60°. The inductance from -30° to 0° and that from 0° to 30° is symmetrical.

Table 4.1. Measured Inductance Characteristics of Switched Reluctance Motor

Angle	**0°**	**5°**	**10°**	**15°**	**20°**	**25°**	**30°**
Phase Current	**Inductance**						
1A	113.9	95.8	70.3	44.5	21.3	13.97	13.97
2A	117.4	97.1	74.5	44.5	27	15.2	14.2
3A	118.6	100.8	78.5	47.4	24.5	13.9	13.6
5A	106.3	94.2	70.0	48.4	24.1	14.5	13.9
7A	84.6	80	69.1	45.4	26.3	15.2	13.6
9A	70.4	67.2	59.4	42.0	24.7	14.7	13.6

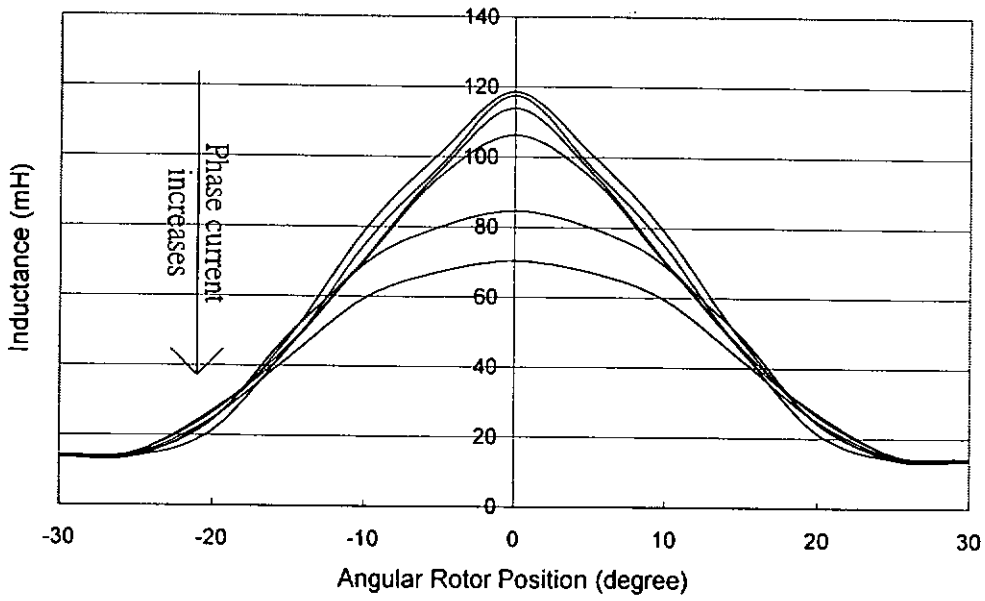

Fig. 4.5. Graph of Measured inductance of switched reluctance motor

To simplify the motor model for computer simulation, effect of the variation of phase current on phase inductance is neglected. Inductance of each phase becomes a periodic function in terms of the angular rotor position. As the maximum input power of the switched reluctance motor drive is 500W, the set of measured phase inductance at 2A phase current is chosen for modelling. The phase inductance of all phase windings is assumed identical with 15° phase shift to each other. Let L_a, L_b, L_c and L_d be the phase inductance of Ph_A, Ph_B, Ph_C and Ph_D, respectively. By discrete Fourier Series method, the approximate periodic functions of the phase inductance are:

$$\begin{aligned} L_a \approx 0.001\{&52.016 - 48.561\cos(6\omega_m t) + 8.857\cos(12\omega_m t) \\ &- 0.088\cos(18\omega_m t) + 2.999\cos(24\omega_m t) \\ &- 1.0315\cos(30\omega_m t) + 0.122\cos(36\omega_m t)\} \end{aligned} \tag{4.8}$$

$$L_b \approx 0.001\Big\{52.016-48.561\cos\Big[6\omega_m(t-\frac{\pi}{12\omega_m})\Big]$$
$$+8.857\cos\Big[12\omega_m(t-\frac{\pi}{12\omega_m})\Big]-0.088\cos\Big[18\omega(t-\frac{\pi}{12\omega_m})\Big]$$
$$+2.999\cos\Big[24\omega(t-\frac{\pi}{12\omega_m})\Big]-1.0315\cos\Big[30\omega(t-\frac{\pi}{12\omega_m})\Big] \quad (4.9)$$
$$+0.122\cos\Big[36\omega(t-\frac{\pi}{12\omega_m})\Big]\Big\}$$

$$L_c \approx 0.001\Big\{52.016-48.561\cos\Big[6\omega_m(t-\frac{\pi}{6\omega_m})\Big]$$
$$+8.857\cos\Big[12\omega_m(t-\frac{\pi}{6\omega_m})\Big]-0.088\cos\Big[18\omega(t-\frac{\pi}{6\omega_m})\Big]$$
$$+2.999\cos\Big[24\omega(t-\frac{\pi}{6\omega_m})\Big]-1.0315\cos\Big[30\omega(t-\frac{\pi}{6\omega_m})\Big] \quad (4.10)$$
$$+0.122\cos\Big[36\omega(t-\frac{\pi}{6\omega_m})\Big]\Big\}$$

$$L_d \approx 0.001\Big\{52.016-48.561\cos\Big[6\omega_m(t-\frac{\pi}{4\omega_m})\Big]$$
$$+8.857\cos\Big[12\omega_m(t-\frac{\pi}{4\omega_m})\Big]-0.088\cos\Big[18\omega(t-\frac{\pi}{4\omega_m})\Big]$$
$$+2.999\cos\Big[24\omega(t-\frac{\pi}{4\omega_m})\Big]-1.0315\cos\Big[30\omega(t-\frac{\pi}{4\omega_m})\Big] \quad (4.11)$$
$$+0.122\cos\Big[36\omega(t-\frac{\pi}{4\omega_m})\Big]\Big\}$$

4.3. Principles of Operation

Fig. 4.6 shows a circuit diagram of the proposed active-clamp resonant converter for 8/6 SRM. To provide zero-voltage switching conditions for all chopping transistors, Q_a and Q_b, under any dwell angle the SRM drive may operate with, including long dwell angle as shown in Fig. 4.7, two resonant tanks and two active-clamp circuits are used in the circuit.

The proposed circuit, shown Fig. 4.6, is a kind of 2(n+1)-switch SRM drive, shown in Fig. 1.5. To obtain zero-voltage switching and resonant voltage clamping, a resonant tank and a clamping circuit is added for each chopping transistor, i.e., for serving two phases of windings. To simplify the description of the principles of operation of the circuit, per-phase operation is considered. Fig. 4.8 shows an equivalent circuit of a per-phase of the active-clamp converter. C_r is a resonant capacitor and L_r is a resonant inductor. They form a resonant tank with an anti-parallel diode of the chopping transistor, D_r. The active-clamp circuit consists of an auxiliary transistor, Q_x, an anti-parallel diode of auxiliary transistor, D_x, and a clamping capacitor, C_c. For clamping the drain-to-source voltage of Q_a, C_c is much larger than C_r.

Idealised waveforms and per-phase equivalent circuits of each state of operation of the active-clamp resonant converter for SRM in motoring stage are shown in Fig. 4.9 and Fig. 4.10, respectively. In this stage, the commutation transistor, Q_1, is always on as the SRM is operated by soft-chopping. Since the switching frequency of the chopping transistor is high and rate of change of

phase current is low, phase current is assumed to be a constant. The phase winding of the motor is considered as a current source. Let I_L be the current of the equivalent current source. There are a total of seven states of operation in one switching period.

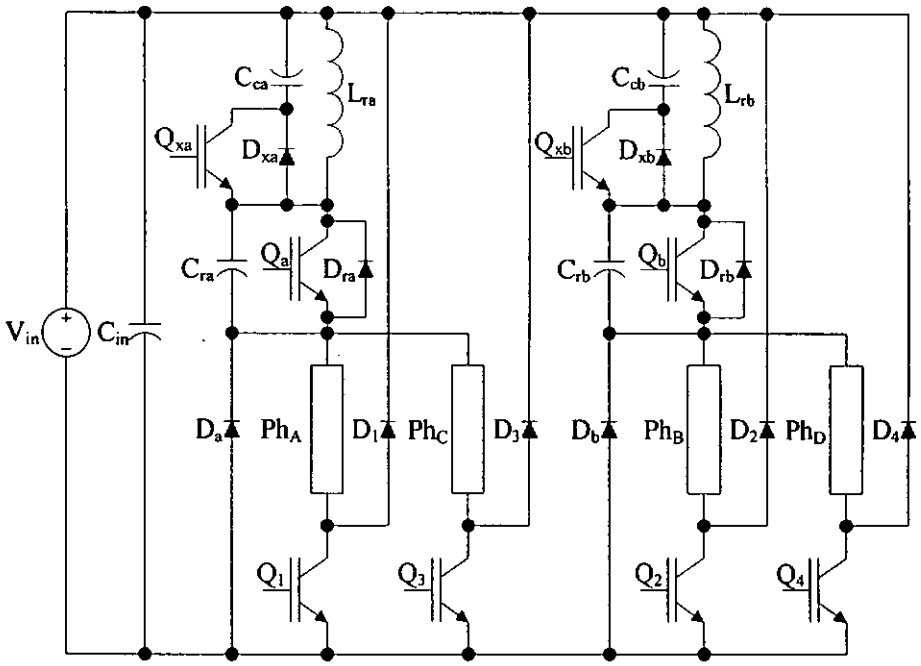

Fig. 4.6. Proposed active-clamp partial soft-switching converter for switched reluctance motor

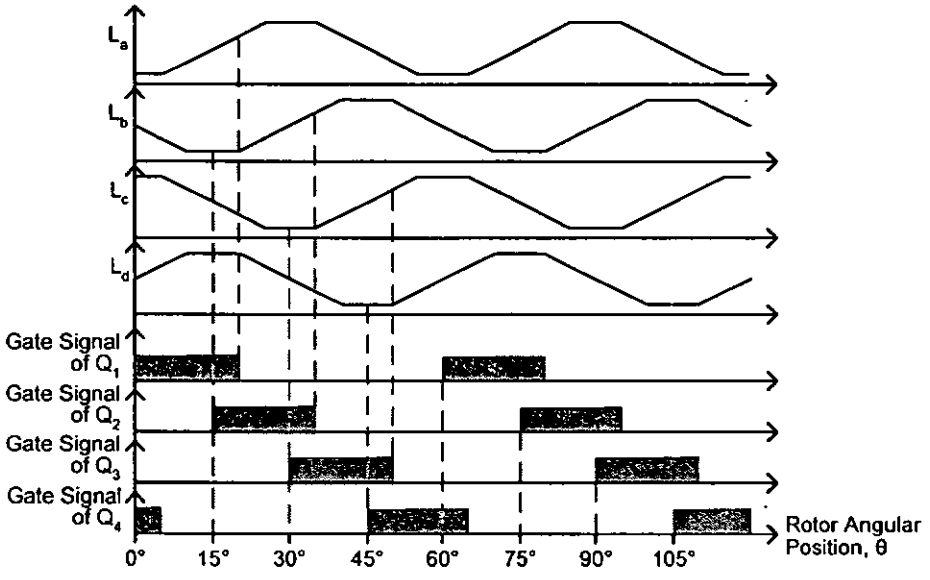

Fig. 4.7. Gate signals of commutated transistors under long dwell angle operation

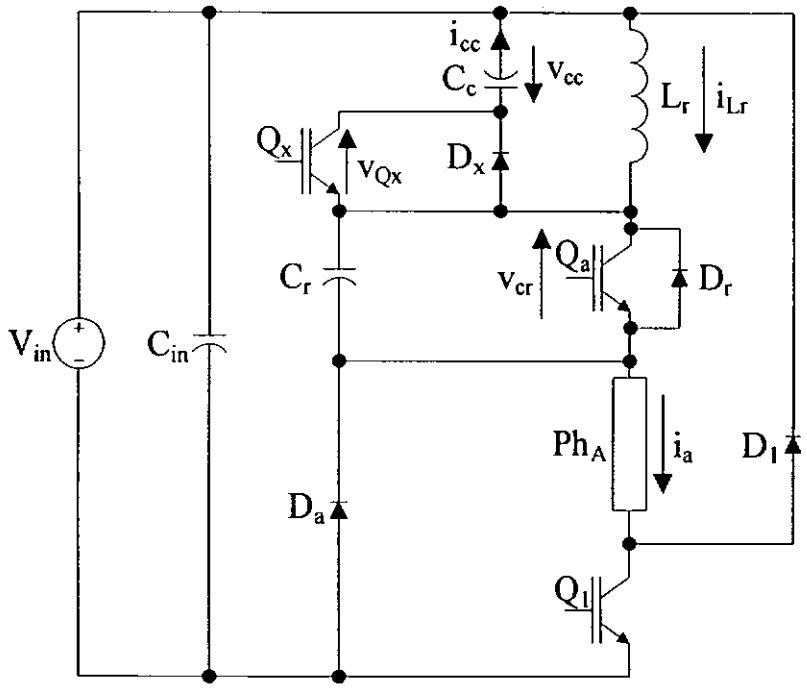

Fig. 4.8. Per-phase Equivalent circuit of active-clamp resonant converter

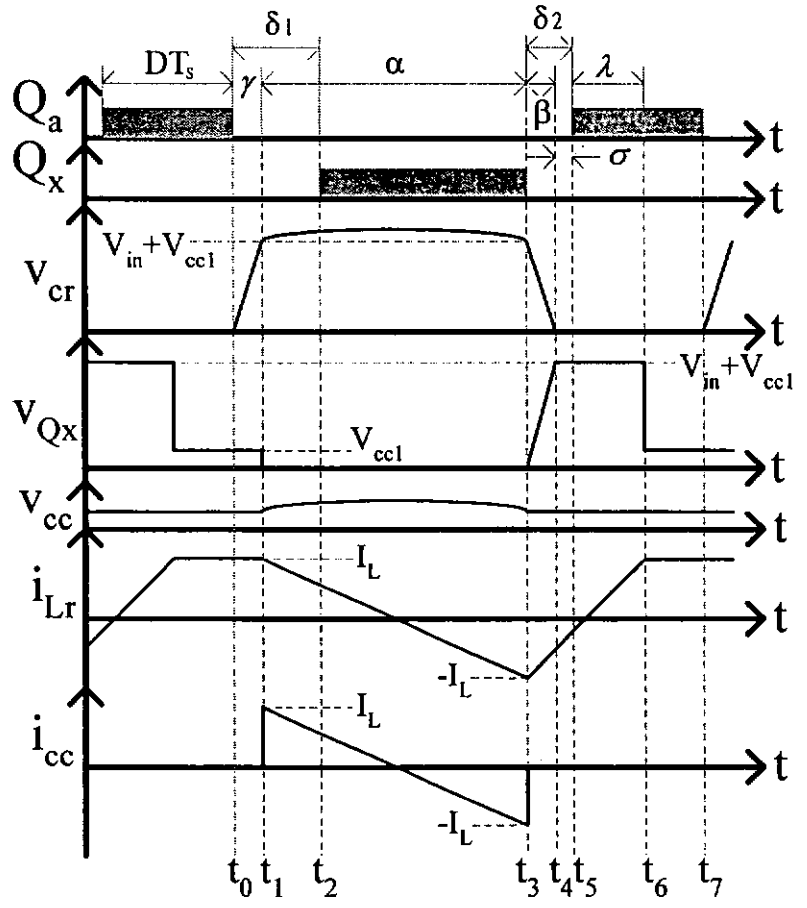

Fig. 4.9. Idealised waveforms of active-clamp resonant converter in motoring stage

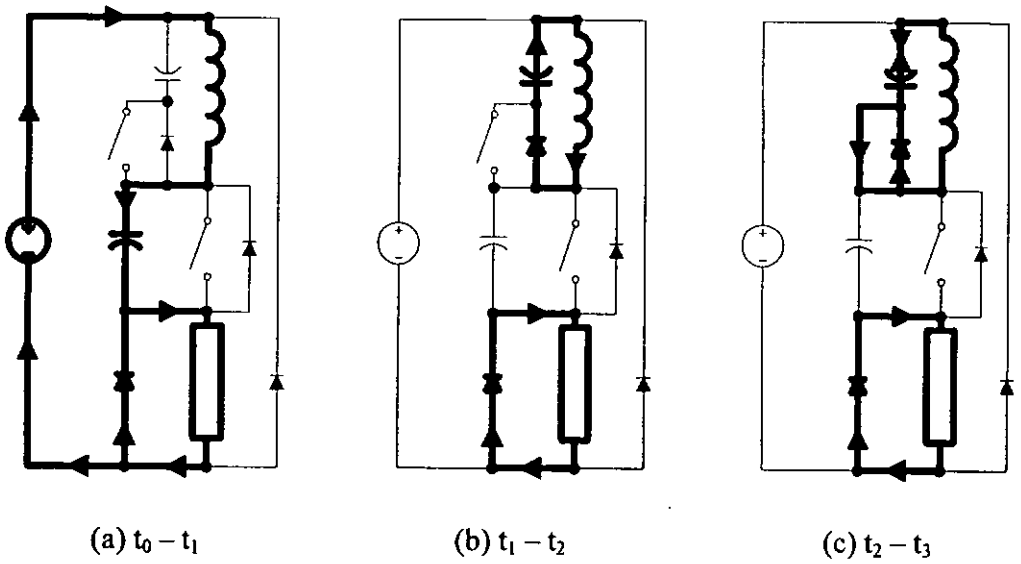

(a) $t_0 - t_1$ (b) $t_1 - t_2$ (c) $t_2 - t_3$

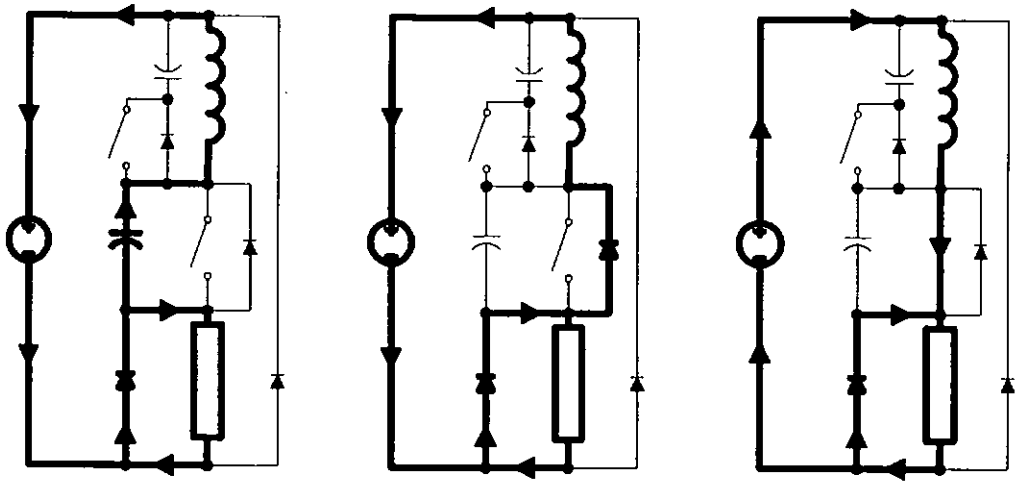

(d) $t_3 - t_4$ (e) $t_4 - t_5$ (f) $t_5 - t_6$

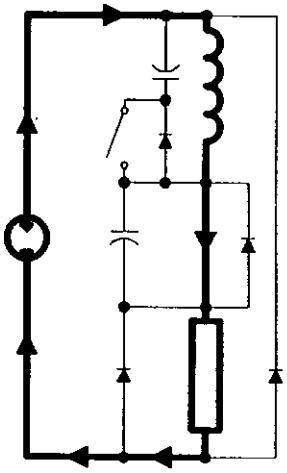

(g) $t_6 - t_7$

Fig. 4.10. Per-phase equivalent circuits of states of operation of active-clamp resonant converter

4.3.1. State I $[t_0 - t_1]$

Fig. 4.10(a) shows the equivalent circuit of this state. At t_1, Q_a is switched off. Q_x is off. The free-wheeling diode, D_a, is in forward bias. It starts freewheeling with Ph_A. C_r is charged. V_{cr} rises from zero gradually and resonates with L_r. Since the duration of charging C_r is very short compared to the whole resonant period, C_r is assumed to be linearly charged. Q_a is switched off under zero-voltage switching. In this state, i_{Lr} is positive. Initial values of i_{Lr} and v_{cr} of State I are:

$$i_{Lr0} = I_L \text{ and } V_{cr0} = 0 \tag{4.12}$$

Equations of this state are:

$$V_{cr} = \frac{I_L}{C_r}(t - t_0) \tag{4.13}$$

$$i_L = I_L \tag{4.14}$$

4.3.2. State II $[t_1 - t_2]$

Fig. 4.10(b) shows the equivalent circuit of this state. At t_2, Q_a and Q_x are still off. D_f is still freewheeling with Ph_A. D_x is in forward bias while v_{cr} reaches $V_{in}+V_{cc1}$ where V_{cc1} is the voltage across C_c, v_{cc}, at t_1. L_r resonates with C_c and C_r. i_{Lr} is still positive. Because capacitance of C_c is much larger than that of C_r, i_{Lr} is approximately equal to i_{cc}.

4.3.3. State III $[t_2 - t_3]$

Fig. 4.10(c) shows the equivalent circuit of this state. At t_2, i_{Lr} is still positive and Q_x is switched on under zero-voltage condition. Q_a is still off at t_2. D_x is in forward bias. After switching on Q_x, i_{Lr} can be negative. At t_3, i_{Lr} is negative. Q_x is switched off at t_3. Equations of State II and State III are:

$$v_{cr} = V_{in} + v_{cc} \tag{4.15}$$

$$v_{cc} + L_r \frac{di_{Lr}}{dt} = 0 \tag{4.16}$$

$$i_{Lr} = C_c \frac{dv_{cc}}{dt} \tag{4.17}$$

Solving the equations (4.15) and (4.16) gives:

$$v_{cc} = I_L Z_c \sin \omega_c (t - t_1) + V_{cc1} \cos \omega_c (t - t_1) \tag{4.18}$$

$$i_{Lr} = I_L \cos \omega_c (t - t_1) - \frac{V_{cc1}}{Z_c} \sin \omega_c (t - t_1) \tag{4.19}$$

where V_{cc1} is the value of v_{cc} at t_1. Z_c and ω_c are the resonant impedance and angular resonant frequency of L_r and C_c, respectively. They are:

$$Z_c = \sqrt{\frac{L_r}{C_c}} \tag{4.20}$$

and

$$\omega_c = \frac{1}{\sqrt{L_r C_c}} \tag{4.21}$$

In steady state, V_{cc1} is equal to the value of v_{cc} at t_3, V_{cc3}. Let α be the total duration of State II and State III, which is controlled by a gate signal

generator or a controller of the converter, the value of v_{cc} at t_2 is:

$$V_{cc1} = \frac{I_L Z_c \sin \omega_c \alpha}{1 - \cos \omega_c \alpha} \tag{4.22}$$

And value of i_{Lr} at t_3 is:

$$i_{Lr3} = -I_L \tag{4.23}$$

4.3.4. State IV $[t_3 - t_4]$

Fig. 4.10(d) shows the equivalent circuit of this state. i_{Lr} is negative. Q_a remains off. Q_x is switched off at t_3. Since D_x is in reverse bias, L_r ceases to resonate with C_c. v_{cc} remains unchanged and equal to V_{cc1} until t_1 in the next switching period. Energy stored in L_r is released by discharging C_r to the voltage source in a resonant manner. Equations of this state are:

$$V_{in} = v_{cr} + L_r \frac{di_{Lr}}{dt} \tag{4.24}$$

$$i_{Lr} = C_r \frac{dv_{cr}}{dt} \tag{4.25}$$

Solving the equations (4.22) and (4.23) gives:

$$v_{cr} = V_{in} + V_{cc1} \cos \omega_r (t - t_3) - I_L Z_r \sin \omega_r (t - t_3) \tag{4.26}$$

$$i_{Lr} = -I_L \cos \omega_r (t - t_1) - \frac{V_{cc1}}{Z_r} \sin \omega_r (t - t_3) \tag{4.27}$$

Resonant impedance and resonant angular frequency of L_r and C_r are:

$$Z_r = \sqrt{\frac{L_r}{C_r}} \tag{4.28}$$

$$\omega_r = \frac{1}{\sqrt{L_r C_r}} \tag{4.29}$$

At t_4, v_{cr} is zero. Duration of this state, β, is solved as:

$$\beta = \frac{1}{\omega_r}\left(\sin^{-1}\frac{V_{in}}{\sqrt{{V_{cc1}}^2 + {I_L}^2 Z_r^2}} - \tan^{-1}\frac{-V_{cc1}}{I_L Z_r}\right) \tag{4.30}$$

Substituting β and V_{cc1} in the equation (4.27), the value of i_{Lr} at t_3 is:

$$I_{Lr4} = -I_L \cos\omega_r\beta - \frac{I_L Z_c \sin\omega_c\alpha \sin\omega_r\beta}{Z_r(1-\cos\omega_c\alpha)} \tag{4.31}$$

4.3.5. State V $[t_4 - t_5]$

Fig. 4.10(e) shows the equivalent circuit of this state. At t_4, both Q_a and Q_x are off. D_a is in forward bias. C_r stops discharging and remains zero voltage. L_r releases energy to the voltage source through D_a instead of through C_r in the previous state.

4.3.6. State VI $[t_5 - t_6]$

Fig. 4.10(f) shows the equivalent circuit of this state. At t_6, Q_x remains off. To obtain zero-voltage switching on of Q_a, Q_a is switched on when i_{Lr} is still flowing in negative direction through D_a. When i_{Lr} has increased to zero, D_a

becomes reverse bias. Current flows through Q_a instead of through D_a from the voltage source to the phase winding of the motor. At t_6, i_{Lr} reaches I_L. D_f becomes reverse bias and stops free-wheeling. Equations of State V and State VI are:

$$v_{cr} = 0 \tag{4.32}$$

$$i_{Lr} = \frac{V_{in}}{L_r}(t - t_4) + I_{Lr4} \tag{4.33}$$

4.3.7. State VII [$t_6 - t_7$]

Fig. 4.10(g) shows the equivalent circuit of this state. At t_6, Q_a, is on and Q_x is off. All diodes are in reverse bias. Current flows from the voltage source to the phase of the motor. i_{Lr} is equal to I_L. The electrical power of the motor is controlled by varying the duration of this state. The next switching period begins when Q_a is switched off again at t_7.

4.3.8. Electrical Output Power of the Converters

Input electrical power can be derived by equation:

$$P_{in} = \frac{V_{in}\left(\int_{t_0}^{t_1} i_{Lr}\,dt + \int_{t_3}^{t_7} i_{Lr}\,dt\right)}{T_S} \tag{4.34}$$

where T_s is the duration of one switching period.

From equation (4.34) and referring to Fig. 8,

$$P_{in} = \frac{V_{in}}{T_s}\left[I_L\left(\gamma - \frac{\sin\omega_r\beta}{\omega_r} - \lambda + DT_s \right) + \frac{V_{ccl}\left(\cos\omega_r\beta - 1\right)}{Z_r} \right.$$
$$\left. + \left(\frac{V_{in}\left(\sigma+\lambda\right)}{L_r} + I_{Lr4} \right)\left(\sigma+\lambda\right) \right] \tag{4.35}$$

Assuming the converter is lossless, electrical input power is equal to electrical output power, P_0. In practice, durations of t_0-t_1 and t_3-t_6 are designed to be very short relative to the whole switching period. Let N_S be the number of stator pole pairs, N_r be the number of rotor poles of the SRM, and θ_D be the dwell angle of each phase of the converter, total electrical output power the converter is:

$$P_0 \approx \frac{N_S N_r \theta_D V_{in} I_L D}{2\pi} \tag{4.36}$$

4.4. Criteria of Soft Switching

For chopping transistor and auxiliary transistor, after one transistor is switched off, another one will be switched on after a short delay. As shown in Fig. 4.9, δ_1 and δ_2 are the short delays. To obtain zero-voltage switching condition for both transistors, certain criteria have to be met. Q_x should be switched on before i_{Lr} decreases to zero. Referring to equations (4.13), (4.14), (4.19), (4.22), (4.30), (4.31) and (4.33), criteria are of δ_1 and δ_2 are derived:

$$\frac{C_r\left(V_{in}+V_{ccl}\right)}{I_L} \geq \delta_1 \geq \frac{1}{\omega_c}\tan^{-1}\frac{\left(1-\cos\omega_c\alpha\right)}{\sin\omega_c\alpha} \tag{4.37}$$

and

$$\beta \le \delta_2 \le \beta + \frac{I_L L_r}{V_{in}} \tag{4.38}$$

v_{cr} in equation (4.26) in State IV has to reach zero to provide zero-voltage switching for Q_a. State-plane analysis of this state is done. The state-plane diagram of State IV is shown in Fig. 4.11.

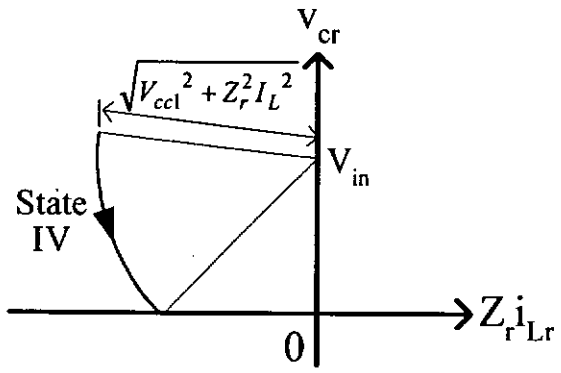

Fig. 4.11. State-plane of State IV of operation

From equations (4.22) and (4.24) and Fig. 4.11, it shows that one of the criteria of achieving zero-voltage switching is:

$$\sqrt{V_{ccl}^{\ 2} + Z_r^2 I_L^{\ 2}} \ge V_{in} \tag{4.39}$$

4.5. Simulation Results

The active-clamp resonant converter driving an 8/6 switched reluctance motor was simulated by Saber Designer. The circuit was controlled by pulse width modulation (PWM). Its input voltage, V_{in}, was 150V DC. Duty ratios of each chopping transistors in their motoring stages were 0.5. Angular speed of the motor is 650 rpm. The simulation results are shown in Fig. 4.12

to Fig. 4.15.

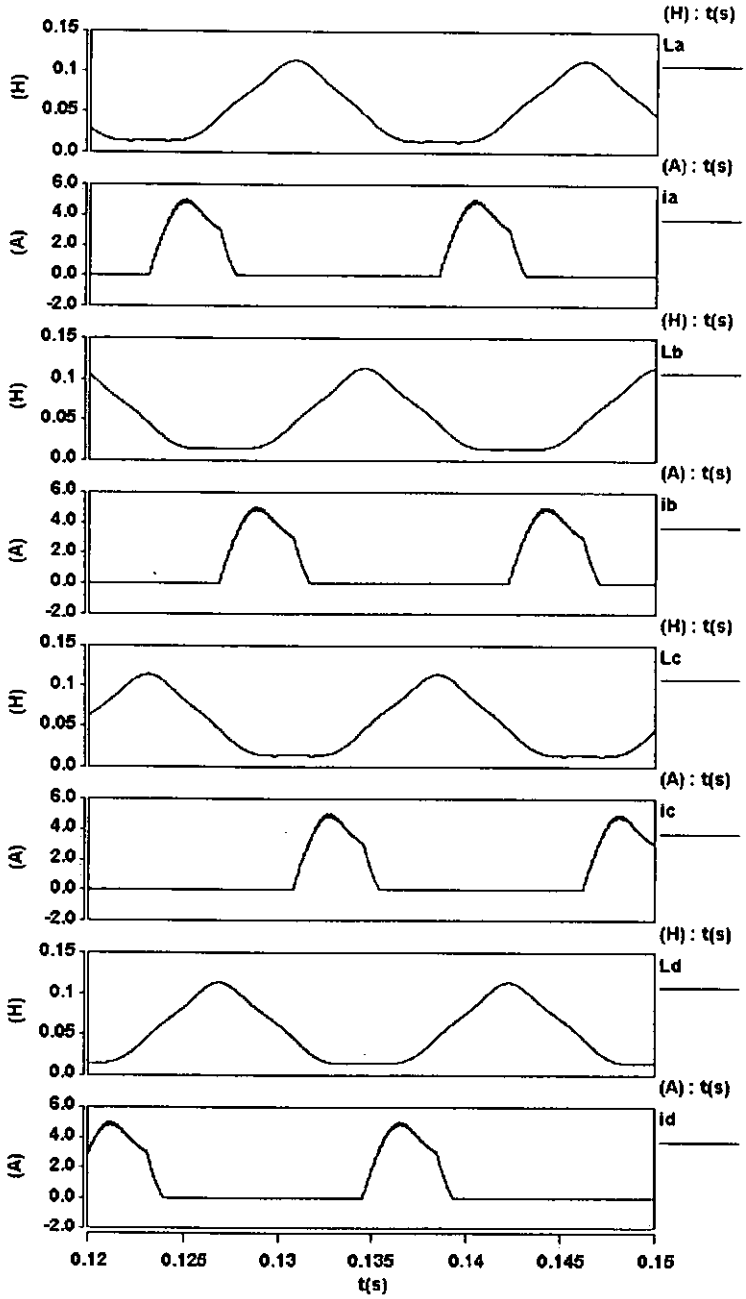

Fig. 4.12. Simulation waveforms of phase currents of active-clamp resonant converter for switched reluctance motor

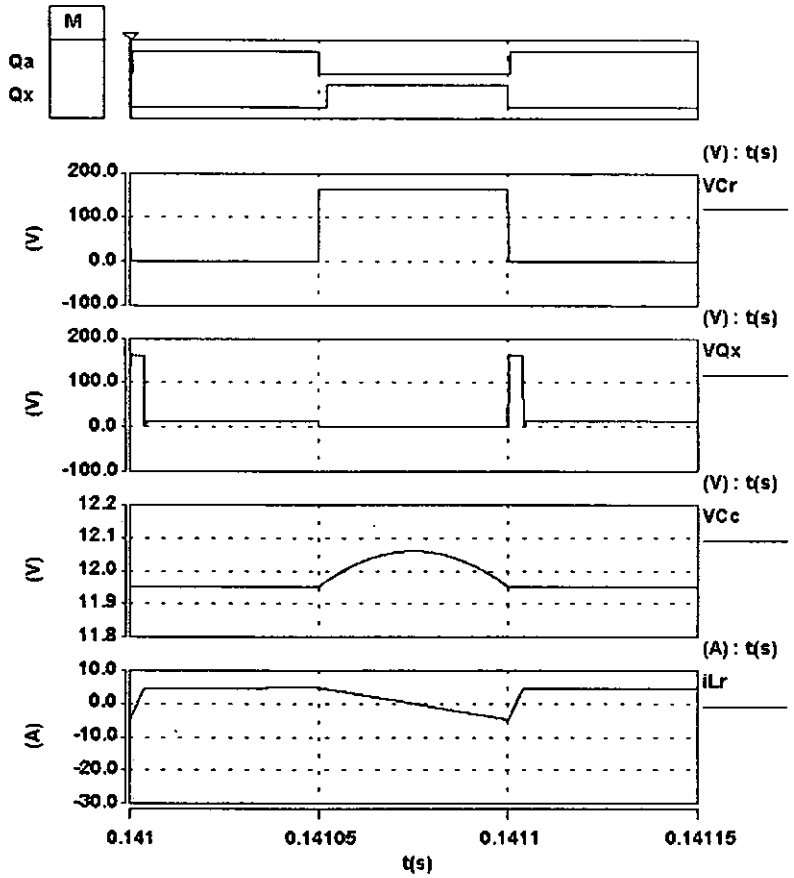

Fig. 4.13. Simulation waveforms of switching of chopping transistor of the active-clamp resonant converter

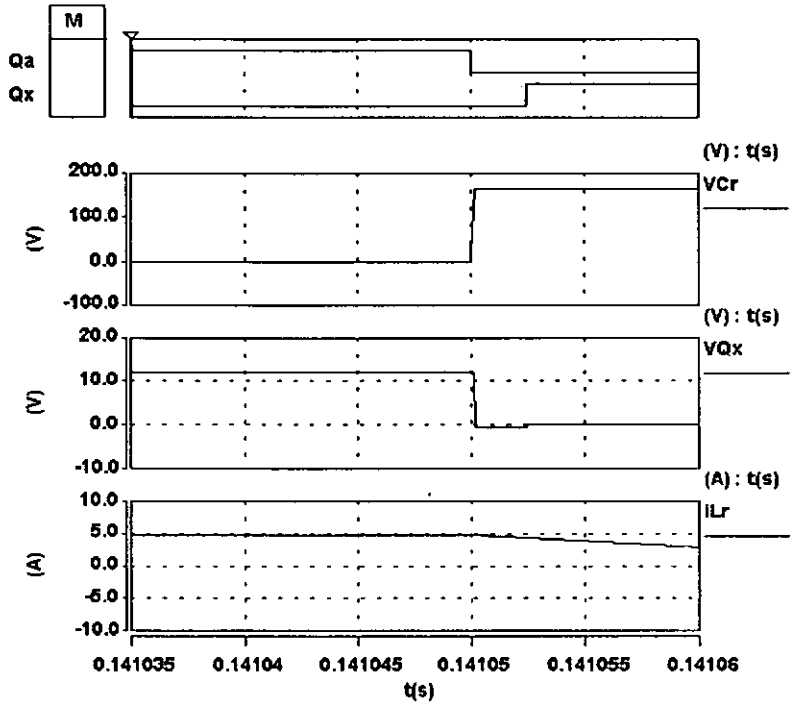

Fig. 4.14. Simulation waveforms of auxiliary transistor of active-clamp resonant converter obtaining zero-voltage switching

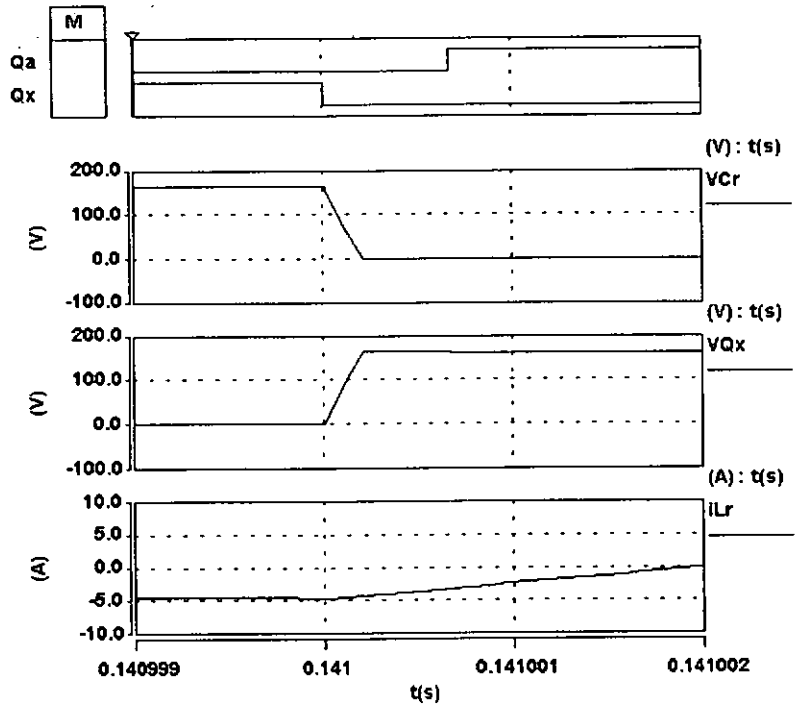

Fig. 4.15. Simulation waveforms of chopping transistor of active-clamp resonant converter obtaining zero-voltage switching

Fig. 4.12 shows the simulation result of phase current of all phase windings. Ph_A Ph_B, Ph_C, and Ph_D were fired at -30°, -15°, 0° and 15°, respectively. Their dwell angles were 15°. Fig. 4.13 shows the simulation result of Ph_A of the converter in one switching period. They show that the maximum values of v_{Cr} and v_{Qx} were slightly higher than V_{in}. Voltage of the chopping transistor was clamped. Fig. 4.14 shows the simulation result of the auxiliary transistor, Q_x. Q_x was switched on under zero-voltage switching when i_{Lr} was positive. Fig. 4.15 shows the simulation result of v_{Cr}. It shows that Q_a was switched on when v_{Cr} was zero and i_{Lr} was negative. Q_a was switched on under zero-voltage switching because drain-to-source voltage of Q_a was equal to v_{cr}. In other words, all high switching frequency transistors in the converter were switched under zero-voltage switching condition. Their drain-to-source voltage was actively clamped.

4.6. Experimental Results

A prototype of active-clamped resonant converter for switched reluctance motor was built. The circuit was tested with an 8/6 SRM. In the experiments, the SRM was connected to a dynamometer as a load. Rated power of the SRM is 4kW. Its rated speed is 1500 rpm. Rated continuous power of the dynamometer without compressed air for cooling is 350W. Its rated speed is 3000 rpm. Fig. 4.16 shows the photo of the 8/6 SRM and the dynamometer used in the experiments.

Fig. 4.17 and Fig. 4.18 show the photos of the prototype converter and the hardware for computer interfacing and driving the transistors. Insulated gate bipolar transistors (IGBTs) were used as all transistors in the prototype. Block diagram of the system in the experiment is shown in Fig. 4.19. A dSpace DS1102 DSP controller board with a Texas Instruments TMS320C3X™ DSP was used for encoding the position sensor signals from the SRM and generating gate signals for the IGBTs.

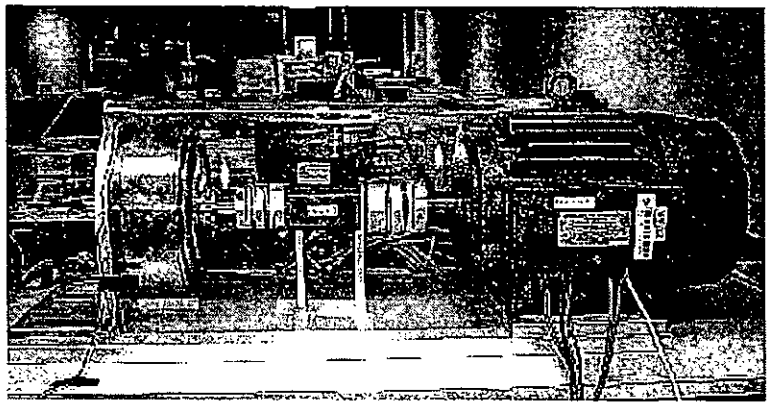

Fig. 4.16. 8/6 switched reluctance motor (right) and its dynamometer (left) for experiments

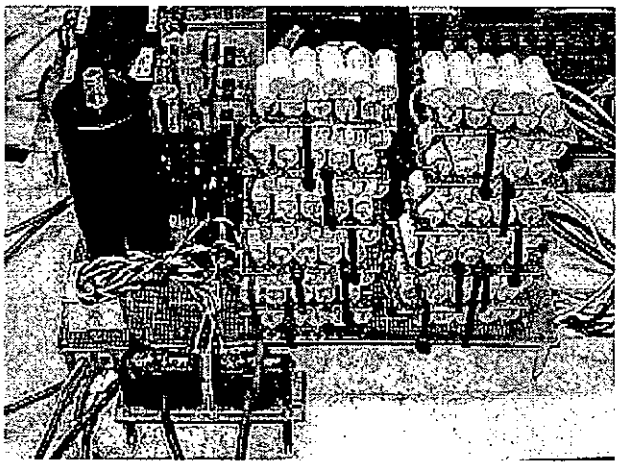

Fig. 4.17. Prototype of active-clamp resonant converter for switched reluctance motor

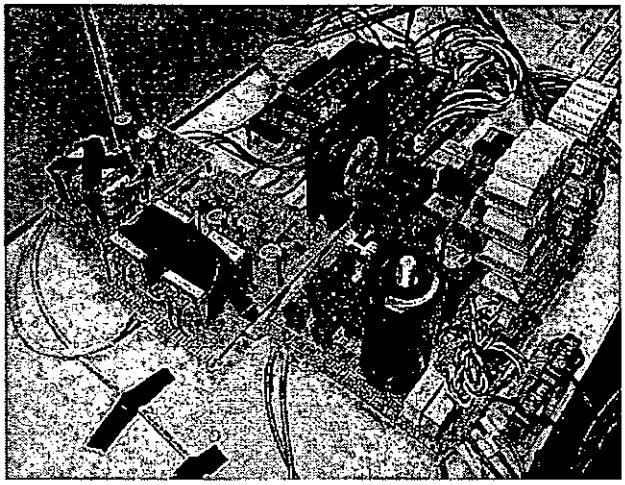

Fig. 4.18. Hardware of the active-clamped resonant converter

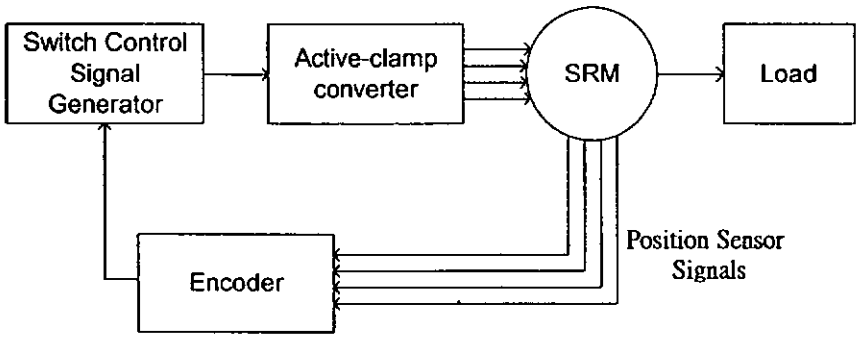

Fig. 4.19. Block diagram of SRM system in the experiment

Testing conditions and list of components of the prototype referring to Fig. 4.6 are shown in Table 4.2 and Table 4.3, respectively. As the values of the

resonant capacitors were very small, internal junction capacitors of the IGBTs were used as both C_{ra} and C_{rb}. As switching frequency of chopping transistors was high, 10kHz referring to Table 4.3, ultra-fast recovery diodes were used for all diodes in the prototype. Filtering capacitor, $C_{in,}$, was built by a 1000μF electrolytic capacitor connected in parallel with two 220nF polyester capacitors. As the ESRs of the polyester capacitors are low, they are used for filtering the high frequency noise. All clamping capacitors, C_{ca} and C_{cb}, were polypropylene capacitors providing fast response and high frequency resonance.

Measured waveforms of the prototype are shown in Fig. 4.20. The speed of the motor in this experiment was 706 rpm. Output torque of the SRM was 4.4Nm. The SRM was controlled by pulse width modulation (PWM) method. Duty ratios of the gate signals of each chopping transistors in motoring stages of their phases were 80%.

Table 4.2. Testing Conditions of the Prototype Active-clamp Converter

Description	**Values**	**Units**
Input Voltage (V_{in})	150	V DC
Maximum Mechanical Output Power for Testing	378	W
Switching Frequency of Chopping Transistors and Auxiliary Switches	10	kHz
Maximum Speed of SRM	998	rpm

Table 4.3. List of Components of the Prototype Active-clamp Converter

Components	Part Numbers	Values	Units
Q_a, Q_b, Q_{ca}, Q_{cb}, and $Q_1 - Q_4$	IRG4PC30U		
$D_1 - D_4$	MUR1660		
D_a, D_b, D_{ra} and D_{rb}	RURP1560		
D_{ca} and D_{cb}	MUR860		
C_{in}		1000.44	μF
C_{ra} and C_{rb}		73	pF
C_{ca} and C_{cb}		550	μF
L_{ra} and L_{rb}		63	μH

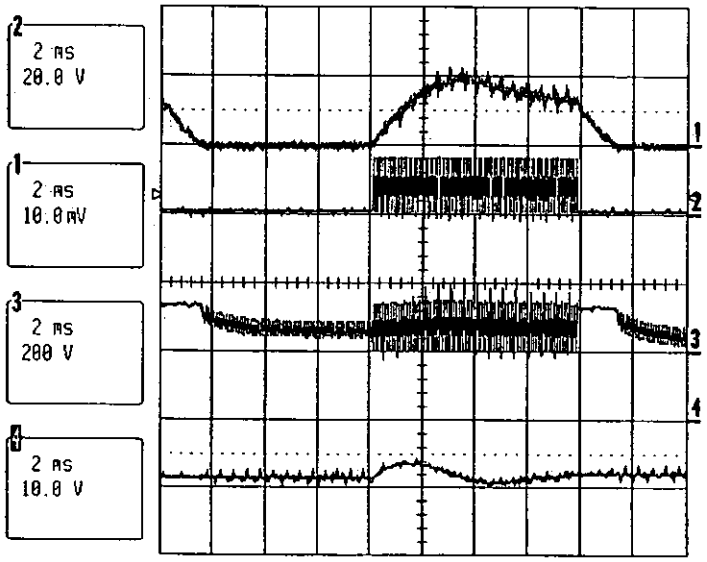

1: phase current (5A/Div); 2: gate signal of chopping transistor;

3: V_{DS} of chopping transistor; 4: v_{cc} of clamping capacitor

(a)

Fig. 4.20. Measured waveforms of obtaining chopping transistor zero-voltage switching in 706rpm 4.4Nm test

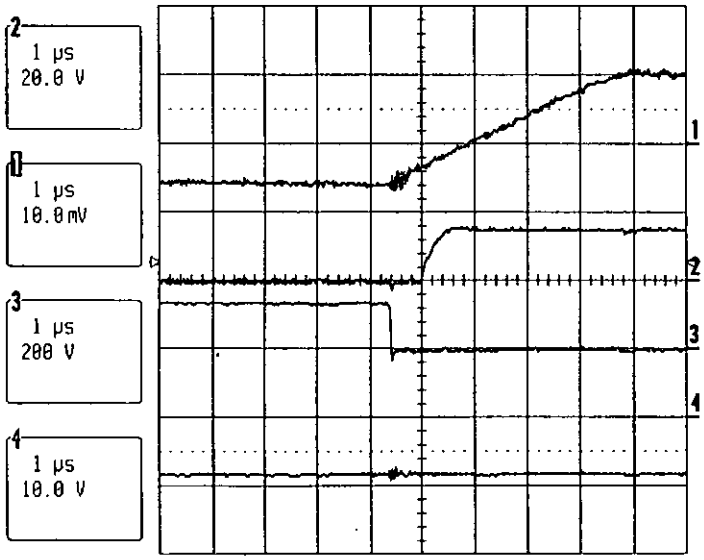

1: i_{Lr} resonant inductor current (10A/Div); 2: gate signal of chopping transistor;

3: V_{DS} of chopping transistor; 4: v_{cc} of clamping capacitor

(b)

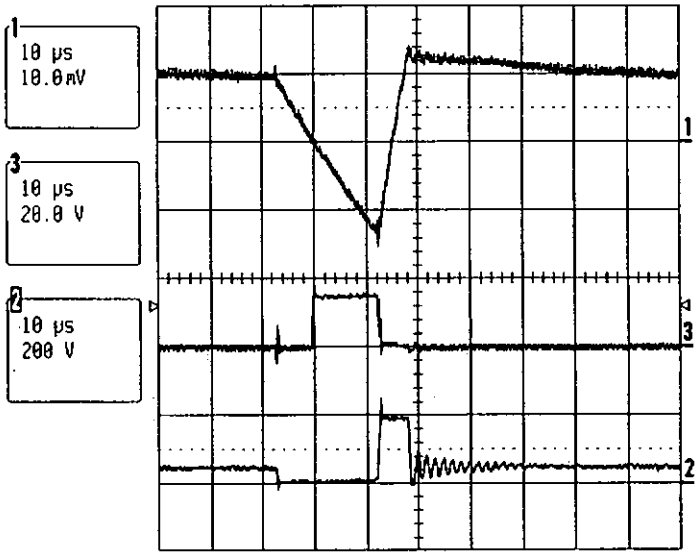

1: i_{Lr} resonant inductor current (10A/Div); 2: gate signal of auxiliary transistor;

3: V_{DS} of auxiliary transistor

(c)

Fig. 4.20. Measured waveforms of obtaining chopping transistor zero-voltage switching in 706rpm 4.4Nm test

Fig. 4.20(a) shows measured waveforms in one commutation period of Q_a.

In Fig. 4.20 (b), trace 2 shows the gate signal and trace 3 shows the drain-to-source voltage of a chopping transistor. They show that the drain-to-source voltage of the chopping transistor is zero when the transistor was switched on. The resonant inductor current, as shown in trace 1, was negative at the moment that the chopping transistor was switched on. Fig. 4.20(c) shows that the auxiliary transistor was switched on at zero-voltage when the resonant inductor current is positive. Zero-voltage switching is achieved for all high switching frequency transistors in the proposed active-clamp resonant converter.

Efficiency of the switched reluctance motor driven by the active-clamp resonant converter has been measured. The measured results are shown in Fig. 4.21 and Fig 4.22. They show that the efficiency is low at high speed. This is because inertia, friction between the rotor and the stator, and other damping factors of the motor produce mechanical losses. Another reason of this efficiency characteristic is that conduction loss due to regenerating period is higher. Details of the effect of the regenerating period of SRM will be discussed in next chapter.

The maximum measured efficiency of the motor shown in Fig. 4.22 is about 74% when the SRM operated at 378W of output power. In the experiment, operation output power of the SRM is relatively low compared with the rated power of the motor. It is common that efficiencies are the highest when the output power of the motor is close to rated power. Consequently, if the motor operates at higher output power, the efficiency of the system will be higher.

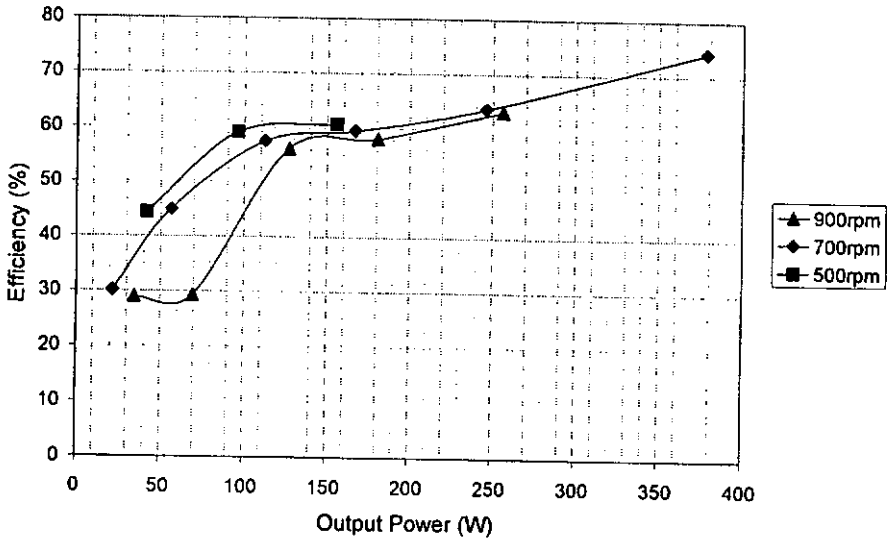

Fig. 4.21. Measured efficiency of the switched reluctance motor with active-clamp resonant converter

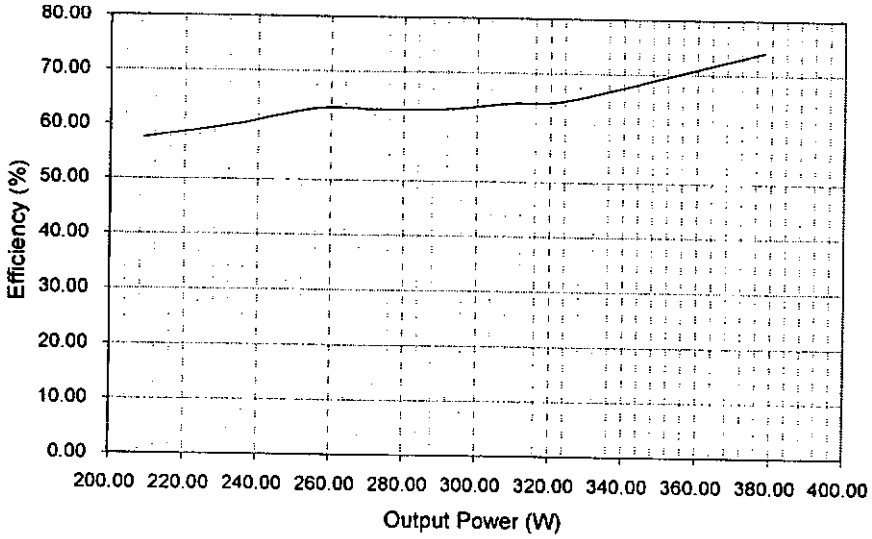

Fig. 4.22. Measured efficiency of the switched reluctance motor with active-clamp resonant converter at chopping with 80% duty ratio

4.7. Discussion

The zero-voltage switching characteristics can reduce both the switching loss and EMI of the chopping transistors. The clamping circuit can reduce the resonant voltage stress of the chopping transistors. The clamping circuit is

also a resonant circuit with the resonant inductor. The resonance is obtained by the clamping capacitor and the resonant inductor. The resonant frequency is much lower than that in the resonance with the resonant capacitor. To provide low resonant frequency, the capacitance value of the clamping capacitor is high. The clamping capacitors can be found in the photo in Fig. 4.7 and Fig. 4.8. There are two clamping capacitors built by two groups of 63V 10μF capacitors.

In the experiment, the circuit has some high voltage and current ratings IGBTs. The tested circuit was designed for the applications with higher power level than that in the experiment. In practical, transistors with lower voltage and current ratings can be used in this power level.

4.8. Summary

An active-clamp partial soft-switching converter for switched reluctance motors has been introduced. Two active-clamp circuits and two resonant tanks have been added in a conventional 2(n+1)-switch converter for 4-phase SRMs. Zero-voltage switching condition is obtained by the resonant tanks and the active-clamp circuits. Resonant voltage of the transistor is clamped by the active-clamp circuits. Switching loss and voltage stress of the chopping transistor are reduced. Principles of operation of the converter has been explained. Equations and simulation results have been provided. A prototype of the converter has been built. The prototype has been tested with a 8/6 switched reluctance motor in the experiments. Soft-switching

characteristic of the converter has been verified by computer simulation and experiments.

Chapter 5. Modification of Shapes of Commutation Current of Switched Reluctance Motor by Using Front-end Switched-capacitor Resonant Converter

5.1. Introduction

One advantage of the resonant switched-capacitor circuits discussed in the Chapter 2 and Chapter 3 is that they have simple structures. They also provide stable voltage conversion ratios without closed-loop control over a wide range of output power. Their features benefit that inverting or non-inverting fractional step-down voltage conversion ratio, or multiple step-up voltage conversion ratios can be obtained for power conditioning in easy ways. An example of their application for power conditioning is acting as front-end converters for DC motor drive. Fig. 5.1 and Fig. 5.2 show the applications of the single-stage inverting and multi-stage resonant switched capacitor converters on power conditioning for switched reluctance motor drives, respectively.

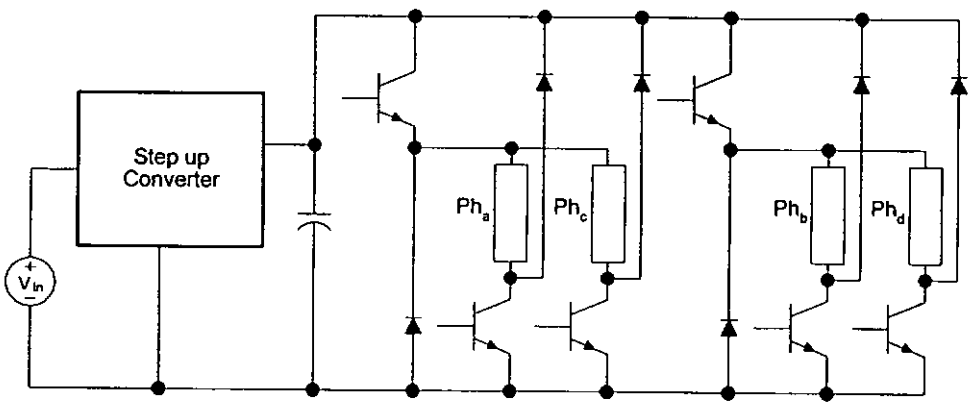

Fig. 5.1. Step-up converter for power conditioning for switched reluctance motor drive

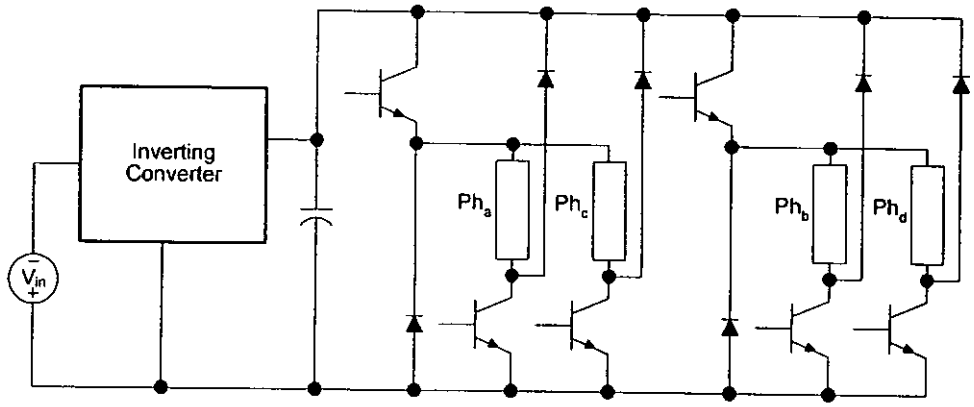

Fig. 5.2. Inverting converter for power conditioning for switched reluctance motor drive

The voltage sources of most power converters for SRM are DC voltage. For many applications, AC to DC conversion is needed to provide a DC link voltage for the SRM drive. Due to the problems of low power factor and high total harmonic distortion, bridge rectification is not suitable for converting AC voltage to AC voltage in high power applications. In this case, power factor correction (PFC) AC-DC converters are usually used to produce high DC electrical power. One of the popular topologies of PFC converter for high power applications is continuous current mode (CCM) boost converter. Its major disadvantage is that output voltage of the PFC boost converter is much higher than the input voltage to obtain high power factor. If the PFC converter is used for providing power to the DC link of a converter for SRM drives directly, the motor will suffer a higher voltage that may not be desirable. Therefore, a front-end converter for the SRM drive is needed to provide lower DC link voltage.

In regenerating mode, energy is released from the phase winding. For most SRM drives, the energy is stored in a voltage source or a capacitor. The

stored energy is re-used by other phases. For high-speed operation, efficiency of switched reluctance motor is poor [B12]. One of the reasons is that commutation current cannot decrease to zero immediately. When the rotor is close to aligned position, rate of change of inductance of the phase is very small. At this moment, the phase does not produce torque although it is conducting. The ratio of conduction loss and the mechanical output power is very small. If the speed is very high, commutation may keep conducting when the rotor is past the aligned position. The conducting phase will produce negative torque. Its mechanical power is wasted. Torque ripple of the total torque of the motor will increase [B19].

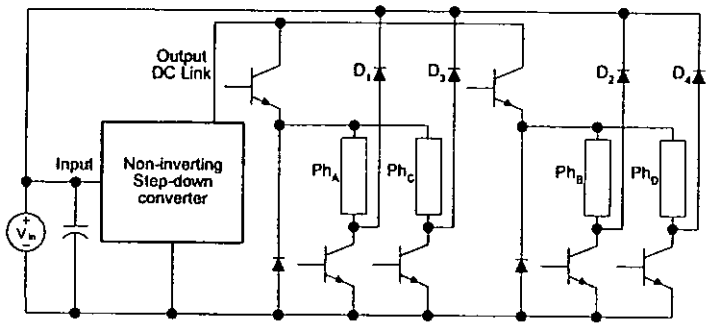

Fig. 5.3. Equivalent diagram of 2(n+1)-switch converter for switched reluctance motor drive with front-end step-down converter

In this chapter, an application of switched-capacitor zero-current switching quasi-resonant step-down converter is introduced. The switched-capacitor resonant converter is used as a front-end converter to step-down DC link voltage as shown in Fig. 5.3. To improve performance of the SRM, recovery diodes of the SRM drive, D_1 to D_4, are connected to the input of the front-end converter to decrease the duration of regenerating period of the phase by the high input voltage. Energy released from the phase in the regeneration can be stored in

the capacitor of the input of the front-end converter and used for driving the motor. Purely power factor correction converter as the front-end converter has not been considered in this study as the techniques are well known and has been proposed by other literatures.

5.2. Implementation of High Power Switched-capacitor Resonant Converter

Chapter 2 has introduced two families of single-stage switched-capacitor zero-current switching quasi-resonant step-down converters. Because of the high efficiency and simple structure, the non-inverting switched-capacitor step-down converters are suitable as the front-end converter shown in Fig. 5.4. Computer simulation and experiments of the front-end converter will be described in the following sections.

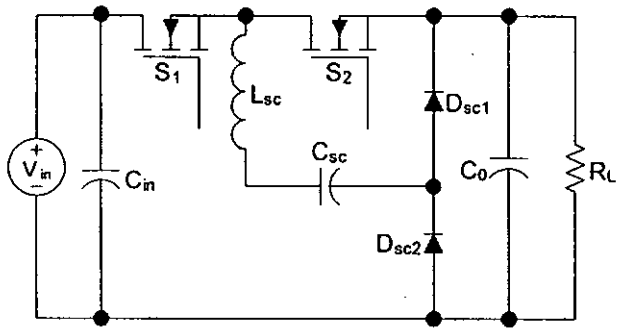

Fig. 5.4 Circuit diagram of the prototype of 1/2-mode switched-capacitor resonant front-end converter

5.2.1. Prototype of the Front-end Converter

A prototype of the 1/2-mode non-inverting switched-capacitor zero-current switching quasi-resonant step-down converter has been built for experiments. Fig. 5.5 shows the photo of the prototype converter. Specification of the circuit and list of components are shown in Table 5.1 and Table 5.2, respectively. For storing energy released from the phase windings of the SRM in the regenerating stage, a large capacitor, C_{in}, was added in the input of the front-end converter.

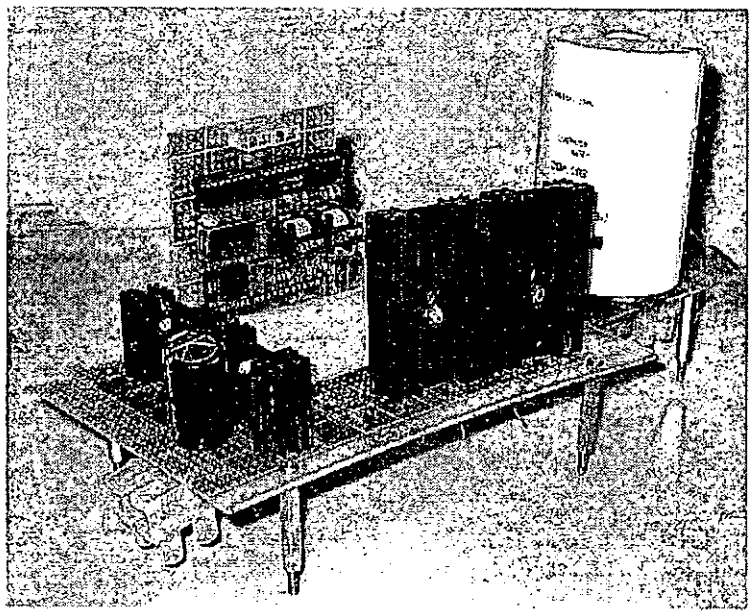

Fig. 5.5 Prototype of 1/2-mode switched-capacitor resonant front-end converter

Table 5.1. Specification of Prototype of 1/2-mode Switched-capacitor Resonant Front-end Converter

Descriptions	Values	Units
Input Voltage	300	V DC
Expected Output Voltage	150	V DC
Switching Frequency	125	kHz
Maximum Testing Output Power	517	W

Table 5.2. List of Components Prototype of 1/2-mode Switched-capacitor Resonant Front-end Converter

Descriptions	Model Numbers	Values	Units
S_1 and S_2	IRF840		
D_{sc1} and D_{sc2}	MUR860		
C_{sc}		0.47	μF
C_{in}		470	μF
C_0		33	μF
L_r		1	μH

5.2.2. Computer Simulation and Experimental Results

The 1/2-mode switched-capacitor zero-current switching quasi-resonant front-end converter with the same values of capacitors and resonant inductor shown in Table 5.2 were simulated by a computer simulation programme. In the simulation, ideal components of all diodes and transistors were applied. The simulation waveforms are shown in Fig. 5.6.

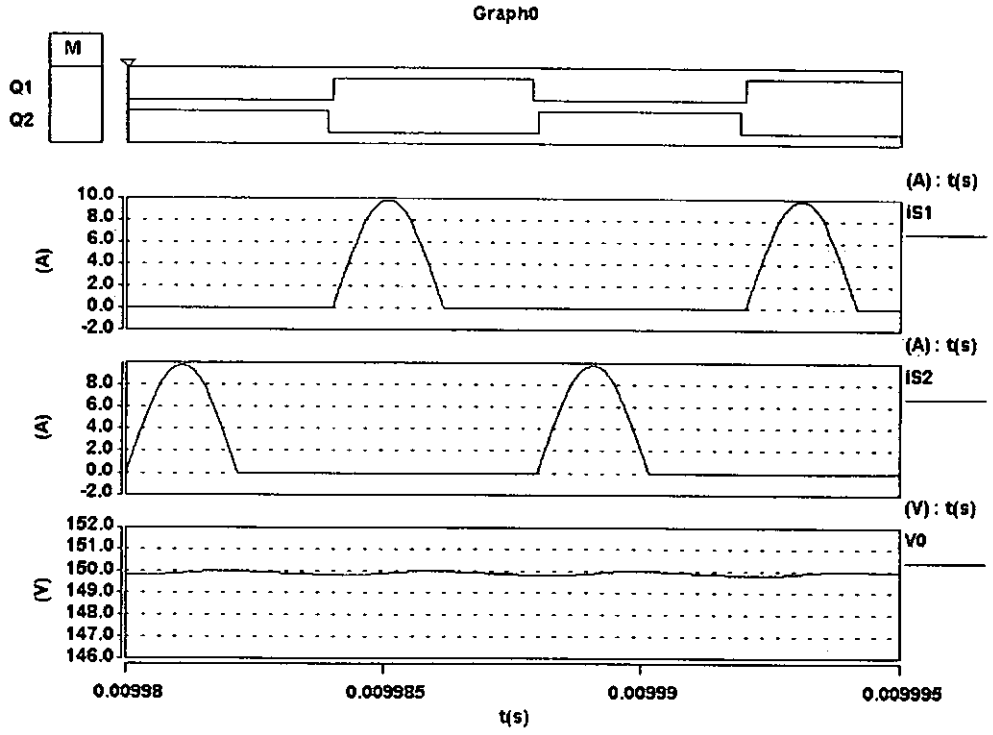

Fig. 5.6. Simulation result of 1/2 mode switched-capacitor resonant front-end converter with 500W output voltage

Waveforms measured in an experiment of the front-end converter with 300W output power are shown in Fig. 5.7. From both computer simulation results and experimental results, all transistors are switched on and off under zero-current switching condition. Switching loss of the transistor can be reduced by this characteristic. In Fig. 5.7 (a) and (b), there are some current transients in the transistor current, i_{S1} and i_{S2}, because junction capacitor of one transistor was charged when another transistor was switched on. Further verification of low switching loss in the transistors by measured v-i trajectories in the experiment is shown in Fig. 5.8.

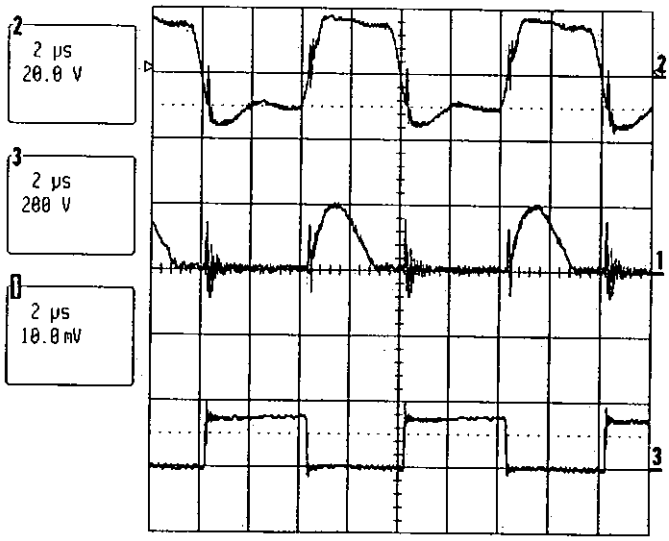

2: Gate signal of S_1

1: Drain current of S_1,i_{S1}, (5A/div)

3: Drain to source voltage of S_1, v_{S1}

(a)

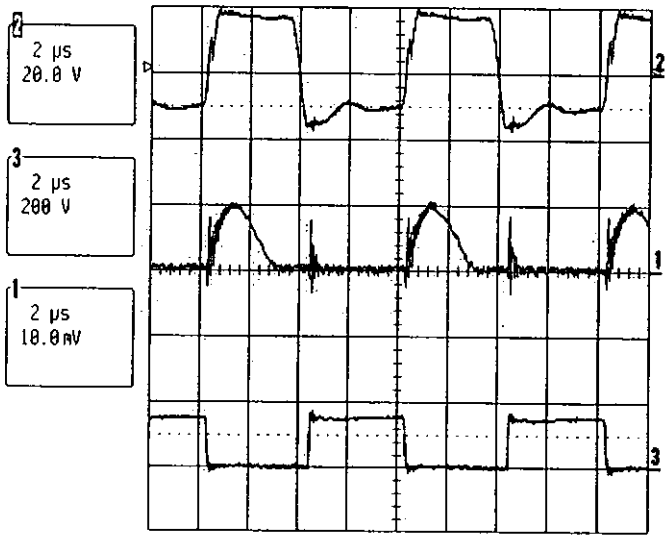

2: Gate signal of S_2

1: Drain current of S_2, i_{S2}, (5A/div)

3: Drain to source voltage of S_2, v_{S2}

(b)

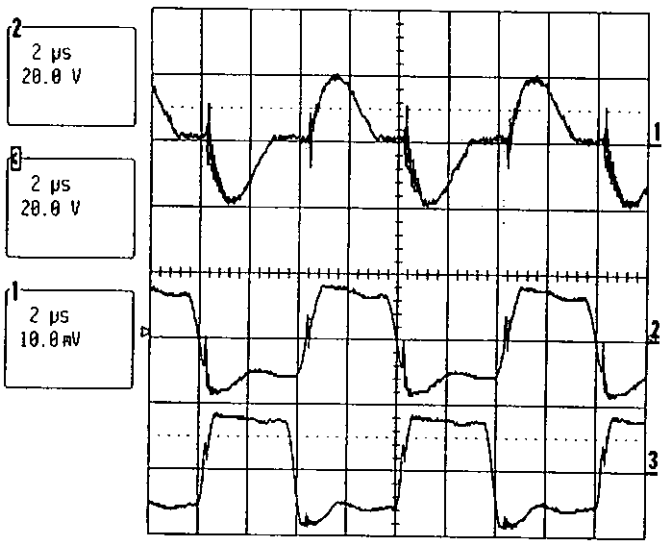

1: Inductor current, i_{Lsc} (5A/div)

2: Gate signal of S_1

3: Gate signal of S_2

(c)

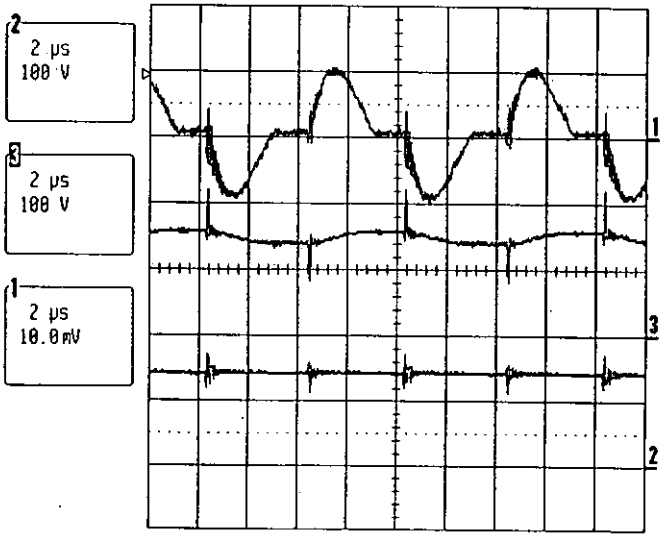

1: Inductor current, i_{Lsc}, (5A/div);

2: Switched capacitor voltage, v_{csc}

3: Output voltage, V_0

(d)

Fig. 5.7 Measured waveforms of the prototype of 1/2-mode switched-capacitor resonant front-end converter

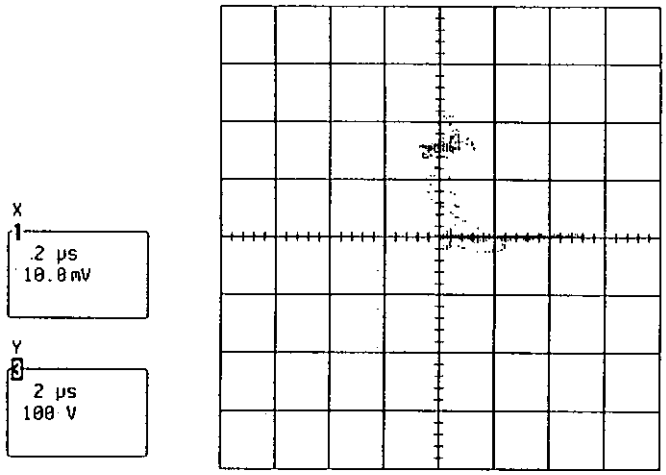

X-axis: i_{S1} (2A/div)

Y-axis: v_{Sc1}

(a) v-i trajectory of S_1

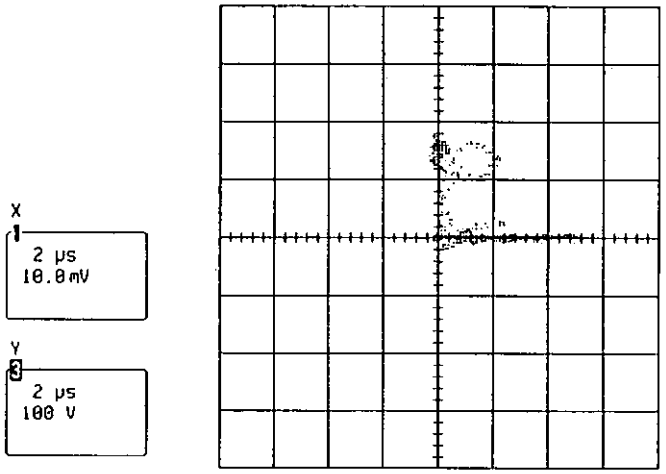

X-axis: i_{S2} (2A/div)

Y-axis: v_{Sc1}

(b) v-i trajectory of S_2

Fig. 5.8 Measured v-i trajectories of the prototype of 1/2-mode switched-capacitor resonant front-end converter

Efficiency and output voltage of the prototype were measured in the testing. The graphs of these characteristics are shown in Fig. 5.9 and Fig. 5.10, respectively. The maximum tested output power was 517W. The figure

shows that the efficiency of the circuit was over 90% if its output power was over 30W. The circuit obtains this high efficiency because the zero-current switching techniques reduce the switching loss of the transistors. Also, comparing with hard-switching counterpart, the half-sinusoidal manner charging and discharging current much reduces the current stress of the switched-capacitor so that the conduction loss of the ESR of the switched-capacitor is reduced. Similar to the switched-capacitor resonant converters described in the previous chapters, the efficiency of the converter is relatively low at light load because the influence of the forward bias voltage of the diodes to the efficiency is high. The efficiency also decreases slightly from the peak efficiency when the output power increases. The experimental results also show that the output voltage of the converter decreased when the load increased due to conduction loss, but the variation is small. The measured output voltage was 141V DC at 517W output power. The voltage drop was less than 6 % in this high power condition.

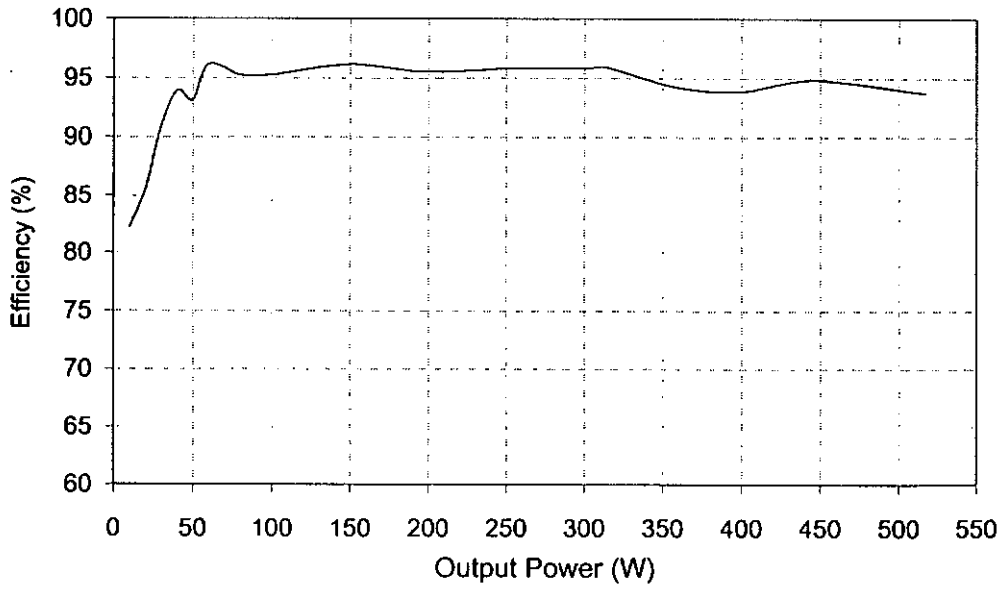

Fig. 5.9. Measured efficiency characteristics of the prototype of 1/2-mode switched-capacitor resonant front-end converter

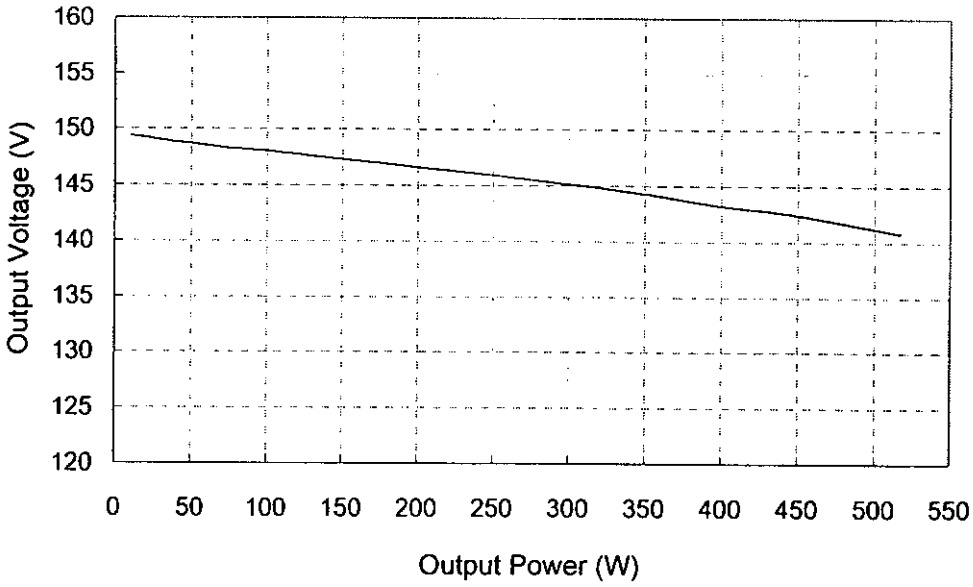

Fig. 5.10. Measured output voltage of the prototype of 1/2-mode switched-capacitor resonant front-end converter

5.3. Modification of Recovery Commutation Current with Front-end Converter

In the regeneration stage of the switched reluctance motor, both commutation transistor and chopping transistor of the phase are switched off. Both the recovery diode and the free-wheeling diode are in forward bias so that a negative voltage is applied to the phase for de-energising the phase. Per-phase equivalent circuit of an SRM in regeneration stage is shown in Fig. 5.11. V_S is the recovery voltage of the phase. L_a is the inductance, R_a is the winding resistance, and E_b is the back electromotive force of the phase. C_S is a large capacitance for storing energy from the motor in regenerating stage.

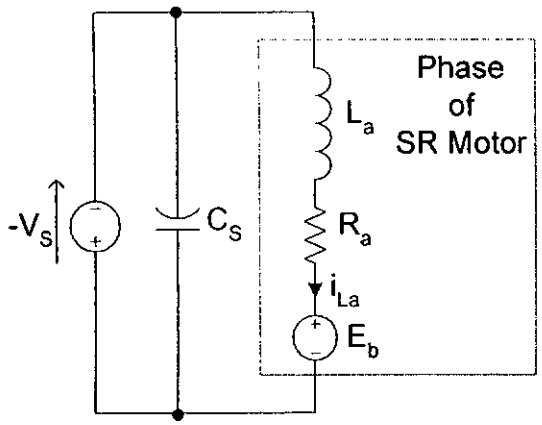

Fig. 5.11. Per-phase equivalent circuit of switched reluctance motor in regenerating stage

Circuit diagram of the proposed SR-motor active-clamp resonant drive system with a front-end converter and high recovery voltage is shown in Fig. 5.12. The front-end converter is a 1/2-mode switched-capacitor zero-current switching quasi-resonant converter. Output voltage of the front-end converter, V_0, is a DC link voltage of the SRM drive. In practice, V_0 is approximately equal to $1/2V_{in}$. Both MOSFETs, S_1 and S_2, in the front-end converter are under zero-current switching. IGBTs, Q_a, Q_b, Q_{xa} and Q_{xb}, in the converter for SRM are under zero-voltage switching. Referring to Fig. 5.11, recovery voltage of the SRM, $-V_S$, is equal to $-V_{in}$ and hence, a voltage higher than DC link voltage for the motor is applied for regenerating stage of each phase to modify their commutation current waveforms. Mathematical analysis and computer simulation of the modification of commutation current are shown in the following sections.

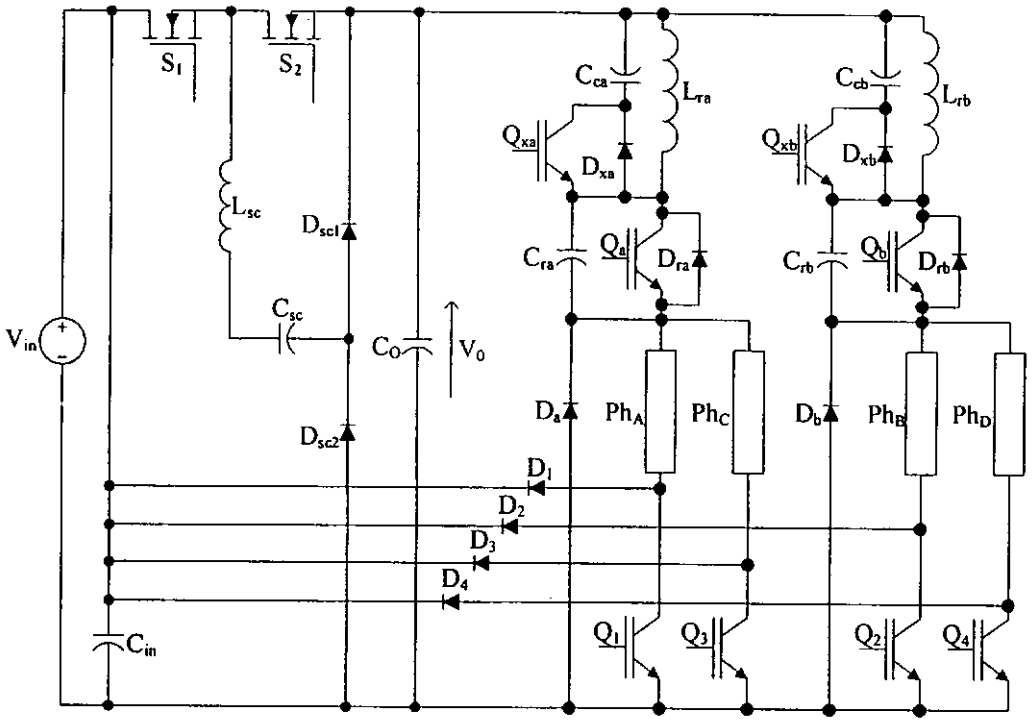

Fig. 5.12. Circuit diagram of switched reluctance motor active-clamp resonant drive with 1/2-mode switched-capacitor zero-current switching front-end converter

5.3.1. Mathematical Analysis

According to Fig. 5.11,

$$-V_S = L_a \frac{di_{La}}{dt} + R_a i_{La} + E_b \tag{5.1}$$

and the back EMF is:

$$E_b = i_{La} \frac{\partial L_a(\theta)}{\partial t} \tag{5.2}$$

Substituting the E_b in the equation (5.2) to the equation (5.1) gives:

$$\frac{di_{La}}{dt} = \frac{V_S - i_{La}\left(R_a + \dfrac{\partial L_a(\theta)}{\partial t}\right)}{L_a(\theta)} \tag{5.3}$$

and

$$\theta = \omega_m t \tag{5.4}$$

where θ is rotor angular position and ω_m is rotor angular speed.

From equation (5.3) is observed that rate of change of current will be more negative if V_S is higher. In Chapter 4, equations of the inductance of all phases were found in equations (4.8) to (4.11). By substituting these inductance equations to equation (5.3), and defining initial value of phase current in regenerating stage, the commutation current of all phases of the SRM is estimated.

Fig. 5.13 shows a per-phase equivalent circuit of regenerating stage of an SRM in another format. The figure shows that in regenerating stage, the phase winding de-energises through D_1 and D_a to the voltage source. Flowing of the commutation current leads to conduction losses due to the forward voltage of the diodes, resistance of copper wires, and phase resistance of the phase winding.

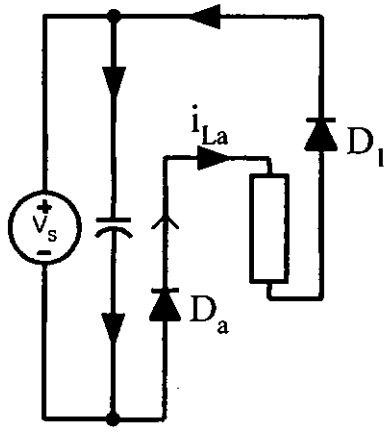

Fig. 5.13. Per-phase equivalent circuit of regenerating stage

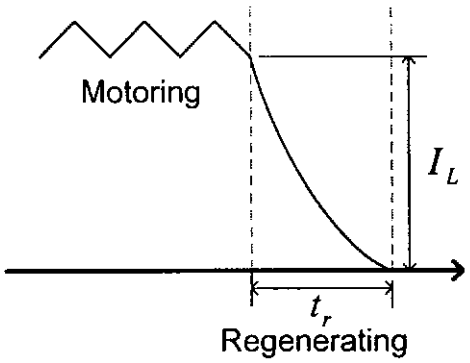

Fig. 5.14. Waveform of commutating current

Referring to the diagram of commutation current of the phase winding shown in Fig. 5.14, I_L is the initial value of commutation current of the phase winding in regenerating stage. Let forward V_F be the forward voltage of the diodes, N_r be the number of pole pairs, and N_y be the number of strokes of the SRM, power loss in regenerating stage is:

$$P_r = \frac{N_r N_y \omega_m}{2\pi}\left(V_F \int_0^{t_r} i_{La} dt + R_a \int_0^{t_r} i_{La}^2 dt \right) \tag{5.5}$$

5.3.2. Computer Simulation

Computer simulation of commutating current in an active-clamp resonant switched reluctance motor drive was done. Fig. 5.15 is the circuit diagram for the computer simulation. As it had been evident by both experiments and computer simulation that the switched-capacitor resonant front-end converter can give the desired results with output power up to 500W, ideal voltage sources with voltage V_{in} and $2V_{in}$ were used to represent output and input voltage of the front-end converter in this computer simulation, respectively.

A comparison of the commutation current between the circuits shown in Fig. 4.5 from Chapter 4 and Fig. 5.15 are shown in Fig. 5.16 and Fig. 5.17. In the figures, Pha represents the time of motoring stage of the phase winding. La is the inductance of the phase winding. iLa_mod and iLa are the current of the phase winding with and without modification, respectively. The computer simulation results show that the duration of regenerating stage of SRM is shorter after adding the commutation current modification front-end converter.

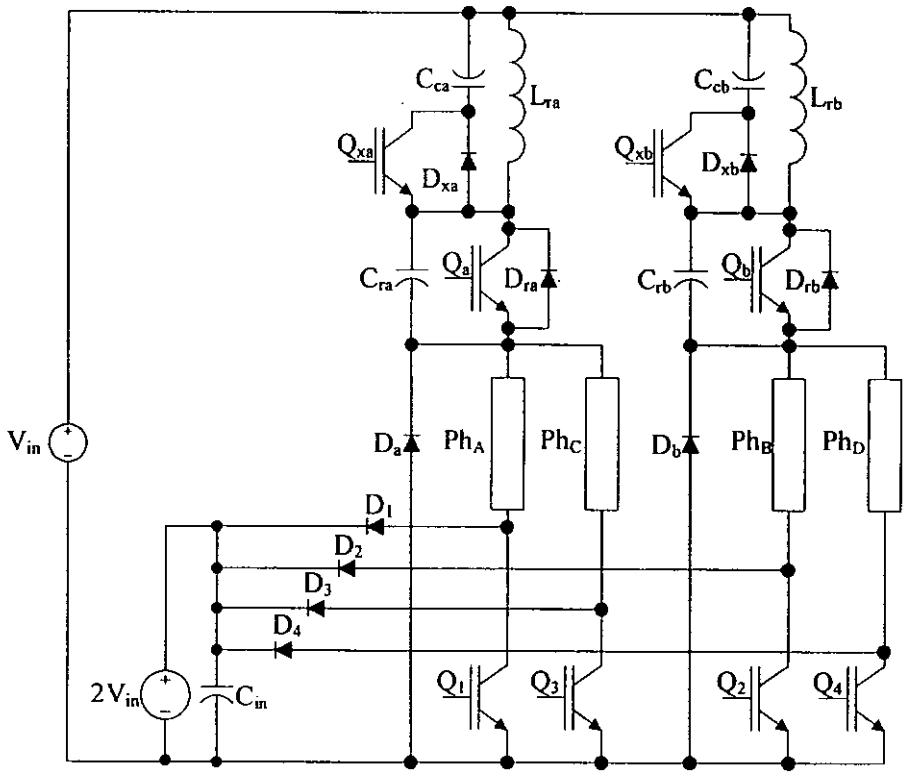

Fig. 5.15. Circuit diagram of modified switched reluctance motor active-clamp resonant drive for computer simulation

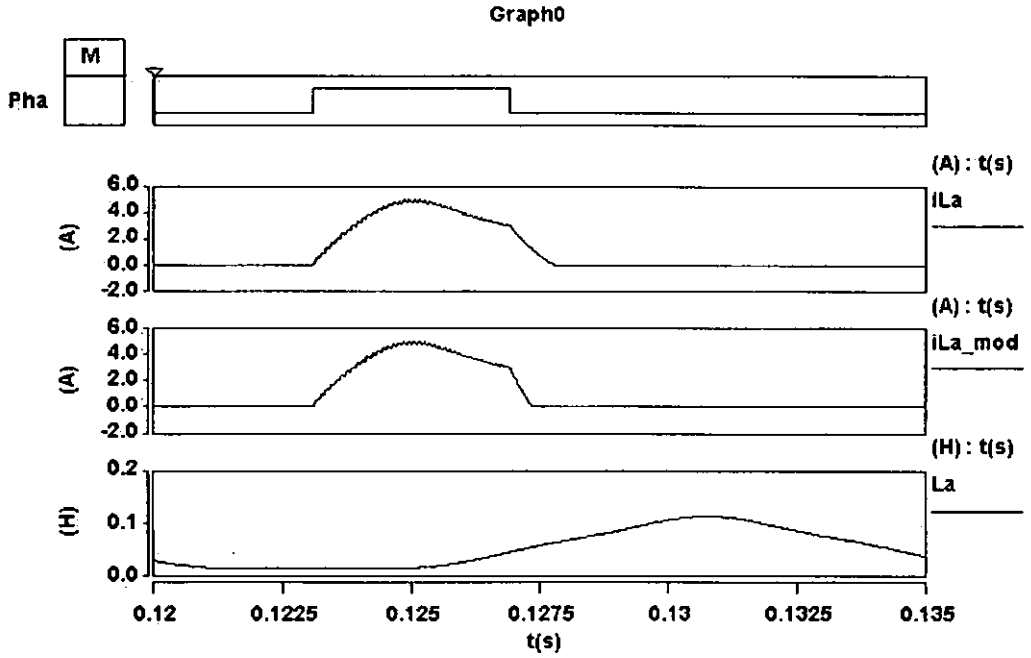

(a)

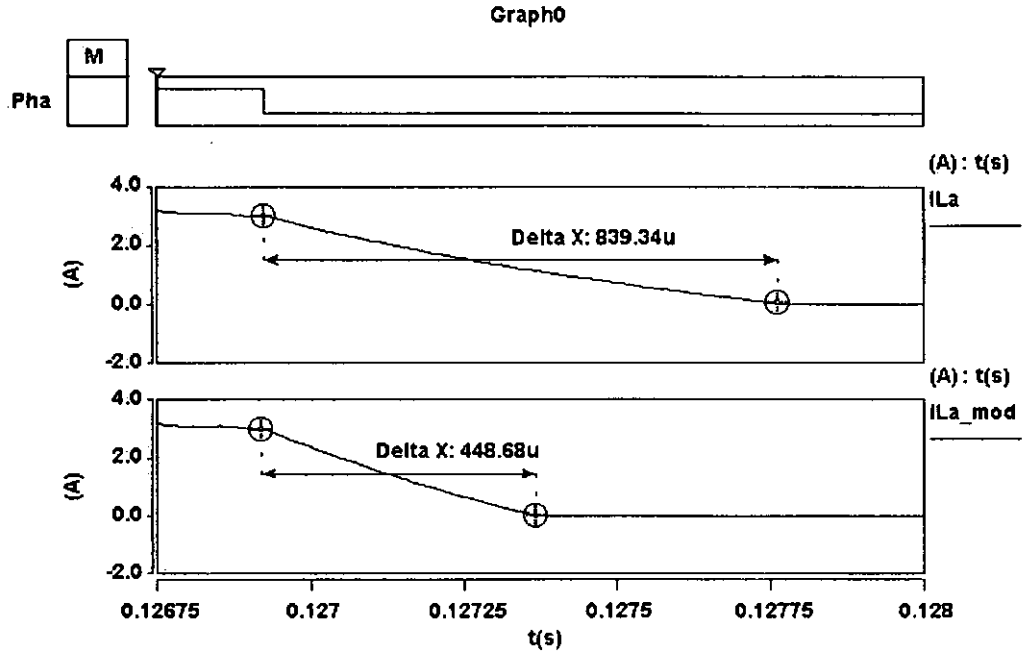

(b)

Fig. 5.16. Simulation results of commutation current of switched reluctance motor at 650 rpm of speed

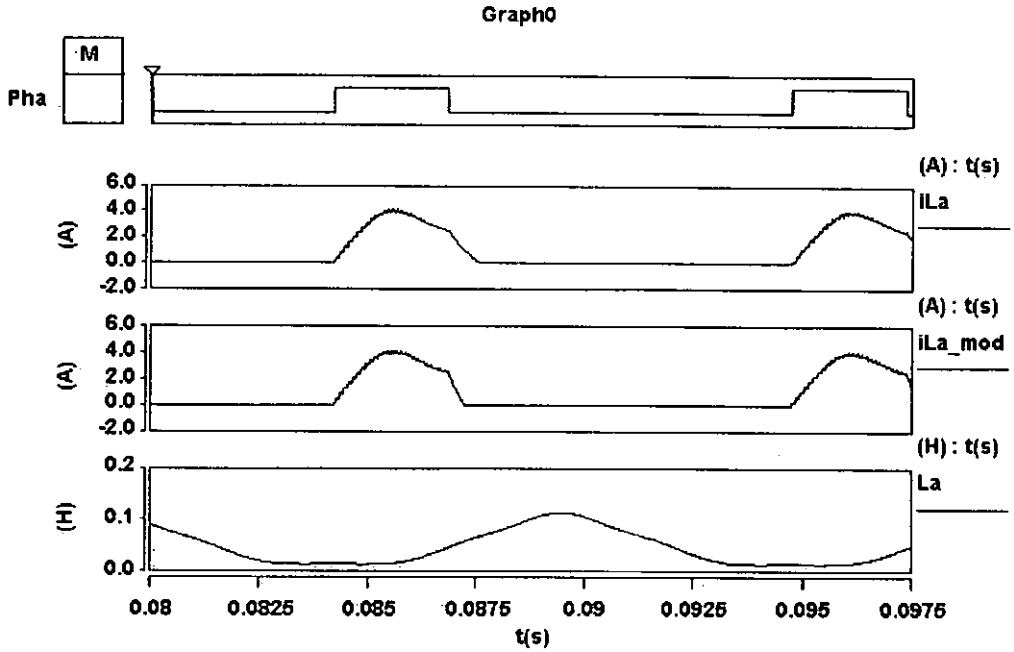

(a)

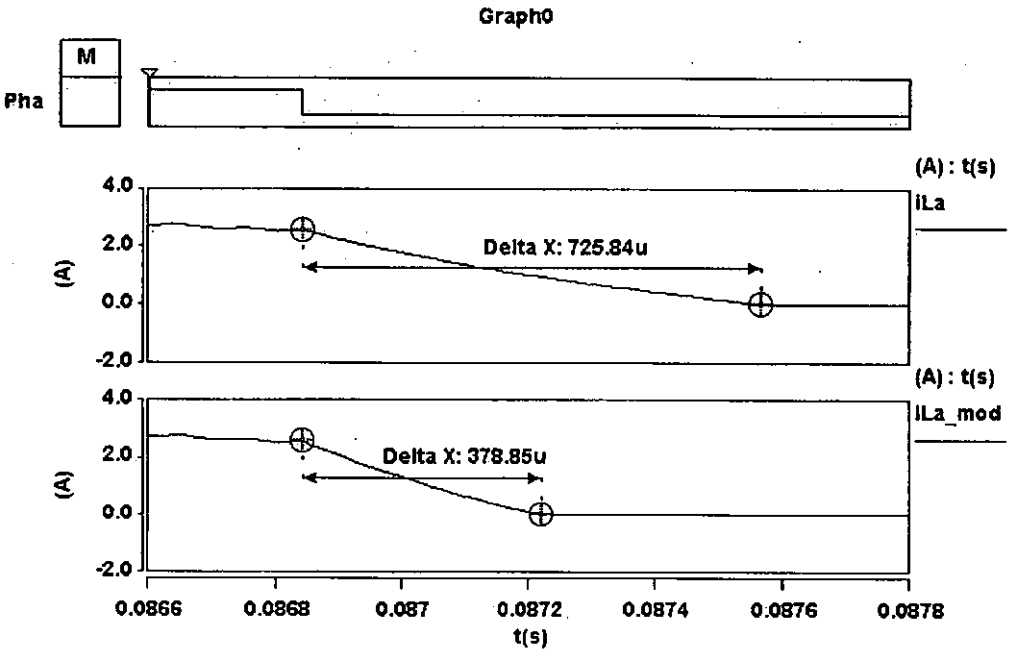

(b)

Fig. 5.17. Simulation results of commutation current of switched reluctance motor at 950 rpm of speed

5.4. Experimental Results

5.4.1. Performance of Switched Reluctance Motor Drive with Front-end Converter

A switched-reluctance motor drive system with an active-clamp resonant converter and a 1/2-mode switched-capacitor zero-current switching quasi-resonant front-end converter has been built. A photo of the system is shown in Fig. 5.18.

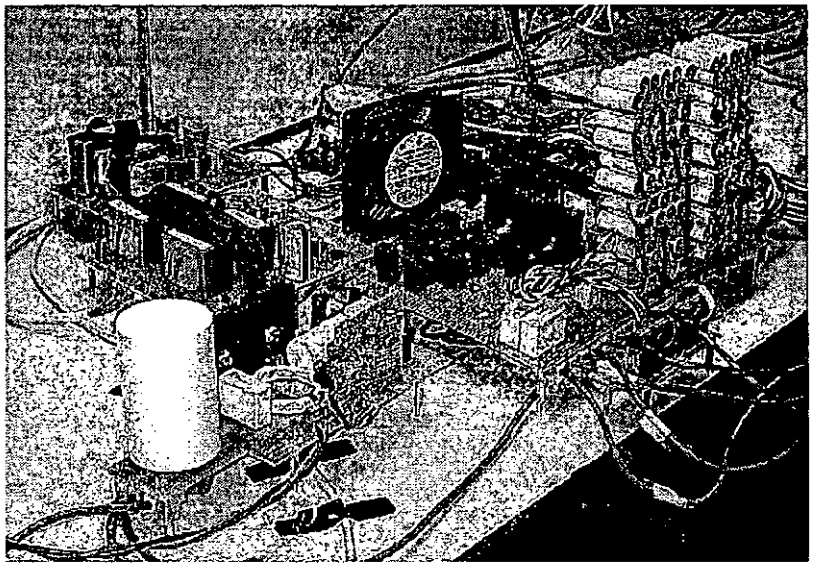

Fig. 5.18. Photo of Soft-switching Switched Reluctance Motor Drive for Commutation Current Modification

The performance of the SRM drive system was tested in the experiment. The system is the same as the circuit diagram shown in Fig. 5.12 in Section 5.3. The active-clamp resonant converter and the switched-capacitor resonant front-end converter in the system are the same as the circuits discussed in Section 4.6 and 5.2.2, respectively, except C_{in} of the active-clamp resonant converter was

removed. Measured waveforms of the active-clamp resonant converter and those of the switched-capacitor resonant front-end converter are shown in Fig. 5.19 and Fig. 5.20, respectively. Input voltage of the front-end converter is 300V DC. Maximum output power in the experiment is 258W when the speed of the SRM is 700 rpm.

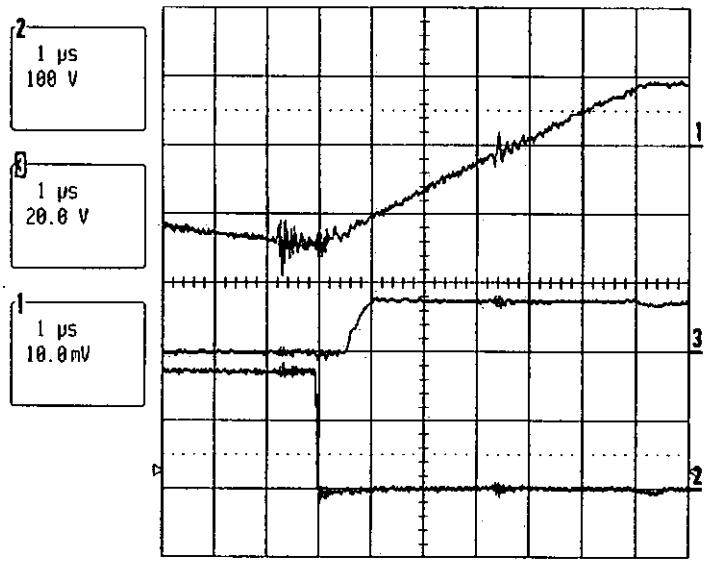

1: i_{Lr} resonant inductor current (10A/Div);

2: gate signal of chopping transistor;

3: v_{DS} of chopping transistor

(a)

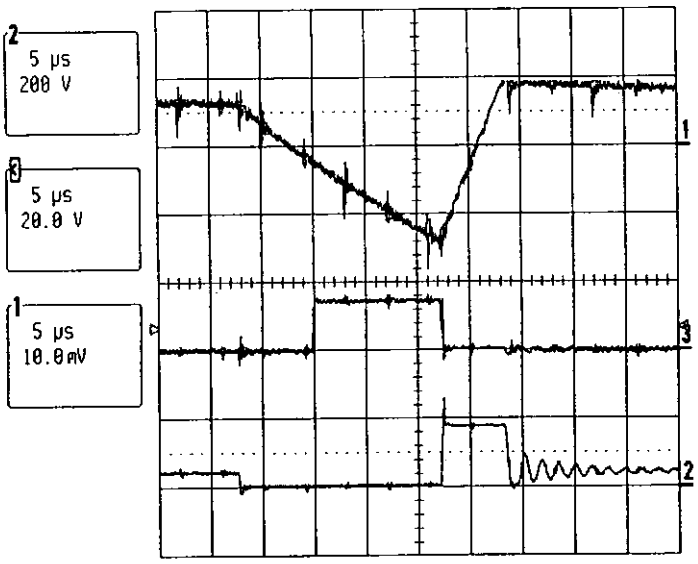

1: i_{Lr} resonant inductor current (10A/Div);

2: gate signal of auxiliary transistor;

3: v_{DS} of auxiliary transistor

(b)

Fig. 5.19. Waveforms of transistors of the active-clamp resonant converter obtaining zero-voltage switching in SRM drive system with front-end converter

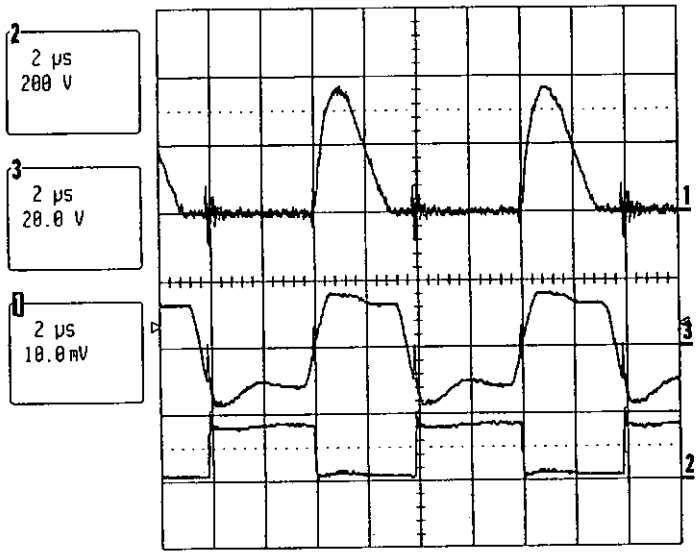

1: current of S_1 (5A/div);

2: v_{ds} of S_1;

3: gate signal of S_1

(a)

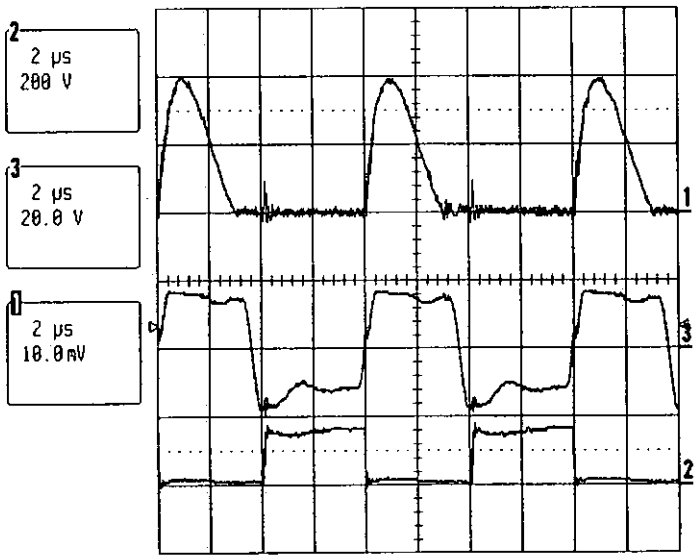

1: current of S_1 (5A/div);

2: v_{ds} of S_2;

3: gate signal of S_2

(b)

Fig. 5.20. Measured waveforms of the switched-capacitor resonant front-end converter obtaining zero-current switching in SRM drive system

Fig. 5.19 shows the waveforms of a chopping transistor and an auxiliary transistor in the active-clamp resonant converter. From the figure, both the chopping transistor and the auxiliary transistor are switched on when their drain-to-source voltage is zero. Fig. 5.20 shows the waveforms of both transistors in the switched-capacitor resonant front-end converter. Both transistors are switched off when their current is zero. These measured waveforms imply that the soft-switching characteristics in the SRM drive system discussed in previous chapters have not been influenced by the commutation current modification characteristic.

Measured efficiency of the SRM drive system is shown in Fig. 5.21. The

graph shows that when the power is higher, the rise of efficiency of the SRM system at higher speed is greater. It is evident that the SRM system can improve the electrical performance of the motor at high speed. More experimental results of the modified commutation current characteristic of switched reluctance motor will be discussed in the next section.

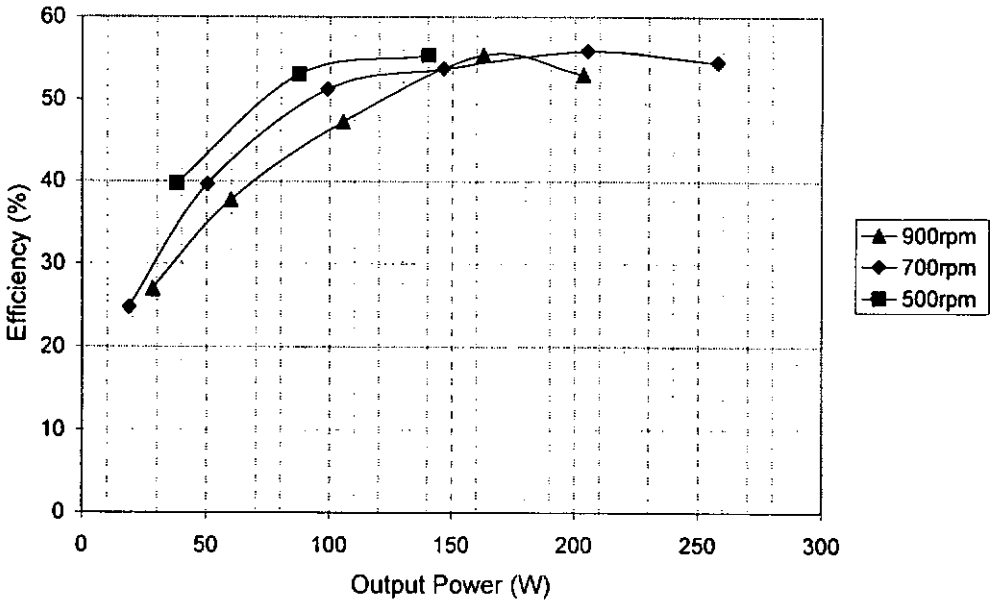

Fig. 5.21. Measured efficiency of soft-switching switched reluctance motor drive for commutation current modification

5.4.2. Comparison of Commutation Current in Different Switched Reluctance Motor Drive Systems

The experimental results of the active-clamp resonant switched reluctance motor drive with switched-capacitor resonant front-end converter were compared with the results of the stand-alone active-clamp resonant converter. In the experiment, the same SRM was used for both drive systems. The waveforms of the commutation current of these drive systems measured at the operation of 900 rpm and 150W are shown in Fig. 5.22 and Fig. 5.23. Using the proposed

circuit, the duration of regenerating stage of the SRM decreased fro 1.1ms to 0.55ms. It is clear that the SRM commutation current in regeneration stage was significant improved.

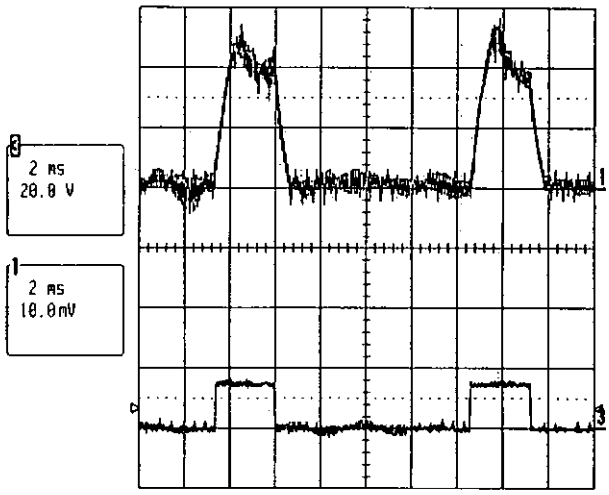

(a) Modified commutation current

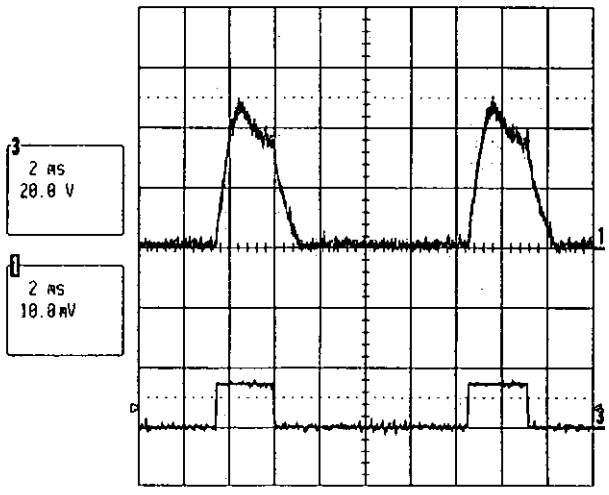

(b) Typical commutation current

1: Commutation of a phase (2A/div)

3: gate signal of the commutating transistor

Fig. 5.22. Measured waveforms of commutation current of switched reluctance motor

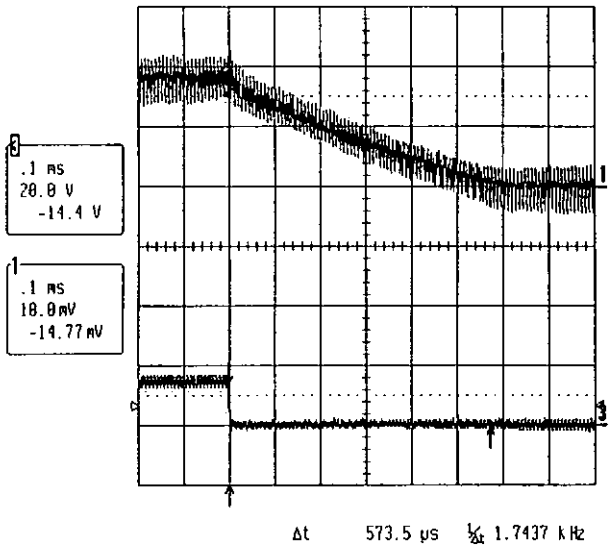

(a) Modified Commutation Current

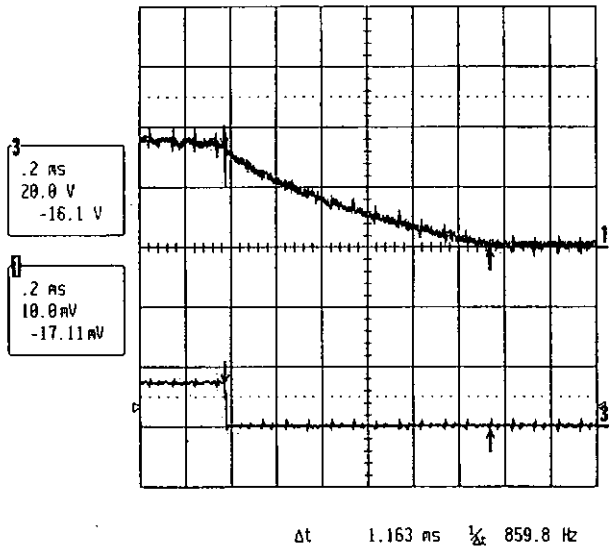

(b) Typical Commutation Current

1: Commutation of a phase (2A/div); 3: gate signal of the commutating transistor

Fig. 5.23. Measured commutation current of regenerating stage of switched reluctance motor

Fig 5.22 shows the efficiency of the SRM system with different operating Speed. Fig 5.22(a), (b) and (c) show the measured efficiency when the speed of the SRM was at 500 rpm, 700 rpm and 900 rpm, respectively.

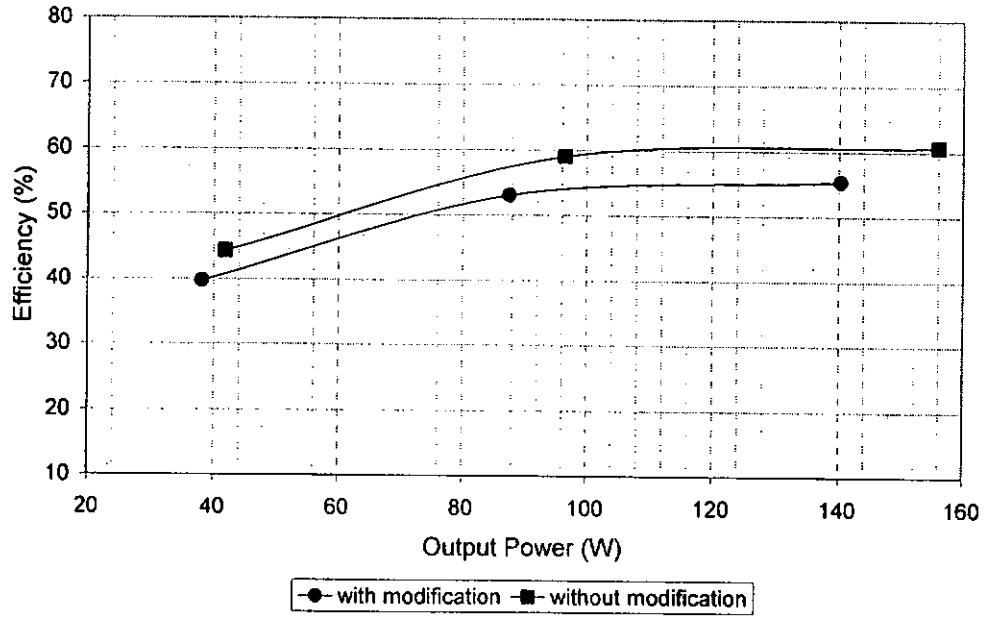

(a) At 500 rpm

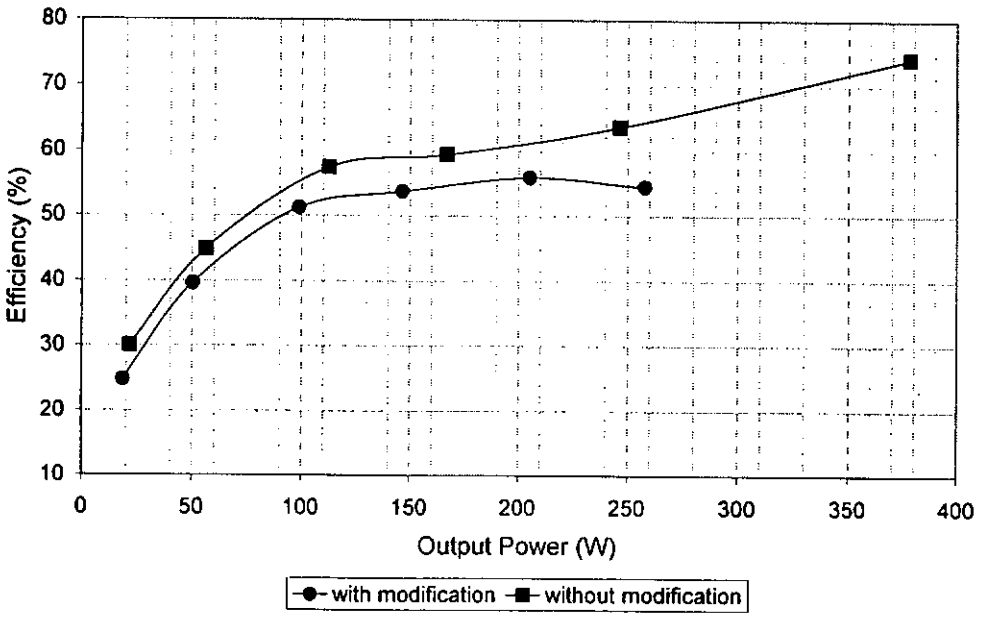

(b) At 700 rpm

Fig. 5.24. Comparison of efficiencies of the switched reluctance motor drive systems

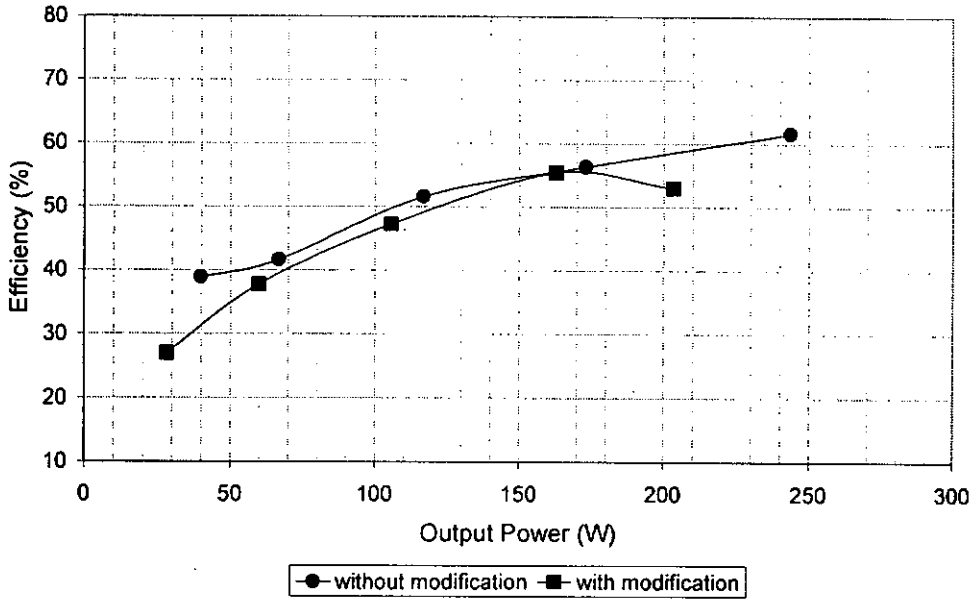

(c) At 900 rpm

Fig. 5.24. Comparison of efficiencies of the switched reluctance motor drive systems

Fig. 5.24 shows the comparison of the efficiency characteristics of the stand-alone circuit and the modified circuit. The results in Fig. 5.24 (a) to Fig. 5.24 (c) show that the efficiency of the modified circuit is lower than that of the stand-alone circuit although the commutation current shape has been modified confirmed by Fig. 5.22 and Fig. 5.23.

5.5. Discussion

In the whole proposed SRM drive system, there are in a total of two electrical power conversion stages by the resonant switched-capacitor converter and the resonant SRM drive. It is normal that the more power conversion stages, the system has higher power loss. As a result, the experimental results shown in Section 5.4 show that the efficiency of the modified circuit is lower than that of the stand-alone circuit although the current waveform of the

modified circuit has been modified to be the expected manner.

According to the efficiency characteristic of the high power resonant switched-capacitor converter shown in Section 5.22, the efficiency of the converter decreases from the peak efficiency when the output power increases. This efficiency decreasing characteristic influences the modified circuit that the differences of the measured efficiencies of the circuits are bigger while the output power increases.

Both the measured efficiencies of the modified circuit and the stand-alone circuit are quite low. It is because the power level in the experiment was only about 10% of the power rating of the SRM.

The SRM used in the experiment is an 8/6 4-phase motor. The firing angle and the dwell angle of the SRM drive in the experiment are 0° and 15°, respectively. In other word, the phase winding starts demagnetizing when the rotor position is at 15°. This position is too far from the aligned position that the modified commutation current cannot benefit the SRM. It is possible that the modified circuit may improve the efficiency in long dwell angle operation, in the SRM with fewer poles, such as 3-phase 6/4 SRM. Fig. 5.25 and Fig. 5.26 show the per-phase simulation result of a 3-phase 6/4 SRM operating with long dwell angle, 0° firing angle and 144° dwell angle, without commutation current modification and with commutation current modification, respectively. The speed of the SRM is 1500 rpm. The resistance of each phase winding is 0.8Ω. Considering the SRM has no mechanical power loss and iron loss, the

mechanical output power of the SRM is 3577.28W in both simulated conditions.

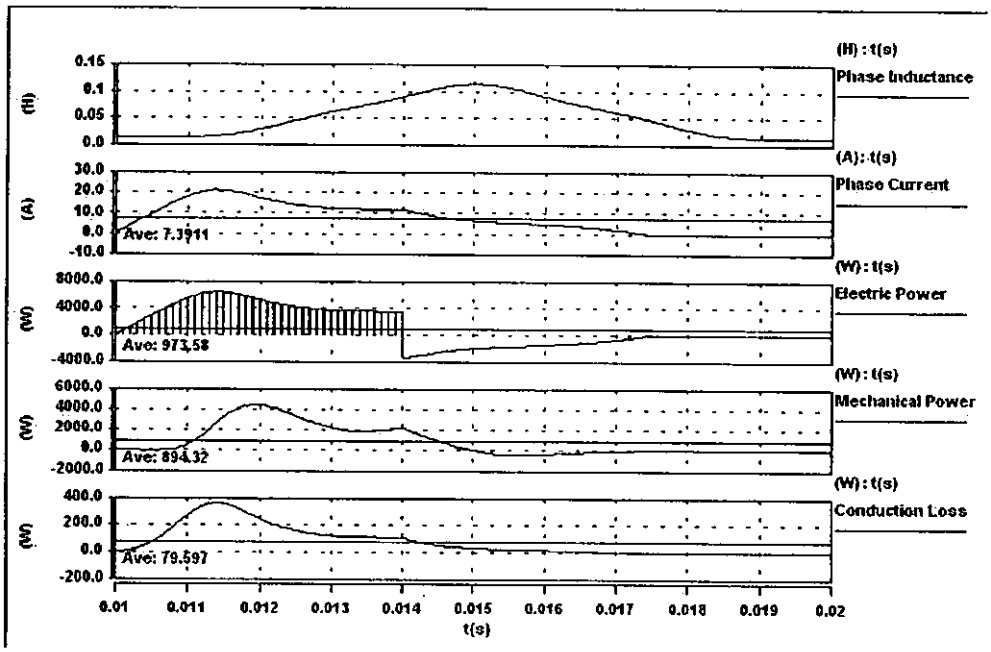

Fig. 5.25 Per-phase simulation results of a 3-phase 6/4 switched reluctance motor with long dwell angle without commutation current modification

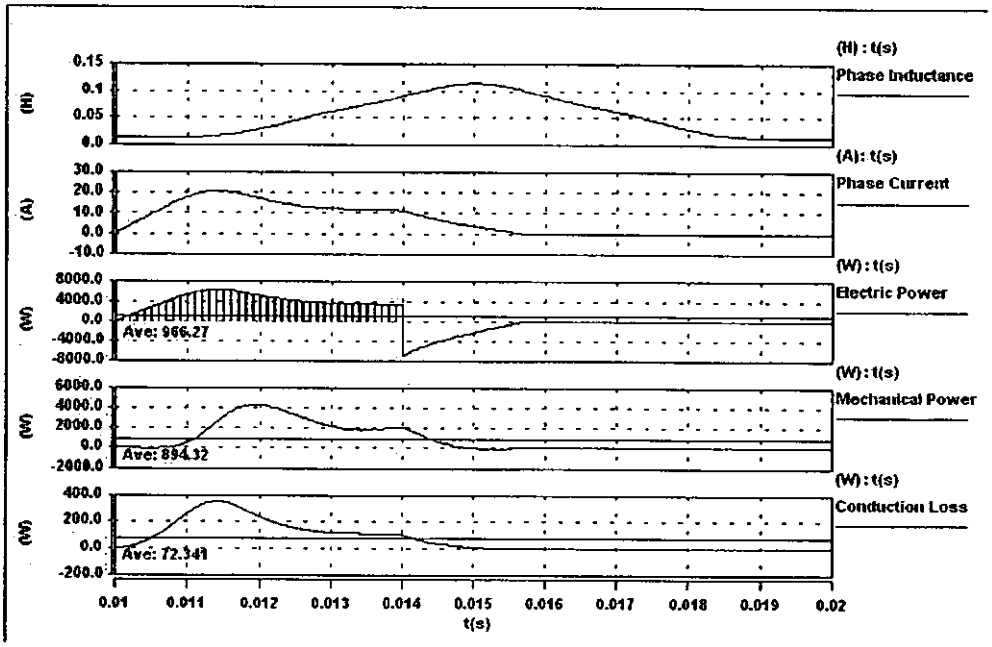

Fig. 5.26 Per-phase simulation results of a 3-phase 6/4 switched reluctance motor with long dwell angle with commutation current modification

Referring to Fig. 5.25 and Fig. 5.26, these simulation results show that the efficiency of the SRM from electric power converting to mechanical power is 91.86% in the condition without commutation current shape modification while the efficiency is 92.55% in the condition with commutation current shape modification. The results show that the commutation current modification method improves the efficiency of the SRM. This is because this method reduces the conduction loss of the phase windings and the negative torque due to the flowing of the phase current when the rate of change of inductance in terms of rotor angular position is negative.

In low to medium power conditions and low to medium speed conditions without commutation current modification, the demagnetising duration is short comparing with the angular period of the rotor of the SRM. The phase current may not flow over the aligned position. The phase may produce only positive torque in both motoring and demagnetising stages. If the SRM is operated with the commutation current modification system, the high demagnetising voltage will shorten the demagnetising duration. The average output torque and power of the SRM may be reduced. The phase current of the SRM with commutation current modification in motoring stage has to be higher than that without modification. This causes the current stress, which the phase of SRM suffers, in the commutation current modification system is higher. The higher current stress causes higher conduction loss on the power converter, the phase windings of the SRM and the conductors and hence, the efficiency of the commutation current modification system in these conditions is lower, such as the conditions in Section 5.4.

Other than the proposed resonant technique, Resonant DC Link (RDCL) technique can also provide a soft-switching condition for power converters [A15]. This technique is popular on inverters. Producing a resonant voltage, applying the voltage to the DC link of the inverter, the transistors may be switched under soft-switching condition. Active-clamped technique is also applied (RDCL) called Active-clamped Resonant DC link (ACRDCL). Some literatures have introduced this technique for SRM drives [B5, B8 and B13]. ACRDCL can reduce the peak value of the resonant DC link voltage and can control the duration of the high level voltage and that of the zero voltage by PWM with fixed switching frequency. This can give a suitable resonant DC link voltage that the transistors can be switched with different duty cycle under soft-switching. Also, there is no current-voltage overlapping problem either when the transistor is switched-on or off. That is, the transistor is switched under fully soft-switching condition. The circuits introduced in [B5] and [B13] can also provide a boosted voltage for demagnetising the phase winding to improve the commutation current shape.

The SRM drive system proposed in this chapter can provide a boosted voltage for demagnetising the phase winding by a resonant switched-reluctance motor. Comparing with the techniques of [B5, B8, and B13], all circuits have two power conversion processes in the whole SRM drive. The circuits in [B5, B8, and B13] are fully soft-switched while the chopping transistors in the proposed circuit may have switching loss because they may have current-voltage overlapping problem when they are switched off. Also, the circuits of [B5, B8, and B13] have fewer transistors comparing with the proposed circuit. The

proposed circuit can provide soft-switching to the chopping transistors when the SRM drive is operated in either PWM control method or constant current control method even with long dwell angle operations. The flexibility of the control method is high. The circuits of [B5, B8, and B13] produce only one ACRDCL for the whole circuit. When more than one phase windings of the SRM are energised, their voltages will be the same. They may have a problem to provide soft-switching condition when the SRM is controlled by constant current control method with long dwell angle operation or any operation that more than one phase winding is energised.

5.6. Summary

Application of the resonant switched-capacitor converters for power conditioning has been brief introduced. Examples of applications of inverting circuit and step-up circuit for switched reluctance motor drive have been provided.

An SRM drive system for modifying shapes of commutation current of phase windings of SRM has been discussed in this chapter. Conduction loss in regenerating stage of SRM can be reduced by this method. This advantage becomes more significant in higher speeds of operation. It has been analysed by both mathematical analysis and computer simulation. The commutation current modification can be achieved by adding a front-end converter before an SRM drive and re-routing the path for regenerating stage to the high voltage power source of the front-end converter.

A switched-capacitor zero-current switching quasi-resonant front-end converter has been introduced. To step down a DC voltage by half, a 1/2-mode switched capacitor resonant converter is chosen. Output power of the converter tested in experiment is up to 500W. The experiment has shown that the converter suits high power applications as its efficiency is highest at its maximum testing output power.

Experiments of the commutation current modification method have been done. By using an active-clamped resonant converter for the SRM drive and the switched-capacitor resonant converter as the front-end converter, soft-switching is obtained for all high switching frequency transistors. The experiment results have been compared with that of a stand-alone SRM drive with active-clamp characteristics. Discussion of the comparison of the experimental results has been provided.

Chapter 6. Conclusions and Recommendations

6.1. Conclusions

The contributions made in the study are summarised as follows:

(i) Two families of single-stage switched-capacitor zero-current switching quasi-resonant step-down DC-DC converters have been proposed. One family of the converters produce different fractional non-inverting stepped down voltage. The other ones produce fractional inverting stepped down voltage. All switching devices in the converters are switched under zero-current switching condition. Mathematical analysis provided generalised equations for all circuits systematically. Computer simulations and experiments have been done to verify the zero-current switching and high efficiency characteristics of the converters.

(ii) A family of multi-stage switching-capacitor zero-current switching quasi-resonant step-up converters has been proposed. The converters convert input voltage to different multiplied output voltage. All switching devices are switched in zero-current. Systematically mathematical analysis, computer simulation and experiments have been done.

(iii) Two switched-capacitor cells are proposed for both proposed single-stage

and multi-stage switched-capacitor converters. The switched-capacitor cells have no transistor in their structures. By adding the cells, different fractional or multiplied voltage can be produced without adding additional transistors.

(iv) The zero-current switching characteristics of the proposed switched-capacitor resonant converters are not only able to reduce switching loss of transistors, but also able to eliminate current stress problem. Power ranges of applications of the proposed switched-capacitor converters are much wider than conventional switched-capacitor converters. The 1/2-mode switched-capacitor resonant converter has been tested in high output power condition. The experiment has verified that the converter provides high efficiency over a wide range of output power.

(v) Model of switched reluctance motor has been done. By discrete Fourier Series method, inductance characteristics of SRM can be defined. This model has been applied on computer simulation for analysing the proposed SRM drives.

(vi) To improve efficiency of converters for SRM, an active-clamp resonant converter is proposed. This is a 2(n+1)-switch SRM converter. By adding resonant tanks and clamping circuits in the converter, zero-voltage switching of all high switching frequency transistors can be achieved. Equations and design method of the converter has been provided. The

performance of the converter has been tested in experiments.

(vii) A switched-capacitor resonant step-down front-end converter has been introduced for SRM drive. This front-end converter helps to step-down the high voltage of the voltage source, such as boost power factor correction converter, to a suitable voltage for DC link of the SRM drive. A commutation current modification method has been discussed for improving performance of SRM in this application, particularly in high speed of operation. This method has been applied on the active-clamp resonant SRM drive. By re-routing the regenerating path of the SRM drive to the high voltage side, duration of the regenerating stage of SRM is shorter. Experiments have confirmed that the soft-switching characteristics of both front-end converter and the SRM drive have not been affected. The modified SRM drive and the stand-alone active-clamp drive has been compared and discussed.

6.2. Recommendations for Future Study

For future study of the active-clamp resonant converter for switched reluctance motor and the commutation current modification, areas of further study are recommended below:

(i) Developing a switched-capacitor circuit with less switching loss, such as zero-voltage switching circuit.

(ii) Developing a family of single stage step-up switched capacitor converter without adding additional transistor.

(iii) Developing a more precise model, such as non-linear model, for switched reluctance motors for computer simulations.

(iv) Investigating the active-clamp resonant SRM drive by using another chopping method, especially constant current mode method.

(v) Testing the SRM drive in higher power level. As the power rating of the dynamometer is not suitable for the SRM used in the experiment, the power level of the SRM drives in the experiments was not high enough to obtain the maximum efficiency. Studying the efficiency characteristic of the SRM drives with higher power level necessary.

(vi) Studying the SRM drive by applying different dwell angles and firing angles. Comparing the results with normal dwell and firing angles.

(vii) Studying the commutation current modification method in longer Dwell angle application.

(viii) Studying the commutation current modification method for another SRM with different number of poles and phases.

(ix) Developing a front-end converter for the SRM drive with more additional

function such as power factor correction and bi-directional power flow.

(x) Developing a method to modify the commutation current without single stage of electrical power conversion.

Appendix A. Other Researches of Switched Capacitor Converters

Other novel switched-capacitor zero-current switching quasi-resonant converters are introduced below. There are no large magnetic components in the circuits. All transistors are switched under zero-current switching condition by the resonance of switched-capacitors and the very small resonant inductors.

A.1. Single Output Circuits

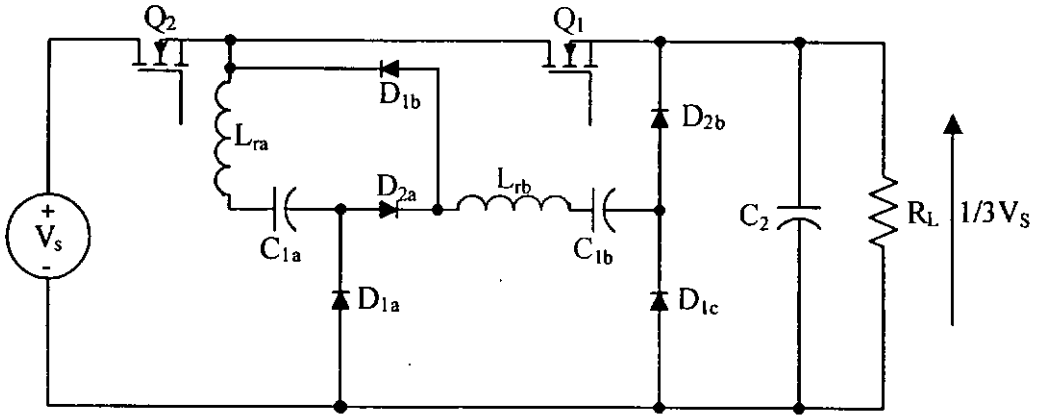

Fig. A1. Step-down 1/3-mode converter

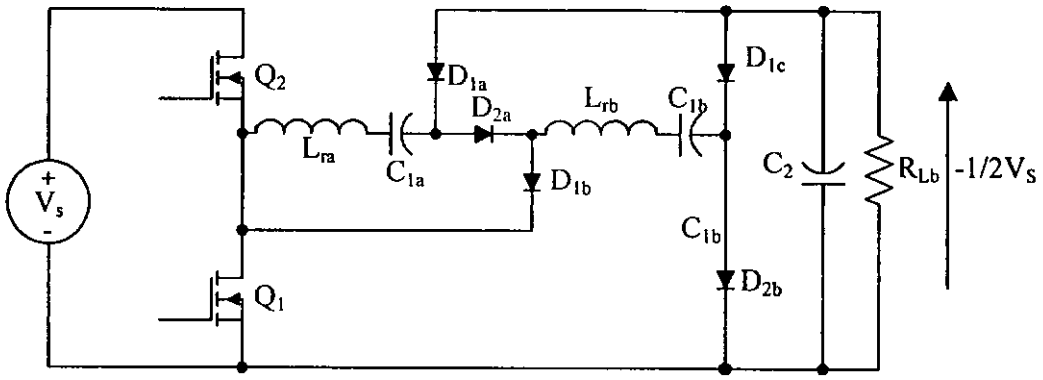

Fig. A.2. Inverting 1/2-mode converter

A.2. Multiple Output Circuits

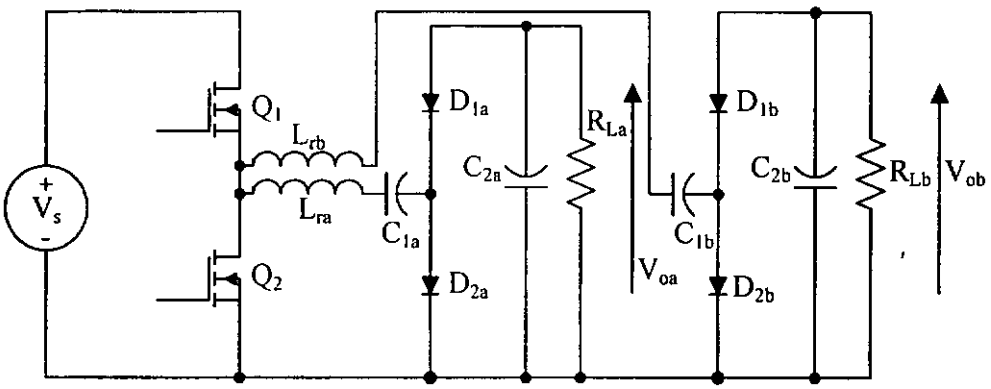

Fig. A.3. Dual output inverting circuit

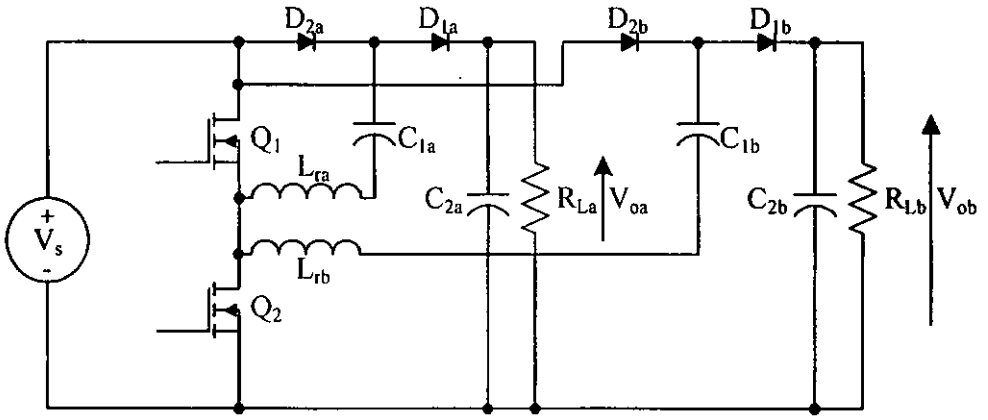

Fig. A.4. Dual output 2-mode step-up circuit

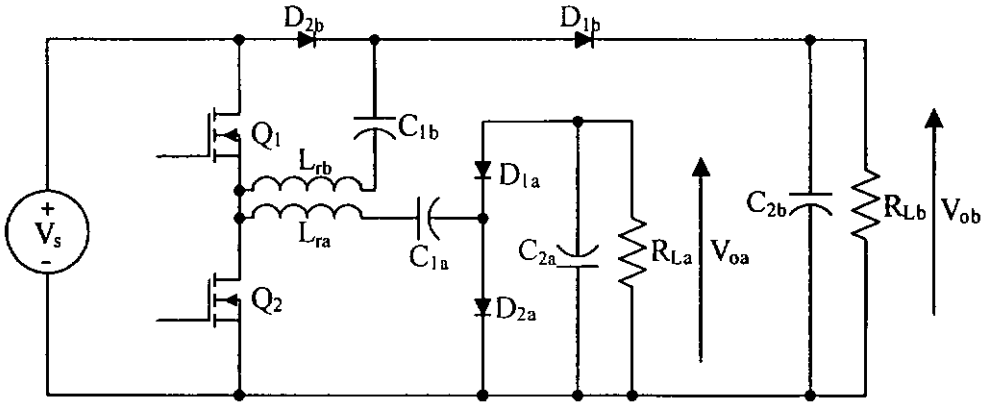

Fig. A.5. -1-mode inverting and 2-mode step-up circuit

A.3. Bi-directional Circuits

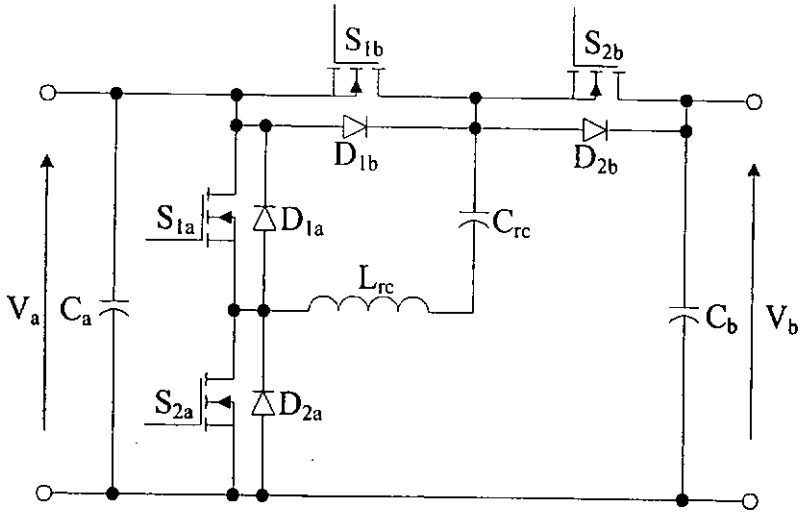

Fig. A.6. Non-inverting bi-directional circuit

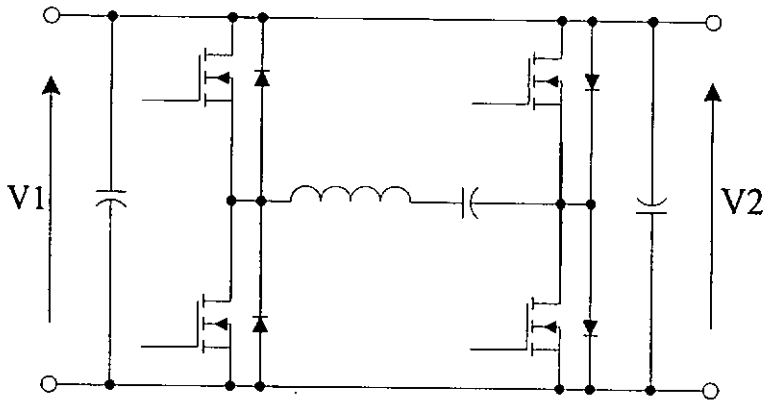

Fig. A.7. Inverting bi-directional circuit

Appendix B. Other Researches of Zero-current Switching Converter

Another family of zero-current switching resonant converters developed in extra research is introduced below. All transistors in the circuits are switched under zero-current switching condition achieved by the resonance of L_r and C_r. Resonant current of Q_1 is clamped by L_2 and C_r.

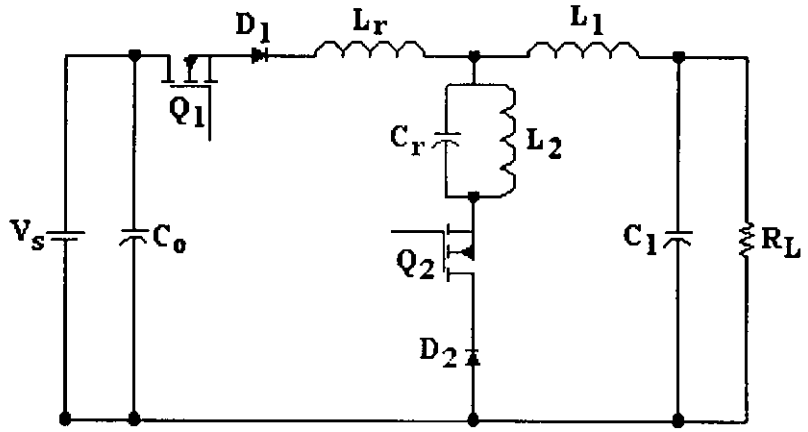

(a) Buck

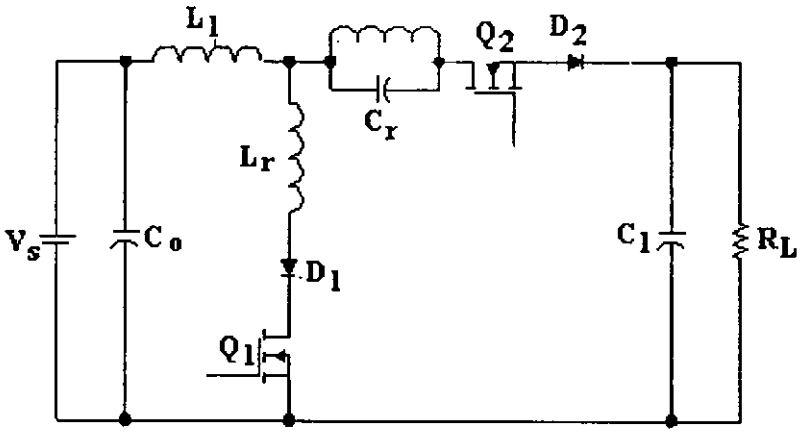

(b) Boost

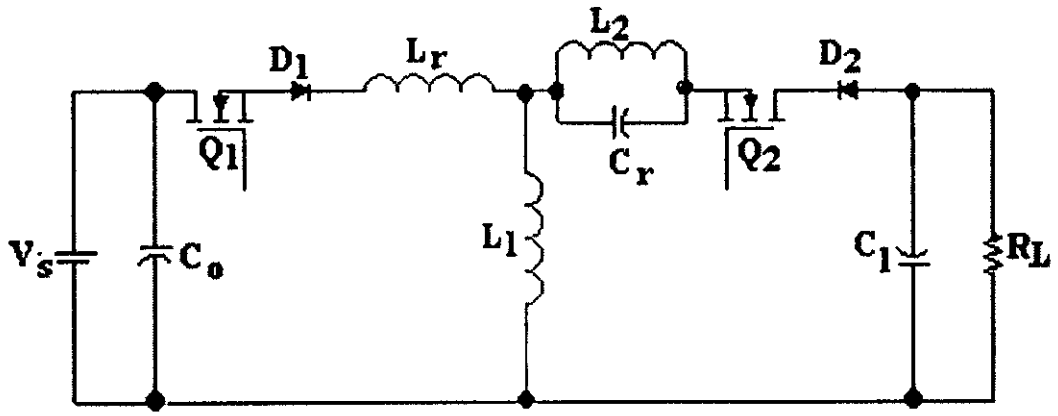

(c) Buck-boost

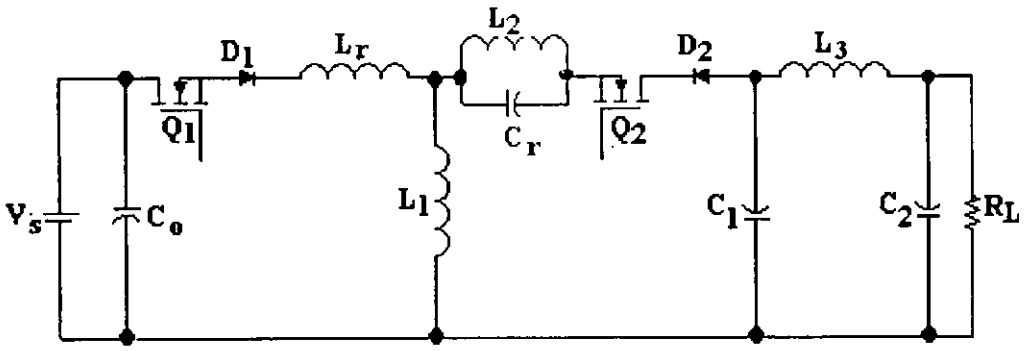

(d) Negative-Luo

Fig. B.1. Family of zero-current switching fixed frequency resonant transition square wave converters

These above circuits have not been used in the SRM circuit. However, these soft-switching circuits can be used as matching voltage between the input voltage source and the DC link voltage for the SRM as illustrated in Fig B2. A family of circuits has been listed and therefore each provides different voltage conversions when needed.

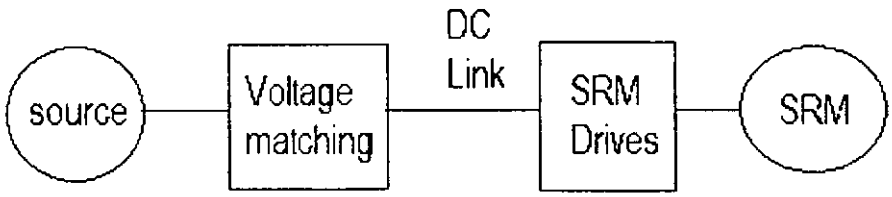

Fig. B.2. Illustration of voltage matching using a DC voltage conversion circuit

References

A. Soft-switching Technique

A1. F.C.Lee, "High-frequency quasi-resonant converter technologies", *Proc. of IEEE,* vol. 76, no. 4, pp. 377-390, Apr. 1988.

A2. K.H.Liu, and F.C.Y.Lee, "Zero-voltage switching technique in DC/DC converters", *IEEE Trans. on Power Electron.,* vol. 5, no. 3, pp. 293-304, July 1990.

A3. K.W.E.Cheng and P.D. Evans, "Parallel-mode extended-period quasiresonant convertor", *IEE Proc. Electr. Power Appl.,* vol. 138, no.5, pp. 243-251, Sept 1991.

A4. W.J.B.Heffernan and P.D. Evans, "Comparative assessment of zero voltage switched off-line power convertor topologies", *IEE Proc Electr. Power Appl.,* vol. 139, no. 2, pp. 71-85, Mar. 1992.

A.5. K.W.E.Cheng and P.D. Evans, "Constant frequency, two-stage quasiresonant convertor", *IEE Proc. Electr. Power Appl.,* vol. 139, no.3, May 1992.

A6. L.Yang, Y.Zhang, and C.Q.Lee, "A family of constant-switching-frequency quasi-square-wave converters", *Electr. and Comp. Engg. Canadian Conf.*, vol. 1, pp. 309-312, 1993.

A7. G.C.Hua, S.L.Ching, Y.M.Jiang, and F.C.Y. Lee, "Novel zero-voltage-transition PWM converters", *IEEE Trans. on Power Electron.*, vol. 9, no.2, pp. 213-219, Mar. 1994.

A.8. S.Y.R.Hui, K.W.E.Cheng and S.R.N.Prakash, "A class of fully soft-switched power factor correction circuits", *PESC '95 Record,* vol. 2, pp. 1165-1170, June 1995.

A9. G.Hua, and F.C.Lee, "Soft-switching techniques in PWM converters", *IEEE Trans. on Ind. Electron.*, vol 42, no. 6, pp. 595-603, Dec. 1995.

A10. F.C.Lee, R.Watson, and G.C.Hua, "Utilization of an active-clamp circuit to achieve soft switching in flyback converters", *IEEE Trans. on Power Electron.*, vol 11, no. 1, pp. 162-169, Jan. 1996.

A11. H.Chung, S.Y.R.Hui and K.K.Tse, "Reduction of EMI emission from power converter using soft-switching techniques", *Electron. Letters, IEE,* vol. 32, no. 11, pp. 977-979, 23 May 1996.

A.12. S.Y.R.Hui, K.W.E.Cheng and S.R.N.Prakash, " A fully soft-switched extended-period quasi-resonant power-factor-correction circuit", *IEEE Trans Power Electron.*, vol. 12, no. 5, pp. 922-930, Sept. 1997.

A13. K.W.E.Cheng, and P.D.Evans, "Unified theory of extended-period quasiresonant converters", *IEE Proc., Electr. Power Appl.*, vol 147, no. 2, pp. 119-130, Mar. 2000.

A14. Y.P.B.Yeung, and K.W.E.Cheng, "Zero-current switching fixed frequency resonant-transition square wave converters", *Electr. Power Appl., IEE Proc.*, vol 148, no. 6, pp. 475-480, Nov. 2001.

A15. D.M.Divan, and G.Skibinski, "Zero-switching-loss inverters for high-power applications", *IEEE Trans. on Ind. Appl.*, vol. 25, no. 4, pp. 634-643, 4 July.-Aug. 1989.

B. Switched Reluctance Motor Drives

B1. S.Vukosovic, and V.R.Stefonovic, "SRM inverter topologies: a comparative evaluation", IEEE Tran. on Ind Appl., vol 27, no. 6, pp. 1034-1047, Nov.-Dec. 1991.

B2. T.J.E.Miller, "Switched Reluctance Motors and Their Control", *Magna Physics Publishing and Clarendon Press, Oxford*, 1993.

B3 Sei Chan and A.M.Omar, "A Modified Split-supply Switched-reluctance Drive Inverter", *Proc. of EMPD'95*, vol. 2, pp. 628-633, Nov. 1995.

B4. C.Y.Wu and C.Pollock, "Analysis and reduction of vibration and acoustic noise in the switching reluctance drive", IEEE Trans Ind. Appl., vol. 31, no. 1, pp. 91-98, Jan.-Feb. 1995.

B5. L.G.B.Rolim, R.Hanitsch, E.H.watanabe, and W.I.Suemitsu, "Development of a high-efficiency switched reluctance drive using soft-switching techniques", *PEVD, 6th International IEE Conf.*, No. 429, pp. 203-207, Sept 1996.

B6. C.Pollock and C.Y.Wu, "Acoustic noise cancellation techniques for switched reluctance drives", *IEEE Trans. Ind. Appl.*, vol. 33, no.2, pp. 477-484, Mar.-Apr. 1997.

B7. Y.Murai, J.Cheng, and M.Yoshida, "A soft-switched reluctance motor drive circuit with improved performances", *Record of PESC 1997, 28th Annual IEEE*, vol. 2, pp.881-886, 1997.

B8. G.Gallegos-Lopez, P.C.Kjaer, T.J.E.Miller, and G.W.White, "Simulation study of resonant dc link inverter for current-controlled switched reluctance motors", *Proc. of PEDS International Conf.*, vol. 2, pp.757-761, 1997.

B9. T.W.Ching, K.T.Chau, and C.C.Chan, "A new zero-voltage-transition converter for switched reluctance motor drives", *Record of PESC 1997, 28th Annual IEEE Conf.*, vol. 2, pp. 887-891, 1997.

B10. K.T.Chau, T.W.Ching, C.C.Chan, and M.S.W.Chan, "A novel zero-current soft-switching converter for switched reluctance motor drives", *Proc. of IEEE IECON Annual Conf.*, vol. 2, pp. 893-898, 1998.

B11. T.W.Ching, K.T.Chau, and C.C.Chan, A novel zero-voltage soft-switching converter for switched reluctance motor drives", *Proc. of IEEE IECON Annual Conf.*, vol. 2, pp. 899-904, 1998.

B12. Y.G.Dessouky, B.W.Williams and J.E.Fletcher, "A Novel Power Converter with Voltage-boosting Capacitors for a Four-phase SRM Drive", *IEEE Tran. on Ind. Electron.*, vol. 45, no. 4, pp. 815-823, Oct. 1998.

B13. L.G.B.Rolim, W.I.Suemitsu, E.H.Watanabe, and R.Hanitsch, "Development of an improved switched reluctance motor drive using a soft-switching converter", *Electr. Power Appl., IEE Proc.*, vol. 146, no. 5, pp. 488-494, Sept. 1999.

B14. Y.Murai, J.Cheng, and M.Yoshido, "New soft-switched/switched-reluctance motor drive circuit", *IEEE Tran. on Ind. Appl.*, vol. 35, no. 1, pp. 78-85, Jan.-Feb. 1999.

B15. Y.Murai, J.Cheng, S.Sugimolo, and M.Yoshido, "A capacitor-boosted,

soft-switched switched-reluctance motor drive", *APEC*, vol. 1, pp. 424-429, 1999.

B16. K.W.E.Cheng, Y.P.B.Yeung, C.Y.Tang, X.D.Xue, and D.Sutanto, "Topology analysis of switched reluctance drives for electric vehicles", *Power Electron. and Var. Speed Drives, 8th International IEE Conf.*, no. 475, pp. 512-517, 2000.

B17. K.I.Hwu and C.M.Liaw, "DC-link voltage boosting and switching control for switched reluctance motor drives", IEE Proc. Electr. Power Appl., vol. 147, no. 5, pp. 337-344, Sept. 2000.

B18. R.Krishnan, "Switched Reluctance motor Drives – Modeling, Simulation, Analysis, Design, and Applications", *CRC Press*, 2001.

B19. A.Oahmane. F.Meebody and F-M.Sargos, "A novel boost capacitor circuit to enhance the performance of the switched reluctance motor", *Record of PESC 2001, 32nd IEEE Annual Conf.*, vol. 2, pp. 844-849, 2001.

C. Switched-capacitor Converters

C1. O.C.Mak, Y.C.Wong, and A.Ioinovici, "Step-up DC power supply based on a switched-capacitor circuit", IEEE Trans. on Ind. Electron., vol 42, no. 1, pp. 90-97, Feb. 1995.

C2. C.K.Tse, S.C.Wong, and M.H.L.Chow, "On lossless switched-capacitor power converters", *IEEE Trans. on Power Electron.*, vol. 10, no. 3, pp. 286-291, May 1995.

C.3 M.S.Makowski, and D.Maksimovic, "Performance limits of switched -capacitor DC-DC converters", *Record of PESC '95, 26th Annual IEEE Conf.*, vol. 2, pp. 1215-1221, 1995.

C4. W.S.Harris, and K.D.T.Ngo, "Power switched-capacitor DC-DC converter: analysis and design", *IEEE Trans. on Aero. and Electron. Sys.*, vol 33, no. 2, part I, pp. 386-395, Apr. 1997.

C.5 K.W.E.Cheng, "New generation of switched-capacitor converters", *Record of PESC '98, 29th Annual IEEE Conf.*, vol 2, pp. 1529-1535, 1998.

C.6 H.S.H.Chung, W.C.Chow, S.Y.R.Hui, and S.T.S.Lee, "Development of a switched-capacitor DC-DC converter with bi-directional power flow", *IEEE Trans. on Circuits and Systems I: Fundamental Theory and Appl.*, vol. 47, no. 9, pp. 1383-1389, Sept. 2000.

C.7 A.Ioinovici, "Switched-capacitor power electronics circuits", *IEEE Circuits and Sys. Magazine*, vol. 1, no. 3, pp. 37-42, 2001.

C.8 K.W.E.Cheng, "Zero-current-switching switched-capacitor converters", *Electr. Power Appl., IEE Proc.*, vol. 148, no. 5, pp. 403-409, Sept. 2001.

C.9 Y.P.B.Yeung, K.W.Cheng, S.L.Ho and D.Sutanto, "Generalised analysis of switched-capacitor step-down quasi-resonant converter", *Electron. Letters,* vol. 38, no. 6, pp. 263-264, 14 Mar. 2002.

C.10 Y.P.B.Yeung, K.W.E.Cheng, D.Sutanto, and S.L.Ho, "Zero-current switching switched-capacitor quasiresonant step-down converter", *Electr. Power Appl.,* IEE Proc., vol. 149, no. 2, pp. 111-121, Mar 2002.

Vita

The author was born in Hong Kong SAR, China in 1974. He received his B.Eng. (Hons) degree in Electrical Engineering from the Hong Kong Polytechnic University in 1998. Since 1999, he has been a Ph.D. research student at the same university. In his studies, he has been published five journal papers and nine conference papers. Most of them were through IEE and IEEE. His main research interests are resonant converters and circuitry of switched reluctance motor drives.